Spring 5-15-2016

OMCP Mediated Cowpox Virulence and its Dependence on the Immune Receptors NKG2D and FCRL5.

Michel Muzi Sun
Washington University in St. Louis

WASHINGTON UNIVERSITY IN ST. LOUIS

Division of Biology & Biomedical Sciences
Immunology

Dissertation Examination Committee:
Anthony French, Chair
Mike Diamond
Mary Dinauer
Brian Edelson
Daved Fremont
Wayne Yokoyama

OMCP Mediated Cowpox Virulence and its Dependence on the Immune Receptors NKG2D and FCRL5.

by
Michel M. Sun

A dissertation presented to the
Graduate School of Arts and Sciences
of Washington University in
partial fulfillment of the
requirements for the degree
of Doctor of Philosophy

May 2016
St. Louis, Missouri

TABLE OF CONTENTS

LIST OF FIGURES AND TABLES

CHAPTER 1

CHAPTER 2

CHAPTER 3

CHAPTER 4

APPENDIX 1

APPENDIX 2

APPENDIX 3

APPENDIX 4

LIST OF ABBREVIATIONS

7AAD	7-aminoactinomycin D
APC	Allophycocyanin
b-	Biotin
BLAST	Basic local alignment search tool
BMDC	Bone marrow dendritic cell
BMDM	Bone marrow derived macrophage
cDNA	complementary DNA
CFSE	Carboxyfluorescein succinimidyl ester
C-type	Calcium-dependent
CPX	Cowpox virus
CrmD	Cytokine response modifier D
DIII	West Nile Virus Domain III
DNA	Deoxyribonucleic acid
EC50	Effective concentration at half maximal
F	Female
FBS	Fetal bovine serum
FcR	Fc Receptor
FcγRI	Fcγ receptor I
FcRL	Fc Receptor-Like
FCRL5	Fc receptor-like 5
FITC	Fluorescein isothiocyanate
FO	Follicular

GFP	Green fluorescent protein
h/hu	Human
HBSS	Hank’s balanced salt solution
HSV	Herpes Simplex Virus
IC50	Inhibitory concentration at half maximal
IFN	Interferon
IFNAR	Interferon α/β receptor
Ig	Immunoglobulin
IRES	Internal ribosomal entry site
ISG	Interferon stimulated gene
ITAM	Immunoreceptor tyrosine based activation motif
ITIM	Immunoreceptor tyrosine based inhibitory motif
LAK	Lymphokine activated killer
L-Q	L-glutamine
LRS	Lymphocyte reduction system
LTR	Long terminal repeat
M	Male
mAb	Monoclonal antibody
m/mu	Murine or mouse
MDM	Monocyte derived macrophage
MEF	Murine embryonic fibroblast
MIC	MHC class I-related chain
MHC	Major histocompatibility complex

MHCISF	Major histocompatibility complex class I superfamily
miRNA	microRNA
MOI	Multiplicity of infection
MPX	Monkeypox
MULT1	Murine ULPB-like transcript 1
MZ	Marginal zone
NA	Neutravidin
NCI	National Cancer Institute
NK	Natural killer
NKG2D	Natural killer group 2D
OMCP	Orthopoxvirus MHC Class I like Protein
PBMC	Peripheral blood mononuclear cell
PBS	Phosphate buffered saline
PCP/PerCP	Peridinin chlorophyll protein complex
PE	Phycoerythrin
PFU	Plaque forming unit
p.i.	Post infection
P/S	Penicillin/streptomycin
qPCR	quantitative PCR
qRT-PCR	quantitative real time PCR
R10	RPMI with 10% FBS
RAE1	Retinoic acid expressed 1
RNA	Ribonucleic acid

RPMI	Roswell park memorial institute (media)
SA	Streptavidin
SB	Sorting buffer
SDS-PAGE	Sodium dodecyl sulfate polyacrylamide gel electrophoresis
SPR	Surface plasmon resonance
TDS	Transient dominant selection
TIR	Terminal inverted repeat
TNF	Tumor necrosis factor
ULBP	UL16 binding protein
UTR	Untranslated region
V018	open reading frame 018 (OMCP)
VACV	Vaccinia virus
VARV	Variola virus
wt/WT	Wild type
ZPXV	Zoonotic orthopoxvirus

ACKNOWLEDGEMENTS

I am immensely grateful for the support provided by my mentor, Tony French. Without his encouragement and steadfast confidence in me, I would never have completed this body of work. His unrelenting faith in me despite my struggles with failure and emotional breakdowns was truly appreciated. I consider myself extremely lucky to have studied under a mentor of his caliber.

I thank all the members of my thesis committee for their insight and advice during the course of my graduate studies. Their comments were invaluable in shaping my professional development.

I thank my fiancé Jeremy Mallari and all of my friends for helping me get through it all. My life is infinitely better with them in it.

I thank my parents and my brother. I owe a tremendous amount to my family for helping me get this far in life.

This research was supported by NIAID R01 AI078994 and AI073552 grants and Washington University Institutional Training Grant T32-AI007172.

Michel Muzi Sun

Washington University in St. Louis

May 2016

ABSTRACT OF THE DISSERTATION

OMCP Mediated Cowpox Virulence and its Dependence on the Immune Receptors NKG2D and FCRL5.

By

Michel M. Sun

Doctor of Philosophy in Biology and Biomedical Sciences

Immunology

Washington University in Saint Louis, 2016

Associate Professor Anthony R. French, Chair

Viruses with large DNA genomes, such as cowpox virus, encode many open-reading frames involved in the modulation of the host immune system, facilitating escape from immune detection or downregulation of specific aspects of the host immune response. Investigation of virally-encoded immunoevasins has been instrumental in understanding host-pathogen interactions. Here, we focus on the cowpox virus immunoevasin Orthopoxvirus MHC Class I-like Protein (OMCP) and demonstrate for the first time that OMCP facilitates cowpox virus virulence *in vivo.* We have previously documented that OMCP binds the activating receptor NKG2D on NK cells as well as the orphan receptor FCRL5 on innate B cells. By using NKG2D-deficient, FCRL5-deficient, and wild type mice, as well as recombinant cowpox viruses lacking OMCP or expressing a mutated form of OMCP that does not bind NKG2D, we were able to delineate the impact of OMCP targeting of each receptor. We found that OMCP's virulence *in vivo* could

largely be attributed to blocking NKG2D-mediated NK cell responses with no apparent effect due to binding to FCRL5 bearing innate B cells. Interestingly, the delay in weight recovery observed in mice surviving WT cowpox compared to OMCP-deficient cowpox infection was not observed in NKG2D-deficient mice and was abrogated in WT mice by the depletion of NK cells on day 8 post-infection. Additionally, we show that monomeric OMCP has a low affinity for FCRL5, although OMCP tetramers bind FCRL5 bearing cells well. We further demonstrate that the OMCP binding interfaces for NKG2D and FCRL5 are distinct, raising the possibility that the low affinity binding to FCRL5 may be overcome by multivalent presentation of OMCP through clustering of OMCP complexes on cells expressing NKG2D. This work delineates the impact of OMCP targeting of NKG2D and FCRL5 on cowpox virus virulence *in vivo* and highlights the importance of NKG2D-mediated control of orthopoxviruses.

CHAPTER 1: Introduction

Orthopoxvirus is a genus of poxviruses that includes several members with the capacity to infect humans, the best known of which is variola virus (VARV). Humans are the only host for variola virus, which causes smallpox, a highly contagious and often fatal infectious disease. Other notable members include vaccinia virus (VACV), which was used in the worldwide eradication of smallpox, and the zoonotic cowpox virus (CPXV) and monkeypox virus (MPXV) both of which can infect man. Humans can become incidentally infected through contact with rodent reservoirs, as in the case of cowpox virus or monkeypox virus infection. During recent decades, there have been increasing reports of human monkeypox outbreaks in Africa and North America [1, 2], illustrating that these zoonoses are important emerging health threats, especially in this era of increasing encroachment on animal reservoir habitats, expanding foreign travel, and importation of exotic animal species. Monkeypox virus was involved in a large multi-state outbreak linked to importation of prairie dogs in 2003. In total, 71 cases of monkeypox were reported in 5 states within a 1 month span, emphasizing that orthopoxviruses are capable of large scale, epidemiologically relevant outbreaks. Additionally, the cessation of routine childhood vaccination for smallpox, has rendered the population susceptible to possible bioterrorism attacks with smallpox, a Category A biological warfare pathogen. This constant threat to the unvaccinated and increasingly immunosuppressed population provides additional incentive for the study of orthopoxviruses and their interaction with human hosts. Our study seeks to better understand the mechanism of poxvirus immune evasion, with specific focus on the role of OMCP, a viral protein secreted by cowpox and monkeypox virus. Here we investigate

the role of viral OMCP on immune function in mice, the natural reservoir for these poxviruses, during both intraperitoneal and intranasal infection. We demonstrate that OMCP is involved in inhibition of NKG2D mediated NK cell killing *in vivo*, which may be critical for poxvirus clearance following infection.

Previous Evaluation of OMCP

Poxviruses have very large DNA genomes, allowing them to carry many accessory genes that are not required for viral replication and assembly. Many of these genes are involved in the manipulation of the immune system, facilitating escape of immune detection or downregulation of the immune response [3]. Members of the mammalian MHC Class I superfamily (MHCISF) in particular have been shown to be common targets for viral subversion. Many viral antagonists of the MHCISF, including viral NKG2D ligands, are known or predicted to adopt a class I-like fold themselves [4]. However, these viral antagonists have very low sequence homology to mammalian MHC Class I molecules, and fail to align with simple BLAST analysis. Faced with this problem, a structurally-constrained hidden Markov model was designed to search viral genomes for previously uncharacterized class I-like members that may serve as novel viral immunoevasins. Once identified these immunoevasions could be used to probe pathways important in host defense [4]. Using this hidden Markov model (trained with class-I like sequences and constrained by crystallographic data), the orthopoxvirus protein OMCP (also known as CPXV018 or V018) was identified as a viral protein with a putative class I-like fold and therefore predicted to be involved in immune evasion. OMCP variants are encoded by both CPXV and MPXV. The form isolated from the

CPXV-Brighton Red strain will be referred to as $OMCP_{br}$, and that isolated from the MPXV-Zaire 1979 strain referred to as $OMCP_{mpx}$. (The majority of the work described here is performed using $OMCP_{br}$, hence OMCP will refer to $OMCP_{br}$ unless otherwise noted. For experiments involving receptors, both human and murine proteins were initially tested. Data reported will be with murine proteins unless specifically noted.)

OMCP is secreted from infected cells [4]. Investigating whether OMCP recognized the NKG2D receptor was of particular interest, due to its putative MHC class I-like structure (proposed to be similar to the α1 and α2 domains of classical MHC class I), and because inhibition of NKG2D and its endogenous ligands is a common immune evasion strategy used by herpesviruses [5]. Subsequent crystal structure determination confirmed the MHC class I-like nature of OMCP (Fig 1). Upon examination, it was found that OMCP indeed recognizes both mouse and human NKG2D with high affinity, and is effective at inhibiting NKG2D dependent NK cell cytotoxicity by chromium release assay [4]. Thus, OMCP high-affinity binding to NKG2D prevents NK cell recognition of host stress ligands normally upregulated during viral infections.

OMCP is a unique viral immunoevasin, in that it is the only known NKG2D antagonist from poxviruses. Previously identified NKG2D antagonists from HCMV and MCMV act by specifically inhibiting expression of some of the 8 human NKG2D ligands or 9 murine NKG2D ligands [6]. OMCP may therefore be a more efficient NKG2D antagonist, as it is directed toward the receptor itself, rather than suppressing expression of the host derived ligands. Crystallographic evidence suggests that OMCP binds orthogonally

across the NKG2D binding site in a way that at least partially overlaps with the binding of endogenous NKG2D ligands (Lazear et al, submitted). Notably, all other known NKG2D antagonists are surface expressed molecules, making OMCP the only known antagonist that is actively secreted from infected cells. Therefore, we hypothesize that secreted OMCP acts in a paracrine fashion around orthopoxvirus infected cells to saturate NKG2D receptors on approaching NK cell effectors and preventing NKG2D-dependent killing.

Given that OMCP is actively secreted into the inflammatory milieu, it is possible that it has additional actions on other host immune cells distinct from its inhibitory activity on NK cell mediated killing. When murine splenocytes and human PBMCs were tested for binding to OMCP, it was found that F4/80^{+} monocytes/macrophages and innate B cells (CD21^{hi} CD23$^{+/lo}$ splenic marginal zone B cells and CD5^{+} peritoneal B-1a B cells) displayed significant OMCP binding in both mouse and humans (Fig 2) [7]. Because B cells do not express NKG2D, this observation suggested that additional receptors on B cells and macrophages are also capable of binding to OMCP. To identify these putative receptors, a retroviral cDNA library was constructed using a WEHI-231 B cell line with high surface expression of an OMCP binding receptor. This library was transduced into an OMCP receptor negative C1498 cell line, and repeated flow cytometric enrichment with OMCP tetramers was used to sort for OMCP staining cells. Genomic DNA was extracted from OMCP tetramer positive clones, retroviral inserts were amplified and sequenced, and FCRL5 was subsequently identified as the receptor responsible for

OMCP binding on innate B cells [8]. Binding of OMCP was validated by demonstrating binding to FCRL5 receptor transduced Ba/F3 cell lines (Fig 3)

The FCRL5 receptor

FCRL5 is a member of the Fc receptor-like family, a group of poorly characterized receptors that consist of Ig domains homologous to classical Fc receptor family members but do not bind immunoglobulin. Many FCRL's, including FCRL5 are orphan receptors with unidentified endogenous ligands and unknown function. The contribution of FCRL5 to immunity has not been reported, and how the impact of FCRL5 is modified by OMCP binding remains unknown. In addition, the role of innate B cells in antiviral immunity and host immunity in general, is unclear and poorly understood.

The ligand for FCRL5 has not been identified, and the function of the receptor is complicated by the fact that it contains both a non-canonical ITAM and two canonical ITIMs in its cytoplasmic region [9]. The current paradigm is that FCRL5 has the potential to serve as an inhibitory co-receptor on mature B cells. The FCRL5 $^{-/-}$ mouse is available, but its phenotype has not been published. Consistent with the idea that OMCP may be targeting FCRL5 to give the virus a survival advantage, we expected that the FCRL5 $^{-/-}$ mouse will have a survival advantage compared to WT mouse when both are infected with OMCP-sufficient CPX, since the FCRL5 $^{-/-}$ is capable of avoiding one aspect of viral subterfuge that is likely to be detrimental to the host. However, FCRL5 $^{-/-}$ may have a disadvantage compared to WT when both are infected with OMCP-deficient CPX, since B cells in the FCRL5 $^{-/-}$ are lacking a possible immune

modulating receptor that in the situation without immunevasion targeting is deleterious to the cell.

Despite significant effort by our laboratory to identify a role for OMCP binding to FCRL5 on innate B cell function, no *in vitro* or *in vivo* effect has been established. OMCP incubation does not affect BCR-induced calcium mobilization in WEHI-231 cells stimulated with anti-IgM F(ab')2, nor does soluble OMCP downregulate cell surface FCRL5 [7]. Additionally, no impact was identified on anti-CPX IgM production early during CPX infection. Interestingly, the OMCP-FCRL5 interaction was restricted to mice and not conserved with human FCRL analogs [7].

We thoroughly investigated OMCP binding to NKG2D and the FCRL5 receptors. We present extensive evidence of OMCP targeting of NKG2D on NK cells and FCRL5 on innate B cells and its effects on cowpox virulence *in vivo* in Chapter 2. Here we demonstrate that OMCP has significant inhibitory effect on NKG2D receptors that accounts for the majority of OMCP's virulence following cowpox infection. However, we find no evidence that OMCP binding to FCRL5 on innate B cells has an effect on murine survival or weight loss *in vivo*. Chapter 3 investigates a unique hypothesis of OMCP receptor crosslinking. Although we demonstrate here that OMCP crosslinking is plausible, we have not found conclusive data to confirm redirected NK cell killing. Finally, Chapter 4 offers future directions for continuation of this cowpox OMCP project. A discourse on problems we have encountered during our investigation of the OMCP binding receptor on macrophages is presented in Appendix 1.

Figures:

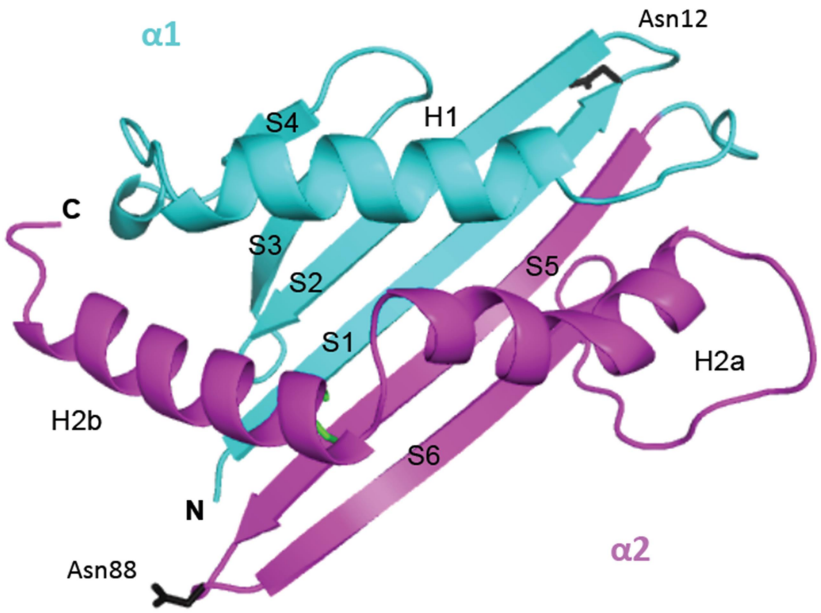

Figure 1: CPX OMCP is an MHC Class I-Like protein

The 2.25 Å resolution crystal structure of Brighton Red OMCP reveals an MHC class I like structure similar to known NKG2D ligands. Ribbon diagram of CPXV OMCP. Secondary structure elements are noted, S for beta strands and H for helix. The α1/α2 portions of the platform domain are indicated in cyan and magenta, respectively. PDB ID = 4FFE

Figure from Lazear et al. J. Virology 2013 [10]

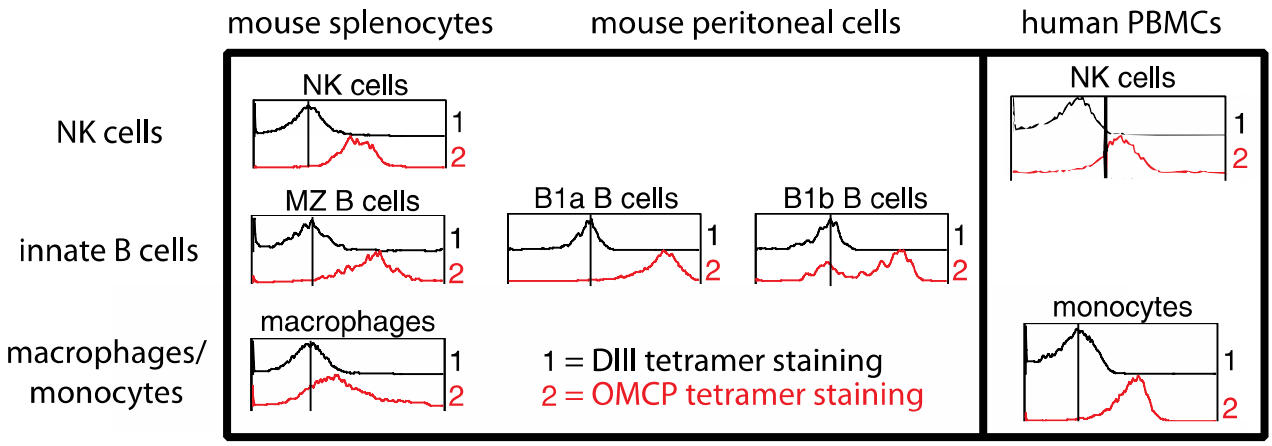

Figure 2: OMCP binds to NK cells, innate B cells, and macrophages/monocytes in murine and human cells.

Primary murine splenocytes or peritoneal lavage cells, or human PBMCs were stained for appropriate cell markers and binding to DIII tetramers (black) or OMCP tetramers (red). Figure taken from experiments presented in [4] and [8]

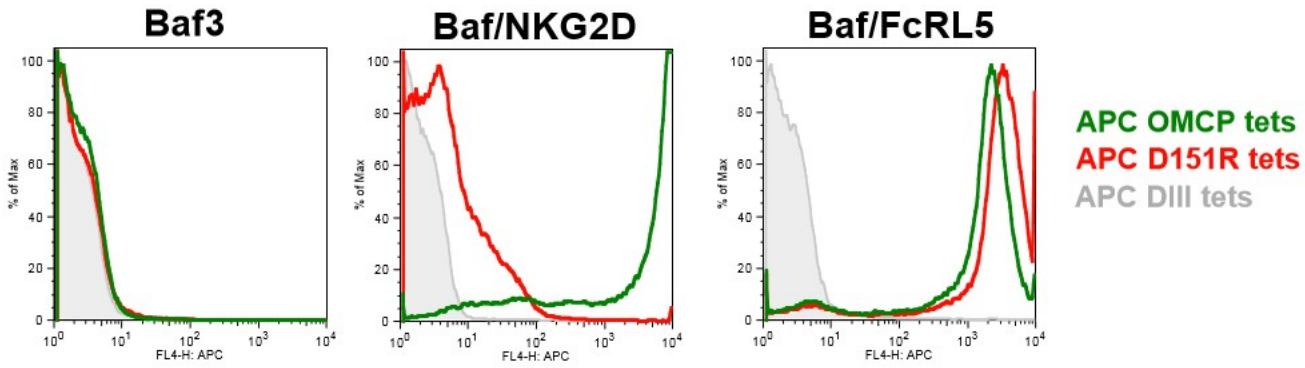

Figure 3: CPX OMCP binds to cells transduced with NKG2D and FCRL5 receptors

Untransduced parental Ba/F3 cells or cells retrovirally transduced for stable expression of the murine NKG2D receptor or FCRL5 receptor were stained with APC labeled OMCP tetramers (green), D132R tetramers (red), or control DIII tetramers (gray shaded).

CHAPTER 2: OMCP virulence *in vivo*

Introduction:

Viral immunoevasins have proven to be powerful tools for probing host-pathogen interactions, revealing cellular pathways that viruses exploit and identifying components of host defense integral for control of a specific virus. We previously described the immunoevasin Orthopoxvirus MHC Class I-like Protein (OMCP) secreted by cowpox virus (CPXV) and monkeypoxvirus [4]. OMCP acts as a competitive antagonist of NKG2D, preventing interactions with cellular stress ligands and inhibiting *in vitro* NK cell-mediated cytolysis [4]. OMCP was also found to engage the orphan receptor FCRL5 on splenic marginal zone (MZ) and peritoneal B-1 B cells, but the functional consequences of this interaction remain unknown [8].

OMCP is the only known NKG2D antagonist produced by poxviruses. In contrast to previously identified NKG2D antagonists encoded by human and murine cytomegaloviruses which act by specifically inhibiting surface expression of one or more of the 8 human or 9 murine NKG2D ligands [11, 12], OMCP is secreted from infected cells. We hypothesize that secreted OMCP acts *in vivo* in a paracrine fashion around orthopoxvirus infected cells, saturating NKG2D receptors on approaching NK cell effectors and preventing NKG2D-dependent killing of virally infected cells. The recent crystal structure of OMCP bound to NKG2D demonstrates a novel orientation of OMCP within the NKG2D binding site that allows for both higher shape complementarity and greater buried surface area (E. Lazear *et al*, *submitted*), resulting in a higher affinity of

OMCP for the NKG2D receptor than the affinity of endogenous NKG2D ligands [4]. This high-affinity binding of soluble OMCP may facilitate more efficient NKG2D antagonism by blocking NKG2D binding to multiple different NKG2D ligands.

OMCP tetramers also bind to innate B cells and macrophages in an NKG2D-independent manner [8]. Although the binding of OMCP to macrophages remains poorly characterized, we have previously identified that FCRL5 is the receptor responsible for OMCP binding to innate B cells [8]. The Fc receptor-like (FCRL) family consists of receptors that encode Ig domains homologous to classical Fc receptor family members but not thought to bind immunoglobulin [13]. A recent report suggests that two human FCRL members may bind IgA and certain subtypes of IgG [14], although there has been no evidence of immunoglobulin binding in other human FCRL family members or any of the mouse FCRL family members. The endogenous ligands of the FCRL family members are unknown, with the exception of human FCRL6 which binds HLA-DR, an MHC class II molecule [15]. The role of FCRL5 in host immunity and the impact of OMCP binding on FCRL5-mediated responses remain incompletely understood.

In this manuscript, we investigate the contributions of the immunoevasin OMCP on CPXV virulence *in vivo*. We isolate the effects of the binding interactions of OMCP to either NKG2D or FCRL5 receptors *in vivo* using NKG2D-deficient and FCRL5-deficient mice, as well as recombinant CPXV lacking OMCP expression or expressing a mutant OMCP that selectively does not bind NKG2D. Using these unique tools, we

demonstrate OMCP's role as a CPXV immunoevasin *in vivo* and the importance of NKG2D-mediated responses to host defense against CPXV.

Experimental Methods:

Cell lines and mice.

The generation of Ba/F3 transductants expressing NKG2D and FCRL5 was previously described [4, 8]. C57BL/6 (B6) mice were obtained from the National Cancer Institute (Charles River, MA). NKG2D-deficient mice on a B6 background were a kind gift from Bojan Polic (University of Rijeka, Croatia) [16], and FCRL5-deficient mice on a B6 background were obtained from Riccardo Dalla Favera (Columbia University). Mice were maintained under specific pathogen–free conditions and used between 8 and 12 weeks of age. All experiments were conducted in accordance with institutional guidelines for animal care and use based on the Guide for the Care and Use of Laboratory Animals of the National Institutes of Health. The protocol was approved by the Animal Studies Committee at Washington University (#20110104). Female mice utilized in survival studies were observed daily after infection for 28 days and moribund mice were euthanized per institutional guidelines.

CPXV and infection of mice.

Brighton Red strain CPXV was obtained from the ATCC and propagated in BS-C-1 cells. Virus was purified from infected BS-C-1 cell lysates by centrifugation through a 36% sucrose gradient. The titer of the viral stock was determined using a standard plaque assay on BS-C-1 cells [17, 18]. Intraperitoneal i.p. infections were done at a dose of

2x106 pfu CPXV/mouse unless otherwise indicated. For intranasal infections, mice were first anesthetized i.p. with ketamine/xylazine short acting sedative. Mice were infected with the appropriate innoculum of virus in a 50µL volume intranasally. All i.n. infections were done at a dose of $2.5x10^4$ pfu CPXV/mouse unless otherwise indicated.

Generation of recombinant cowpox viruses.

Recombinant virus lacking expression of OMCP (ΔV018) and its revertant were produced by transient dominant selection [19, 20]. A PCR product encoding the VACV p7.5 5' UTR and promoter was amplified and spliced to another PCR product encoding the *E. coli gpt* sequence. The final product was cloned into plasmid pUC19 to create pUC19 p7.5 *gpt*. OMCP was then amplified in two fragments in order to insert two tandem early termination codons. This product was cloned into pUC19 7.5 *gpt* to create pUC19 p7.5 *gpt* OMCPSTOP. The revertant plasmid pUC19 p7.5 *gpt* OMCP was generated by excising the OMCPSTOP sequence and replacing it with wild-type OMCP. OMCP D132R mutant CPXV was generated in a similar manner with primers to insert a point mutation at D132. The mutated D132R construct was also spliced to *E. coli gpt* and cloned for transient dominant selection.

Confluent CV-1 cells were then infected with CPXV (for CPXV ΔV018 or D132R generation) or CPXV ΔV018 (for revertant generation) at an MOI of 0.5. Two hours post-infection, the cells were transfected with pUC19 p7.5 *gpt* OMCPSTOP for CPXV ΔV018, pUC19 p7.5 *gpt* OMCP-D132R for D132R generation, or pUC19 p7.5 *gpt* OMCP for revertant generation using Lipofectamine2000. The infected/transfected cells

were lysed after 48 hours, and *gpt*+ viruses were selected by infecting confluent B-SC-1 cells with the transfected virus stock in *gpt* selection medium (DMEM, 2% FCS, 25 µg/mL mycophenolic acid, 250 µg/mL xanthine, and 15 µg/mL hypoxanthine). *Gpt*+ viral plaques underwent two further rounds of selection in *gpt* selection media and two subsequent rounds of purification in non-selective media. Finally, plaques were tested for their ability to grow in both selective and non-selective media. Plaques that grew only in non-selective media (indicating loss of the *gpt* marker) were picked and underwent a total of five plaque purifications. Virus stocks were subsequently propagated in B-SC-1 cells and titered following standard protocols using B-SC-1 cells [18].

Protein, Antibodies, and Flow cytometry.

Recombinant OMCP, D132R OMCP, and West Nile Virus glycoprotein domain III (DIII) were produced and biotinylated as previously reported [4, 21]. APC labeled tetramers were made fresh by incubating biotinylated OMCP protein with APC-streptavidin in a 4:1 molar ratio, incubating for 10 min at room temp, and used for staining cells. APC streptavidin, PE anti-F4/80 (BM8), APC eFlour 780 anti-CD3 (145-2C11), eFlour 450 anti-CD19 (1D3) were purchased from eBioscience (San Diego, CA). FITC anti-CD23 (B3B4), FITC CD19 (1D3), PE anti-NK1.1 (PK136), PE-Cy7 anti-GR1 (1A8), V500 anti-B220 (RA3-6B2), and BV510 anti-CD21 (7G6) were from BD Biosciences (San Jose, CA). FITC anti-CD5 (53-7.3) was from Biolegend (San Diego, CA). Single cell suspensions of splenocytes and isolation of peritoneal cells were performed using standard protocols [22, 23]. To block nonspecific binding of antibodies to FcRs, cells

were incubated in 2.4G2 (anti-FcγRII/III) supernatants (hybridoma from ATCC) prior to staining with labeled Abs. For protein bridging experiments, APC labeled NKG2D tetramers were preincubated with unlabeled OMCP monomer or DIII control monomer in a 2 or 4 monomer:1 tetramer molar ratio. Tetramers were preincubated for 20 min on ice prior to staining of single cell suspensions. 7AAD (CalBiochem) was used on all samples for dead cell exclusion. Data was collected on a FACScan flow cytometer (BD Pharmingen) with DxP multicolor upgrade (Cytek Development, Fremont, CA) and FlowJo CE software (TreeStar, Ashland, OR) or FACSCalibur flow cytometer (BD Biosciences) with CellQuest collection software (BD Biosciences). Data analysis was performed using FlowJo software (TreeStar). Identification of cells is as follows: splenic NK cells (NK1.1+, CD3-), T cells (NK1.1-, CD3+), follicular B cells (CD19+, $CD21^{lo}$. CD23+), marginal zone B cells (CD19+, CD21+, CD23-) peritoneal B1-a (CD19+, CD5+), B1-b (CD19+, CD5-) B cells, macrophages (F4/80+, $GR1^{lo}$), and granulocytes (F4/80-, $GR1^{hi}$).

Plaque assay.

Tissues harvested from mice were weighed and collected in tubes containing 1mL of DMEM and stored at -80^{o}C until processing. Frozen organs wee homogenized using glass dounce homogenizers and collected in 1mL of DMEM. The tissue homogenate was serially diluted in D2.5 media (DMEM, 2.5% FBS, 1% L-glutamine, 1% penicillin-streptomycin, 1% non-essential amino acids) and used in standard plaque assays on BS-C-1 cells [17]. Each organ was titered on $5x10^5$ BS-C-1 cells plated in wells of 6 well plates in duplicate. Infected cell cultures were maintained in D2.5 media at 37^{o}C,

5% CO_2 for 48 hours. Cells were stained at 48 hours post infection using a crystal violet solution and plaques were counted. Viral titers were calculated from a minimum of 3 dilutions done in duplicate.

NK cell depletion.

Mice were depleted of NK cells 8 days p.i. with 100 µg of purified anti-NK1.1 antibody (PK136; BioXcel). Controls were given 100 µg of an isotype matched irrelevant antibody (MAR18.5; BioXcel). The antibodies were diluted in sterile PBS immediately prior to administration, and a 300 µL volume injected intraperitoneally per mouse. Mice were monitored daily for weight loss and survival until 28 days p.i.

Cloning, expression, and purification of FCRL5.

The mature FCRL5 coding sequence was cloned into the AgeI and KpnI sites of the pHL-Avitag3 vector [24]. FCRL5-6His-birA plasmid was transiently transfected into 293F cells (Life Technologies) using PEI and the supernatant was collected on day 3 and day 6. Supernatants were supplemented with 10 mM imidazole and 0.02% sodium azide and purified via Ni-NTA Superflow resin (Qiagen). Protein was bulk eluted with 250 mM imidazole, concentrated, and further purified over a Superdex 200 column (16/60; GE Healthcare Life Sciences). The pooled FCRL5 fractions were then site-specifically biotinylated via the C-terminal birA tag according to the manufacturers specifications (Avidity). OMCP was purified as previously described [10].

Surface plasmon resonance (SPR).

A Biacore T100 instrument (GE Healthcare Life Sciences) was used to assess the binding of OMCP and the conformationally-specific FCRL5 antibody, 9D10 [25]. All experiments were carried out at a flow rate of 50 µl/min, 25°C, and in running buffer containing 10 mM HEPES, pH 7.4, 150 mM NaCl, 3 mM EDTA, 0.005% Triton X-100. CM5 chips (GE Healthcare Life Sciences) with immobilized neutravidin were made as previously described [26]. 500 RUs of biotinylated FCRL5 were coupled to the surface of the chip and then 100 nM OMCP or 9D10 were injected across the chip.

Statistical analysis.

Data analysis was done with Microsoft Excel and GraphPad Prism (GraphPad Software, La Jolla, CA). Unless otherwise noted, unpaired, two-tailed t tests were used to determine statistically significant differences. Error bars in the figures represent SDs from the mean value. The Log-rank (Mantel-Cox) test was used in the comparison of all Kaplan Meier survival curves.

Results:

CPXV lacking OMCP is significantly attenuated *in vivo*.

To facilitate our investigation of the role of OMCP *in vivo* during CPXV infection, we generated an OMCP-deficient (ΔV018) CPXV that does not produce OMCP using a transient dominant selection strategy. Multi-step growth curves of the WT CPXV, OMCP-deficient CPXV, and a revertant CPXV demonstrated nearly identical replication

growth kinetics (Fig. 4), indicating that OMCP is dispensable for viral growth or replication *in vitro*.

Using WT and OMCP-deficient CPXV, we investigated the impact of OMCP during systemic CPXV infection (via the intraperitoneal (i.p.) route) in WT B6 mice. Survival of WT mice infected with WT CPXV demonstrated a dose dependence with an LD50 value of $0.91x10^6$ pfu/mouse (Fig. 5A). Comparison of the survival of WT mice infected i.p. with OMCP-deficient CPXV (Fig. 5B) revealed substantially greater survival in the mice infected with OMCP-deficient CPXV than with WT CPX. Indeed, the LD50 value of $1.64x10^6$ pfu/mouse for mice infected with OMCP-deficient CPXV demonstrated that CPXV lacking OMCP is substantially attenuated *in vivo* compared to WT CPXV. Kaplan Meier survival curves of WT mice infected with the OMCP revertant CPXV (at $0.6x10^6$ and $2x10^6$pfu CPXV/mouse) correlate well with the survival observed following infection with WT CPXV (Fig. 5C), demonstrating that the decreased virulence observed during infection with OMCP-deficient CPXV reflects the absence of OMCP. Together, these results establish for the first time that OMCP facilitates CPXV virulence *in vivo*.

D132R OMCP mutant displays selective loss of NKG2D binding while retaining binding to FCRL5 *ex vivo* on primary cells.

To isolate the effect of OMCP binding to NKG2D from that of binding to FCRL5, we generated OMCP with a point mutation, D132R, that abrogates binding to NKG2D but retains binding to FCRL5 on stably transduced cells *in vitro* as well as in SPR studies (E. Lazear *et al*, *submitted*.) We also generated a recombinant CPXV that expressed

the mutant D132R OMCP, using a transient dominant selection strategy. Multi-step growth curve of D132R CPXV demonstrated identical replication growth kinetics to WT CPXV (Fig. 4).

We subsequently evaluated the ability of the selectively deficient D132R OMCP mutant to bind to primary cells isolated from WT, NKG2D-deficient, and FCRL5-deficient mice. Wild type OMCP tetramers bind to NKG2D bearing NK cells and FCRL5 expressing peritoneal B1-a B cells, and splenic MZ B cells, but not T cells or splenic follicular B cells (Fig. 6A, top panel). Peritoneal B1-b B cells demonstrated similar staining patterns as peritoneal B1-a B cells (data not shown). When OMCP tetramers were used to stain cells from NKG2D-deficient mice, OMCP binding to NK cells was completely abrogated, demonstrating that OMCP binding to NK cells is entirely through NKG2D. However, binding to FCRL5 expressing B cells was retained, confirming that OMCP interactions with innate B cells is NKG2D-independent (Fig. 6A, middle panel). WT OMCP tetramer staining on cells from FCRL5-deficient mice showed loss of binding to peritoneal B1-a B cells and splenic MZ B cells, with retained binding to NK cells (Fig. 6A, bottom panel). The D132R OMCP tetramer demonstrated complete loss of binding to NK cells from WT and FCRL5-deficient mice, yet retained normal binding to FCRL5 bearing peritoneal B1-a B cells and splenic MZ B cells from WT and NKG2D-deficient mice (Fig. 6B, top and middle panels). As expected, the FCRL5 binding was eliminated on MZ B cells from FCRL5-deficient mice (Fig. 6B, bottom panel). These *ex vivo* studies with primary cells from WT, NKG2D-deficient, and FCRL5-deficient mice confirm that the D132R OMCP mutant has a selective deficiency in binding to NKG2D but retains binding to FCRL5.

NKG2D mediates all of the virulence of OMCP during intranasal CPXV infection. We subsequently investigated the impact of OMCP binding *in vivo* to NKG2D and FCRL5 during CPXV infection. Cowpox and its close relatives variola virus, vaccinia virus, and monekeypox can be spread via contact and aerosol transmission [27]; therefore, we choose to study the role of OMCP during acute intranasal i.n. infection. Using our series of WT OMCP expressing CPXV, OMCP-deficient CPXV (ΔV018), and D132R OMCP mutant expressing CPXV in combination with WT, NKG2D-deficient, and FCRL5-deficient mice, we were able to delineate the impact of OMCP on NKG2D and FCRL5 expressing cells during CPXV infection *in vivo*. This unique set of tools allowed us to probe the influence of an orthopoxvirus immunoevasion *in vivo* at a level of detail that has not previously been possible.

Mice were infected i.n. with $2.5x10^4$ pfu/mouse of WT, OMCP-deficient, or D132R CPXV virus. Infection with WT CPXV resulted in similar mortality in WT, NKG2D-deficient, and FCRL5-deficient mice (Fig. 7 solid lines). However, a strong survival phenotype was unmasked when mice were infected with the OMCP-deficient CPXV (Fig. 7, dashed lines). The complete loss of OMCP rendered CPXV severely attenuated in WT and FCRL5-deficient mice, while OMCP-deficient CPXV infection in NKG2D-deficient mice remained similarly lethal as WT CPXV. These results illustrated that under normal circumstances (*i.e.*, WT CPXV infection in WT mice), OMCP is able to effectively abrogate activation through the NKG2D receptor, rendering WT CPXV as lethal in WT mice as it is in NKG2D-deficient mice. Mice infected with the D132R CPXV (which

produces OMCP selectively incapable of binding to and inhibiting NKG2D) phenocopied the mortality of mice infected with a complete OMCP-deficient CPXV (Fig. 7, dotted lines). Despite the fact that OMCP has multiple binding partners, this finding strongly implicated binding to NKG2D in mediating the virulence of OMCP during CPXV infection. The similar mortality observed in NKG2D-deficient mice following infection with D132R or WT CPXV also demonstrated the internal consistency of our infection model since there is no NKG2D receptor available in the NKG2D-deficient mice for WT OMCP to inhibit. The survival studies in NKG2D-deficient mice revealed no significant differences in survival following infection with any of the 3 strains of CPXV (Fig. 7B), supporting the conclusion that OMCP's impact following i.n. CPXV virus infection is mediated entirely through NKG2D. The survival observed in the FCRL5-deficient mice following infection with each of the strains of CPXV closely mimicked that seen in WT mice (Figs. 7C vs 7A), indicating that there is no significant role of the FCRL5 receptor on survival following this route of infection. Despite the striking differences in survival, no significant differences were observed in the lung viral titers in WT mice infected intranasally with WT or OMCP-deficient CPXV (Fig. 7D). The significant attenuation of OMCP-deficient CPXV and the D132R CPXV infection in WT and FCRL5-deficient mice demonstrated the critical importance of NKG2D blockade during WT CPXV infection, and strongly implicates OMCP binding to NKG2D as the primary virulence effect of this viral immunoevasin following acute i.n. infection.

Delayed weight phenotype is absent in NKG2D-deficient mice and abrogated in mice depleted of NK cells.

We assessed daily weights as an additional measure of OMCP virulence during i.n. CPXV infection. Analysis of weight-loss in WT, NKG2D-deficient, and FCRL5-deficient mice during infection with WT, OMCP-deficient, and D132R cowpox viruses generally supported the conclusions drawn from the i.n. survival studies. Mice infected with the less virulent OMCP-deficient CPXV or D132R CPXV lost less weight and surviving mice regained weight faster than their counterparts infected with WT CPXV, emphasizing the viral virulence attenuation when OMCP is absent or unable to bind to NKG2D (Fig. 8). However, in contrast to the prolonged weight-loss observed in surviving WT and FCRL5-deficient mice infected with WT CPXV (compared to OMCP-deficient and D132R CPXV; Fig. 8A & C), weight loss in surviving NKG2D-deficient mice infected with WT CPXV paralleled the weight loss observed in NKG2D-deficient mice infected with the less virulent OMCP-deficient or D132R CPXV (Fig. 8B), consistent with their similar mortality rates in NKG2D-deficient mice. Interestingly, WT mice that were depleted of NK cells on day 8 p.i. regained weight faster during recovery from WT CPXV infection than control mice (Fig. 8D), phenocopying the weight gain observed in surviving WT mice infected with OMCP-deficient or D132R CPXV. These experiments suggested that the NKG2D receptor on NK cells was responsible for the paradoxical delayed weight recovery phenotype observed in the presence of OMCP that is capable of binding to NKG2D receptors.

Low affinity binding of OMCP to FCRL5 can be overcome by multimerization with NKG2D on NK cells.

We hypothesized that the impact of NK cell expressed NKG2D on the paradoxical delayed weight recovery phenotype observed in WT mice infected with WT CPXV could reflect OMCP redirecting NK cell-mediated cytolysis by bridging NK cells and innate B cells or macrophages. The binding interface utilized by OMCP to interact with NKG2D has been recently been described (E. Lazear *et al*, *submitted*), but the OMCP binding sites for FCRL5 and the as yet unidentified receptor on macrophages/monocytes have not been characterized. Therefore, to investigate the plausibility of our bridging hypothesis, we formally evaluated whether the OMCP binding interfaces for NKG2D and FCRL5 were distinct and independent. Using fluorescently labeled NKG2D tetramers, we demonstrated that NKG2D did not bind to FCRL5 transductants or a monocyte cell line. However, preincubation of the labelled NKG2D tetramers with monomeric OMCP resulted in fluorescence specifically associated with FCRL5 expressing cells and monocyte cells, demonstrating that OMCP can simultaneously bind to NKG2D and FCRL5 (or NKG2D and monocytes/macrophages) using different binding interfaces (Fig. 9A), In contrast, preincubation of the NKG2D tetramers with irrelevant protein did not result in NKG2D tetramers interactions with either the FCRL5 transductants or the monocyte cell line, and no OMCP-preincubated NKG2D tetramers were detected on NKG2D transfectants, due to competition for the single NKG2D binding site on the OMCP intermediary. These results indicated that OMCP is capable of binding to NKG2D and FCRL5 (or NKG2D and macrophages/monocytes)

simultaneously, potentially acting as a bridging ligand between NK cells and innate B cells (or monocytes/macrophages).

We have previously reported that OMCP tetramers bind to FCRL5 transductants, innate B cells, and macrophages in an NKG2D-independent manner [8]. Given the lack of observable *in vivo* survival phenotype in the FCRL5-deficient mice during CPXV infection, we further analyzed the binding of monomeric OMCP to FCRL5. A647-labeled OMCP monomer staining demonstrated that OMCP monomers bind strongly to NKG2D but have a much lower affinity for FCRL5 (Fig. 9B). Additional validation by SPR confirmed that any binding of monomeric OMCP to FCRL5 receptors was below the sub-micromolar detection limit of SPR (Fig. 9C). These results suggest that OMCP, which is secreted as a monomer *in vivo* [10], is unlikely to effectively bind FCRL5 in the absence of NKG2D multimerization (Fig. 9A). However, multivalent presentation of OMCP may be achievable on cells expressing NKG2D, which may display OMCP for high avidity binding to FCRL5 expressing B cells and/or macrophages.

NKG2D binding plays a critical role in mediating OMCP's virulence following systemic intraperitoneal infection but NKG2D independent mechanisms also exist. We also investigated the impact of OMCP binding *in vivo* to NKG2D and FCRL5 during systemic CPX infection. Using our series of WT OMCP expressing CPX, OMCP-deficient CPX (ΔV018), and D132R OMCP mutant expressing CPX viruses in combination with WT, NKG2D-deficient, and FCRL5-deficient mice, we were able to

delineate the impact of OMCP on NKG2D and FCRL5 expressing cells during CPX infection *in vivo*.

WT mice were infected with $2x10^6$ pfu/mouse of WT, OMCP-deficient, and D132R CPX virus. WT CPX infection in WT, NKG2D-deficient, and FCRL5-deficient mice was similarly lethal (Fig. 10 solid lines). However, as with intranasal infection, a strong survival phenotype was unmasked when the mice were infected with the D132R expressing CPX virus (Fig. 10, dotted lines). D132R CPX was severely attenuated in WT and FCRL5-deficient mice, while D132R CPX infection in NKG2D-deficient mice phenocopied WT CPX infection in NKG2D-deficient mice. This strongly indicated that under normal circumstances (WT CPX in WT mice), OMCP is able to completely inhibit activation through the NKG2D receptor, rendering WT CPX as lethal in WT mice as it is in NKG2D-deficient mice. The effect of OMCP is uncovered with the D132R mutation that renders OMCP incapable of inhibiting NKG2D. The importance of NKG2D blockade is evidenced by the fact that D132R CPX infection in WT and FCRL5-deficient mice is severely attenuated. D132R CPX in NKG2D-deficient mice has similar mortality as WT CPX infection in those mice (Fig. 10B dotted vs solid lines), demonstrating our infection model is internally consistent, as in this strain there is no NKG2D receptor available for inhibition.

Unexpectedly, we noted that infection with the complete OMCP-deficient virus was less virulent than WT CPX, but more virulent than D132R CPX in WT mice (Fig. 10A, dashed line). This indicates that although the overall effect of OMCP is to promote CPX

virulence, there are some NKG2D independent effects of OMCP that is paradoxically beneficial to the host. The fact that the absence of the NKG2D receptor in NKG2D-deficient mice does not eliminate the difference in survival observed following infection with WT and OMCP-deficient CPX (Fig 10B solid vs dashed) also supports the presence of NKG2D-independent effects of OMCP following i.p. infection.

The survival observed in the FCRL5-deficient mice following i.p. infection with each of the strains of CPX virus closely mimics that seen in WT mice (Figs. 10C vs 10A), indicating that we uncovered no significant role of the FCRL5 receptor on survival following this route of infection. The difference in mortality observed following i.p. infection with the D132R mutant virus compared with the OMCP-deficient virus in both WT and FCRL5-deficient mice, suggested that OMCP may have NKG2D- and FCRL5-independent effects that are paradoxically beneficial to the host. However, the large survival difference between WT CPX and both OMCP-deficient CPX and D132R CPX in WT and FCRL5-deficient mice strongly implicates OMCP binding to NKG2D in providing the primary virulence effect of this viral immunoevasin following i.p. infection.

The conclusions derived from the survival curves were further evaluated by determination of splenic and hepatic viral titers at day 6 p.i. (Fig. 11). There was approximately a 1 log difference in the median splenic and hepatic viral titers between WT mice and NKG2D-deficient mice infected with WT CPX. In WT mice, infection with OMCP-deficient CPX and D132R CPX resulted in lower splenic viral titers than infection with WT CPX, consistent with the increased survival observed in WT mice infected with

OMCP-deficient and D132R CPX. Furthermore, the median splenic titers in WT mice infected with OMCP-deficient CPX virus were similar to the splenic titers observed in NKG2D-deficient mice following infection with WT CPX, consistent with the survival results. However, the splenic titers did not completely correlate with the survival data. For example, similar splenic titers were observed in WT mice infected with OMCP-deficient and D132R CPX, despite the increased survival observed in the WT mice infected with D132R. The hepatic titers as a whole correlated less well with the survival data, suggesting that hepatic titers may not be a primary factor influencing death in this model. Mice inoculated with CPX i.p. have been shown to sustain viral infection in a range of cell types and organs in the peritoneal cavity, including the liver, spleen, pancreas, uterus, ovary, and adipose tissue [27]. Migration of CPX infected peritoneal macrophages into the thoracic cavity is thought to bring virus to the diaphragm, mediastinum, and pulmonary lymph nodes [27]. This diffuse viral dissemination during systemic infection appears to contribute to a multifactoral cause of death, consistent with only modest correlation with individual organ titers.

Discussion:

Viral evasion of NKG2D recognition is integral for the avoidance of innate host defense mechanisms, as evidenced by the many members of the herpesvirus family that have evolved proteins to inhibit expression of a number of NKG2D ligands [28-31]. In contrast to herpesvirus immunoevasins that target individual NKG2D ligands, CPXV utilizes a novel approach of directly targeting the NKG2D receptor using a soluble MHC class I-like immunoevasin. This high-affinity, soluble decoy (OMCP) can theoretically

completely inhibit NKG2D activation by blocking receptor engagement with any of the NKG2D stress ligands upregulated during viral infection, facilitating CPXV escape from immune detection.

After extensive characterization of CPXV OMCP *in vivo* using novel mutant viruses and genetically modified mice, we have shown that the majority of OMCP's effect on host survival can be attributed directly to NKG2D receptor antagonism. In both the intranasal and intraperitoneal routes of infection, NKG2D binding appears to be the main determinant of OMCP-mediated CPXV virulence. Unexpectedly, we did not detect evidence of a direct impact of OMCP interaction with FCRL5 on survival during CPXV infection.

The finding that NKG2D antagonism is the primary contributor to OMCP-mediated virulence during CPXV infection is not unexpected. OMCP has a highly conserved MHC class I like structure and binds murine and human NKG2D with a higher affinity than endogenous NKG2D ligands [4, 10]. Furthermore, OMCP has also been shown to competitively block host NKG2D ligand engagement *in vitro*, suggesting that OMCP binding can successfully inhibit NKG2D activation [4, 10]. Indeed, we have shown that soluble OMCP is sufficient to block *in vitro* NKG2D-mediated NK cell killing of target cells [4]. Therefore, we hypothesized that secreted OMCP from CPXV infected cells creates a gradient of local high concentration of OMCP around infected cells, sufficient to competitively block the interaction of the NKG2D receptor on incoming NK cell effectors with stress ligands induced on virally infected cells, thus preventing NK cell

recognition and killing. The results of our *in vivo* studies support this hypothesis and suggest that NKG2D blockade is important to CPXV virulence. Interestingly, NKG2D has also been implicated in resistance to a related orthopoxvirus, ectromelia [32], suggesting that the NKG2D receptor is essential for innate defense to the extended orthopoxvirus family.

We unexpectedly observed that surviving NKG2D-deficient mice infected intranasally with WT CPXV regained lost-weight faster than WT and FCRL5-deficient mice late during infection (>10 days p.i.). One consideration in explaining this observation is that NKG2D is upregulated on $CD8^+$ T cells during many viral infections [33, 34]. However, we have not observed NKG2D upregulation on CD8 T cells during CPXV, and a recent study demonstrated that two CPVX-encoded immunoevasins (CPX012 and CPX203) neutralized CD8 effector cell responses [35]. Furthermore, WT mice depleted of NK cells day 8 p.i. similarly regained weight faster during the recovery period (Fig. 8D), implicating NKG2D on NK cells in mediating this process. Indeed, the weight gain in the surviving NKG2D-deficient mice or NK cell depleted mice infected with WT CPXV mirrored that of their counterparts infected with OMCP-deficient or D132R virus. One potential explanation for this observation (*i.e.*, OMCP binding to NKG2D bearing NK cells paradoxically delaying murine weight gain during CPXV recovery) is that OMCP may be acting as a bridging ligand facilitating interactions between NKG2D-bearing NK cells and innate B cells (or monocytes/macrophages) and potentially redirecting NK cell lysis against these cells. Indeed, FCRL5 expressing cells (and monocytes/macrophages) were labeled by fluorescent NKG2D tetramers only in the

presence of an OMCP bridge (Fig. 9A), demonstrating that the OMCP binding sites are independent. The observation that monomeric OMCP binds FCRL5 with low affinity (Fig. 9B) and requires multivalent interactions for sustained binding (Figs. 9A & B) may partially explain the lack of survival phenotype we observed during infection in the FCRL5-deficient mice. However, we demonstrate that OMCP is capable of strong binding to FCRL5 when complexed with tetrameric NKG2D (Fig. 9A), a scenario that simulates OMCP presentation on NKG2D receptor bearing NK cells. Furthermore, we have recently reported that artificially cell-associated OMCP (using a cell line transfected with OMCP attached to a Thy1.1 transmembrane domain [4]) resulted in efficient NK cell-mediated cytolysis of the OMCP bearing target cell (E. Lazear et al., *submitted*). Given that we observe delayed weight gain in FCRL5-deficient mice infected with WT cowpox (Fig. 8C), we favor the hypothesis that OMCP is facilitating the redirection of NK cell-mediated responses toward monocytes/macrophages resulting in slower weight gain in surviving mice late during CPXV infection. However, confirmation of this intriguing bridging hypothesis will require additional future studies.

We did not detect any impact of OMCP binding to FCRL5 on survival during CPXV infection. However, it is possible that OMCP binding to FCRL5 mediates other processes that do not directly affect survival or weight loss during acute CPXV infection. FCRL5 is a poorly characterized innate B cell receptor known to modulate BCR signaling [9, 36, 37]. It is expressed on innate splenic marginal zone and peritoneal B1 B cells, subsets of innate B cells with unique developmental lineages [38-40] and specialized roles in the initial stages of humoral defense [41-44]. Despite significant

investigation, our laboratory has not identified an *in vitro* impact of OMCP binding to FCRL5 on innate B cell function or an *in vivo* effect on survival, weight loss, or viral titers.

Taken together, these findings demonstrated the importance of the CPXV immunoevasin OMCP in contributing to the *in vivo* virulence of CPXV. The majority of OMCP's effect can be attributed to binding to NKG2D, and our studies found minimal contributions of OMCP binding to FCRL5 on survival or weight loss. We identified a paradoxical delayed weight gain associated with binding of OMCP to NKG2D on NK cells following intranasal CPXV infection, and have begun to investigate the possibility of OMCP functioning as a bridging ligand between NK cells and FCRL5-bearing cells or macrophages. We have also provided initial evidence that NKG2D-mediated multimerization of OMCP may help overcome the relatively low affinity of monomeric OMCP for FCRL5. This work highlights the importance of NKG2D receptor blockade *in vivo* during CPXV infection and will inform future studies of the host innate immune response to epidemiologically relevant orthopoxviruses.

Figures:

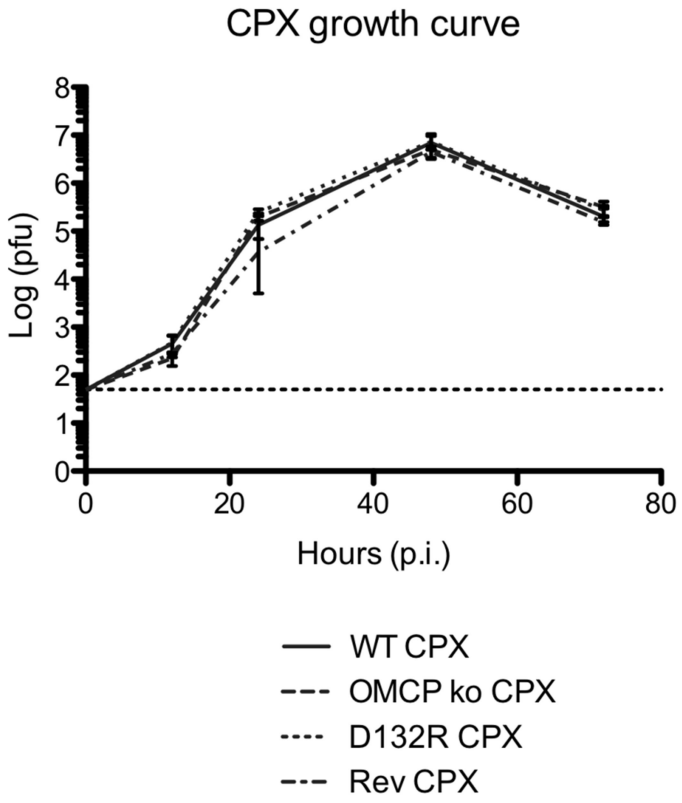

Figure 4: ΔV018 virus and D132R virus do not have a growth defect *in vitro*.

Multi-step growth curves for WT CPX, ΔV018, D132R, and revertant viruses show that all four cowpox virus strains have similar replication kinetics in a multi-step growth curve. B-SC-1 cells were infected at an MOI of 0.01 with the indicated viruses. Infected cells were harvested at the indicated time points and freeze-thawed three times. Lysates were tittered by plaque assay on B-SC-1 monolayers. Results are representative of three experiments done in duplicate.

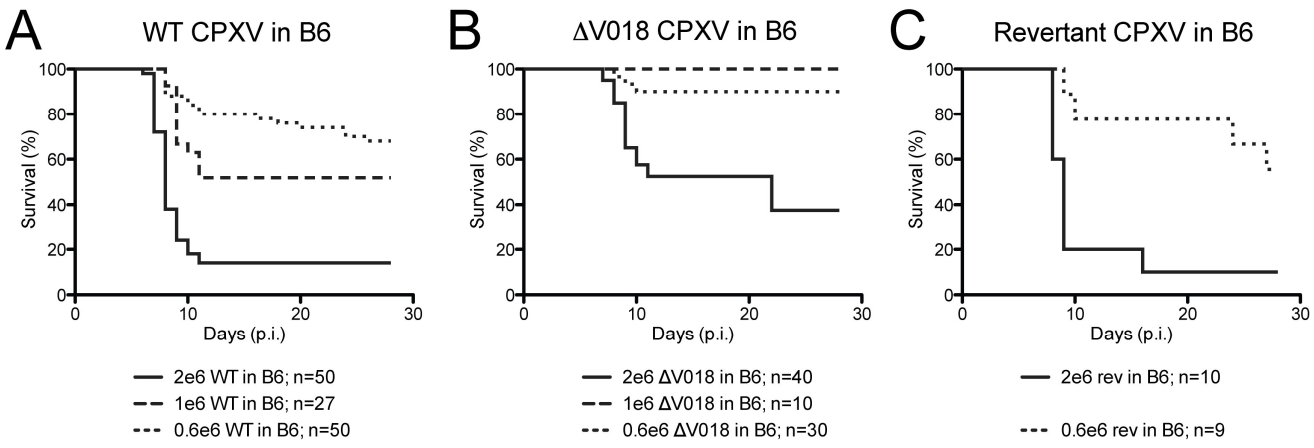

Figure 5: Cowpox virus lacking OMCP is significantly attenuated *in vivo*.

WT CPX **(A)** is more virulent than ΔV018 CPX **(B)**, as evidenced by increased lethality at all tested doses. The Revertant CPX control **(C)** phenocopies WT CPX as is expected. 8-12 week old female WT B6 mice were infected with $2x10^6$ (solid line), $1x10^6$ (dashed line), or $0.6x10^6$ (dotted line) of the indicated CPX strain, and survival was assessed daily for 28 days. Data are aggregated from two-seven independent experiments with 5-10 mice per group.

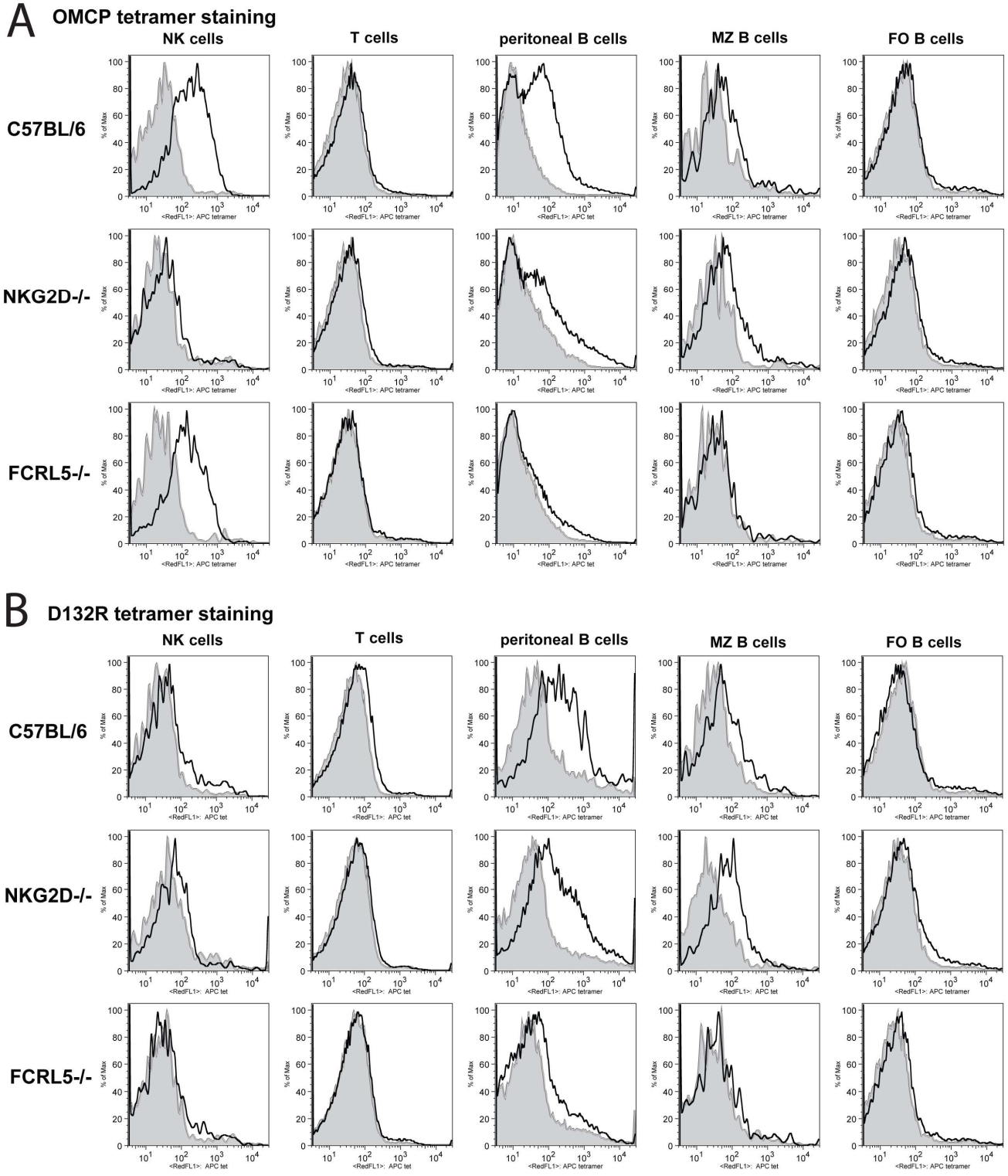
A
OMCP tetramer staining
NK cells
T cells
peritoneal B cells
MZ B cells
FO B cells
C57BL/6
NKG2D-/-
FCRL5-/-
B
D132R tetramer staining
NK cells
T cells
peritoneal B cells
MZ B cells
FO B cells
C57BL/6
NKG2D-/-
FCRL5-/-
% of Max
<RedFL1>: APC tetramer
<RedFL1>: APC tet

Figure 6: WT OMCP binds to NKG2D expressing NK cells and FCRL5 expressing B1 B cells, while D132R OMCP mutant displays selective loss of NKG2D binding with retained FCRL5 binding.

APC labeled OMCP tetramers (solid line) were used to stain splenic NK cells (NK1.1+, CD3-), splenic T cells (NK1.1-, CD3+), peritoneal B1-a B cells (CD19+, CD5+), splenic marginal zone B cells (CD19+, CD21+, CD23-), and splenic follicular B cells (CD19+, CD21+. CD23+).. Peritoneal B1-b (CD19+, CD5-) B cells (not shown) stain similar to B1-a cells. Staining with APC labeled WNV DIII tetramer control shown in gray histograms. **(A)** OMCP tetramer binds selectively to WT NK cells, peritoneal B1-a B cells, and MZ B cells. The NKG2D-deficient mice lose OMCP binding to NK cells while retaining binding to B1-a B cells and MZ B cells. Conversely, the FCRL5-deficient mice lose OMCP binding to B1-a B cells and MZ B cells with retained binding to NK cells. Representative results from four independent experiments. **(B)** OMCP tetramer with the D132R mutation loses binding to NKG2D while retaining binding to FCRL5 expressing cells. The D132R mutant has lost binding to NK cells in WT mice, but it has undiminished binding to peritoneal B1-a B cells and splenic MZ B cells. Peritoneal B1-a B cell and splenic MZ B cell staining is lost only in FCRL5-deficient mice. Representative results from three independent experiments.

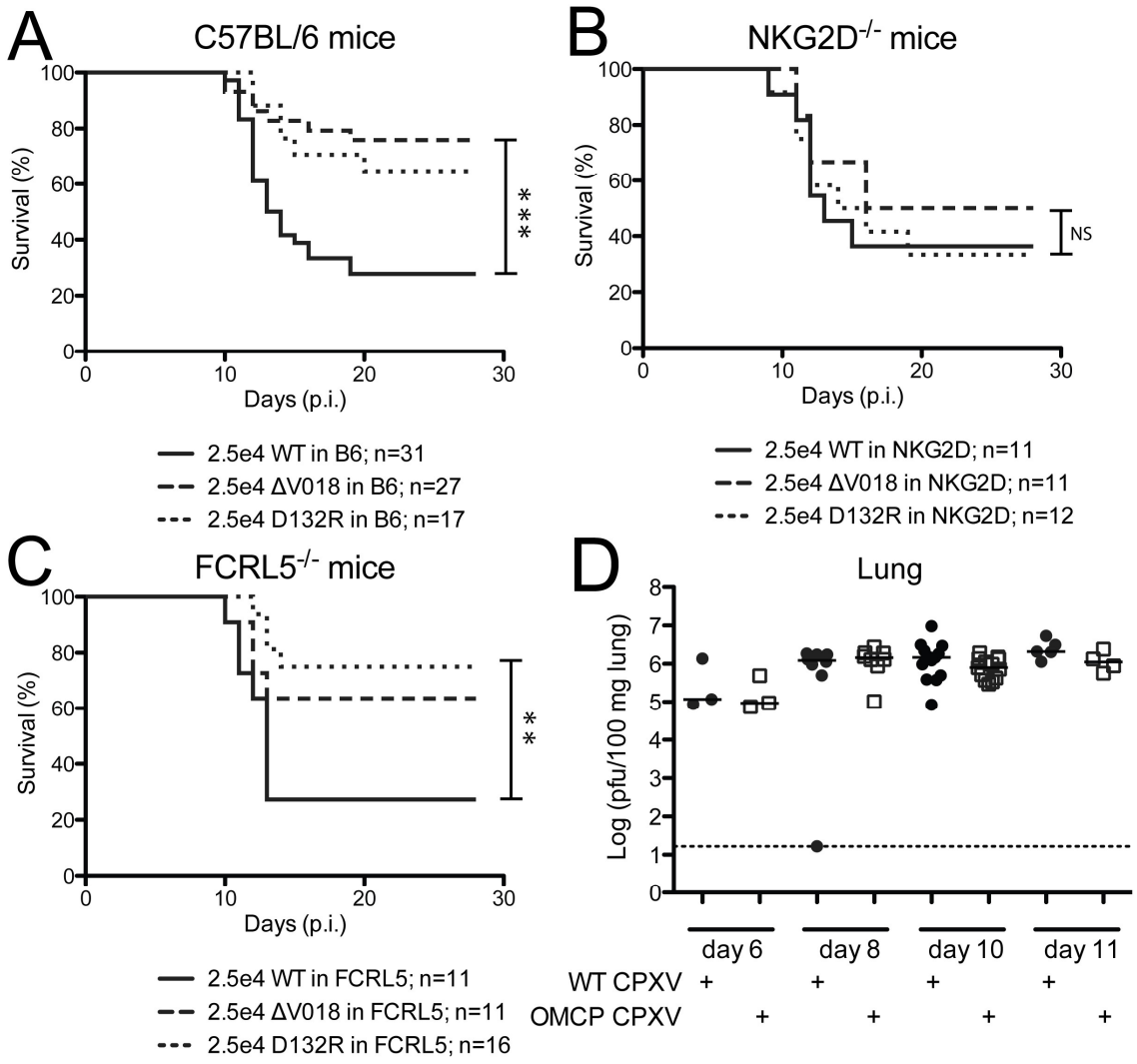

Figure 7: NKG2D mediates all of the virulence of OMCP during intranasal CPXV infection.

WT CPXV (solid line), ΔV018 CPXV (dashed line) and D132R OMCP CPXV (dotted line) infected via the intranasal route differentially influence survival in **(A)** WT B6, **(B)** NKG2D-deficient, and **(C)** FCRL5-deficient mice. Kaplan-Meier analysis shows survival of female mice following intranasal infection with $2.5x10^4$ pfu of the designated CPXV

strain. The data are aggregated from two to four independent experiments. The Log-rank (Mantel-Cox) test was used in the comparison of all Kaplan Meier survival curves. NS not significant, **p<0.01 ***p<0.001 **(D)** Female WT B6 mice were infected intranasally with $2.5x10^4$ pfu of WT or ΔV018 CPXV. Lungs were harvested on the indicated day post infection and tittered by standard plaque assay on BSC-1 cells. Line represents the median value.

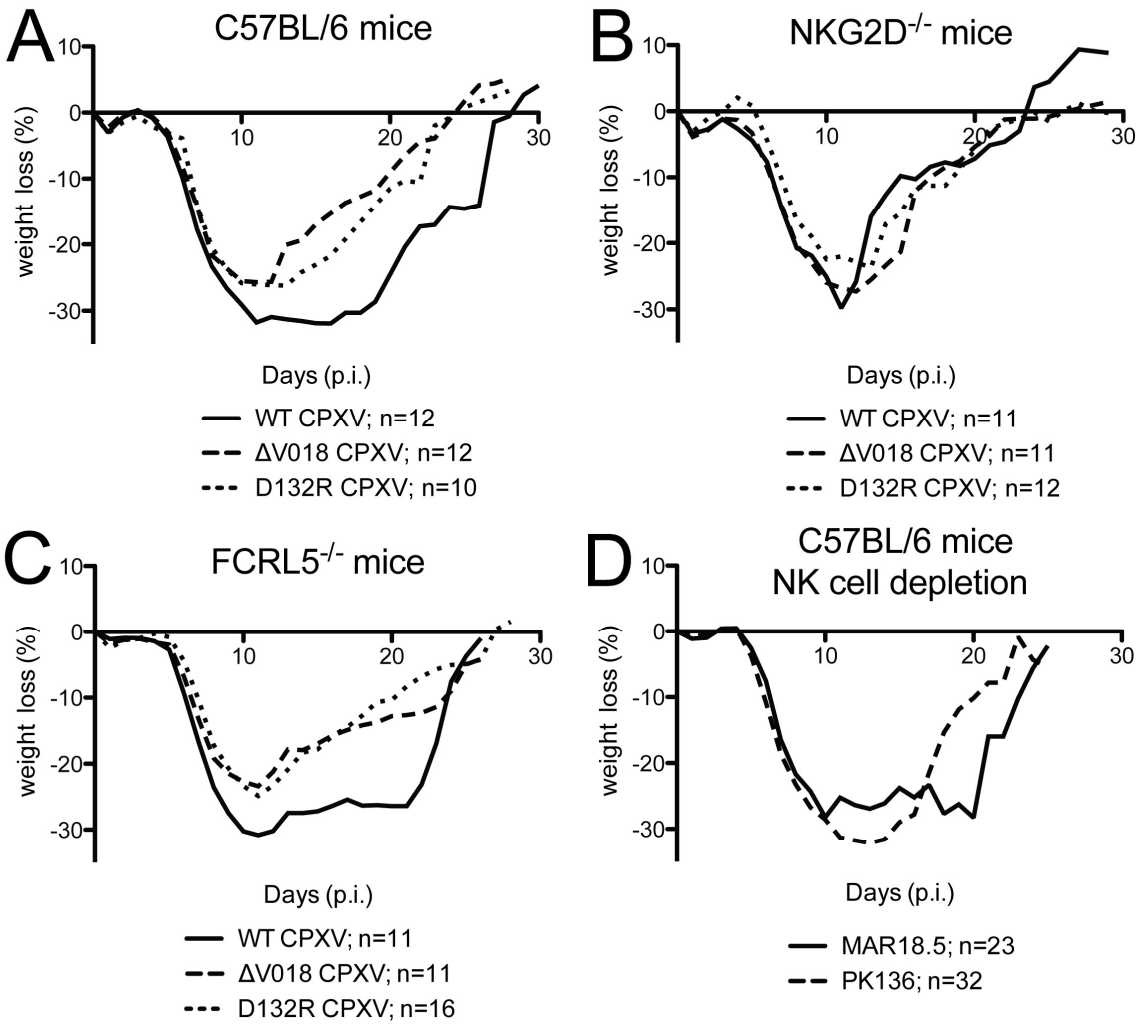

Figure 8: Mice infected with WT CPXV intranasally lose more weight and regain weight slower than mice infected with the less virulent ΔV018 CPXV or D132R CPX .

(A) WT B6, **(B)** NKG2D-deficient, and **(C)** FCRL5-deficient mice were intranasally infected with $2.5x10^4$ pfu of WT CPXV (solid line)**,** ΔV018 CPXV (dashed line) and D132R CPXV (dotted line) and weighed daily. Weights were plotted as percent of initial body mass. The data are aggregated from two to three independent experiments with

4-10 mice per group. **(D)** Weights of WT mice infected with WT CPXV ($2x10^4$ pfu/mouse) depleted of NK cells (PK136) or injected with an isotype control Ab (MAR18.5) on day 8 p.i. were monitored over the course of infection. The data are aggregated from 2 independent experiments with 8-16 mice per group.

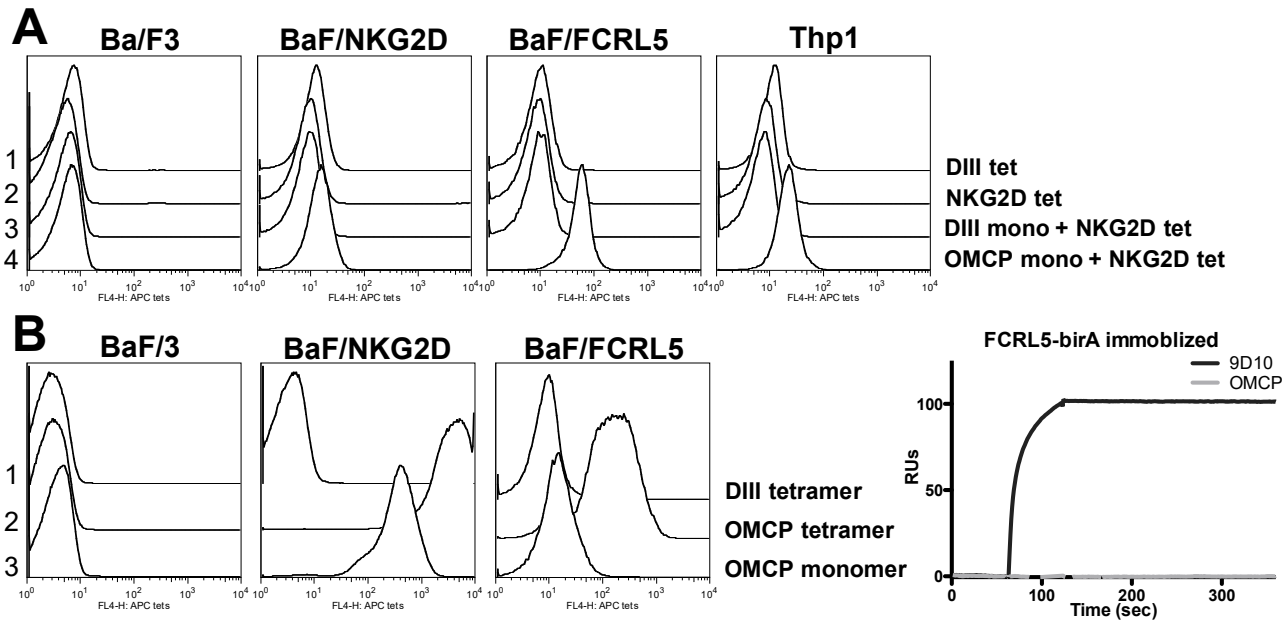

Figure 9: Low affinity binding of OMCP to FCRL5 can be overcome by multimerization with NKG2D on NK cells

(A) Untransduced parental Ba/F3 cells and cells transduced to express the murine NKG2D receptor and murine FCRL5 receptor, as well as a human Thp1 monocyte cell line were used to test OMCP binding in the presence of human NKG2D. Cells were stained with either APC labeled control DIII tetramer (line 1), APC labeled human NKG2D tetramer (line 2), APC labeled human NKG2D tetramer preincubated with DIII control (line 3) or APC labeled human NKG2D tetramer preincubated with OMCP (line 4). Representative results from two independent experiments. **(B)** Parental Ba/F3 cells and cells transduced with the murine NKG2D and murine FCRL5 receptor were tested for binding to APC labeled DIII control (line 1), fluorescent APC labeled OMCP tetramers (line 2) or A647 labeled OMCP monomers (line 3). Representative results

from two independent experiments. **(C)** Purified OMCP monomer or an anti-FCRL5 conformational antibody (9D10) were injected over flow cells containing immobilized murine FCRL5. Binding is detected as an increase in signal.

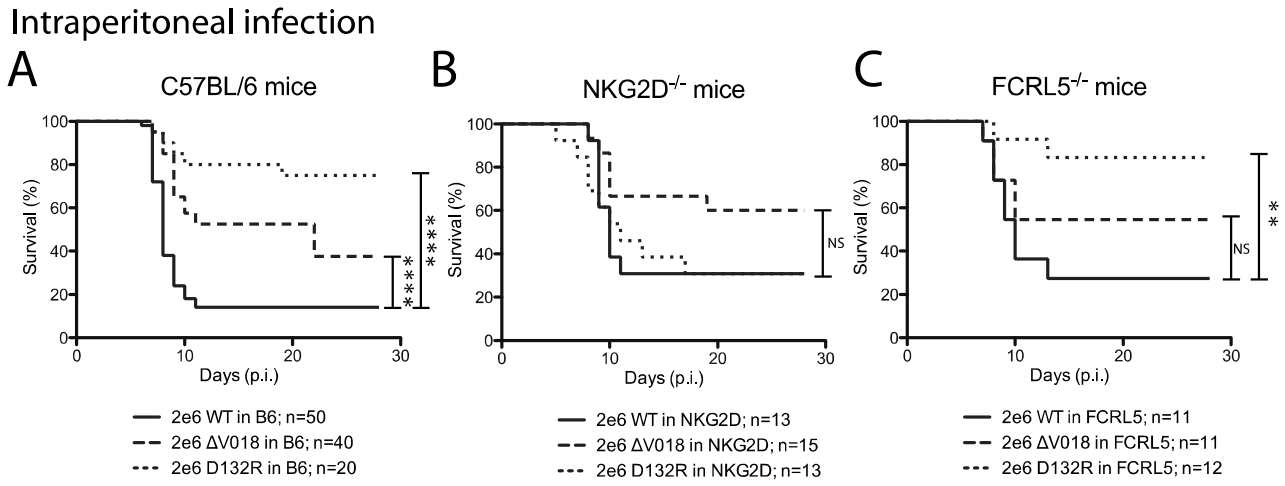

Figure 10: NKG2D binding accounts for the majority of OMCP's virulence during intraperitoneal infection.

WT CPX (solid line), ΔV018 CPX (dashed line) and D132R expressing CPX (dotted line) infected via the intraperitoneal route differentially impact survival in **(A)** WT B6, **(B)** NKG2D-deficeint, and **(C)** FCRL5-deficient mice. Kaplan-Meier analysis shows survival of female mice following intraperitoneal infection with $2x10^6$ pfu of the designated CPX strain. Data are aggregated from three to five independent experiments with 4-10 mice per group. The Log-rank (Mantel-Cox) test was used in the comparison of all Kaplan Meier survival curves. NS not significant, **p<0.01, ****p<0.0001

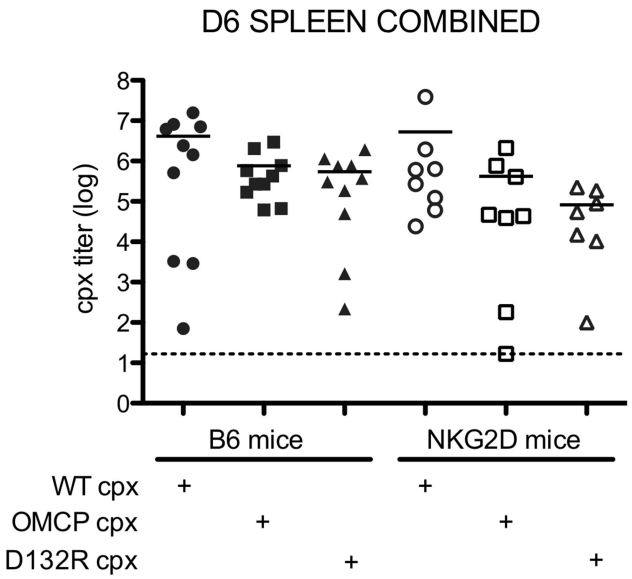
D6 SPLEEN COMBINED
cpx titer (log)
0
1
2
3
4
5
6
7
8
B6 mice
NKG2D mice
WT cpx + +
OMCP cpx + +
D132R cpx + +

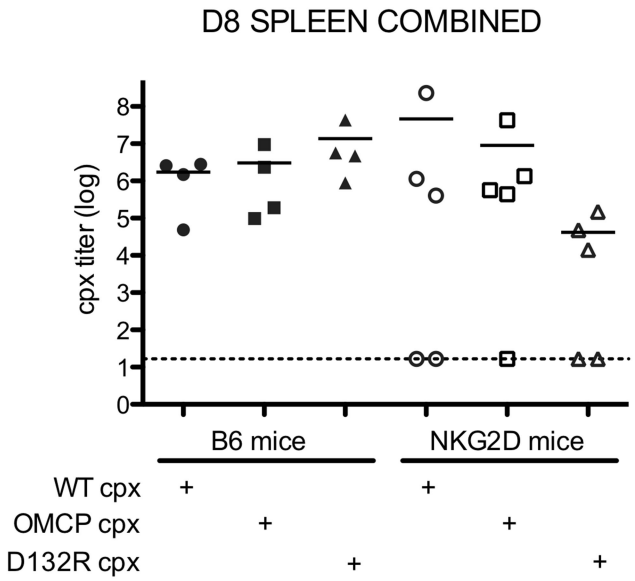
D8 SPLEEN COMBINED
cpx titer (log)
0
1
2
3
4
5
6
7
8
B6 mice
NKG2D mice
WT cpx + +
OMCP cpx + +
D132R cpx + +

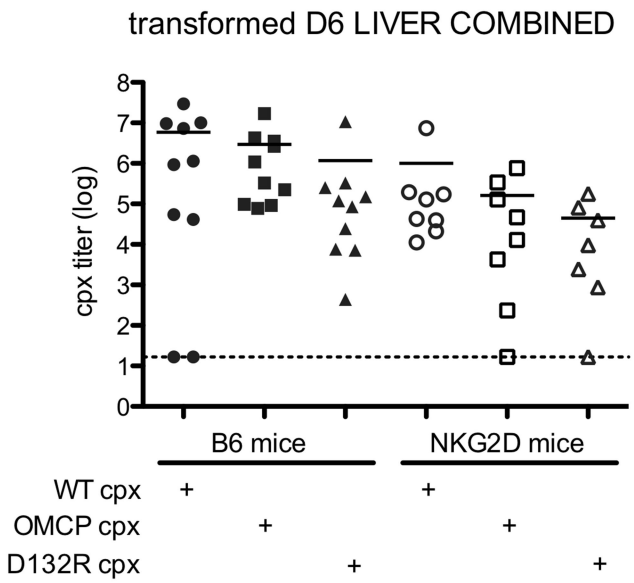
transformed D6 LIVER COMBINED
cpx titer (log)
0
1
2
3
4
5
6
7
8
B6 mice
NKG2D mice
WT cpx + +
OMCP cpx + +
D132R cpx + +

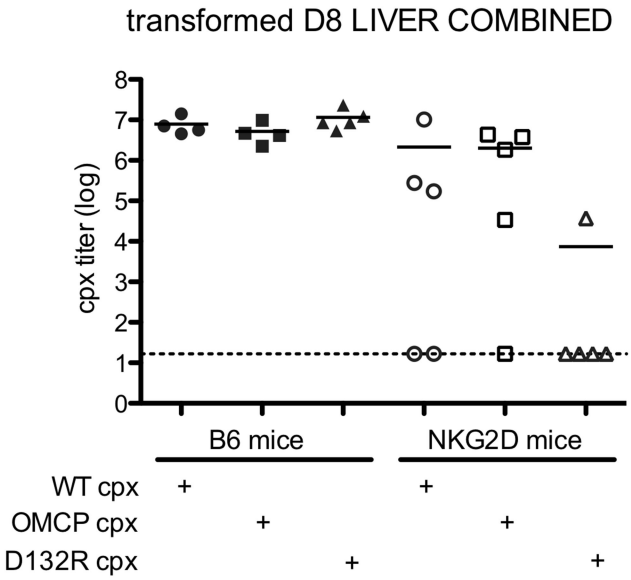
transformed D8 LIVER COMBINED
cpx titer (log)
0
1
2
3
4
5
6
7
8
B6 mice
NKG2D mice
WT cpx + +
OMCP cpx + +
D132R cpx + +

Figure 11: Splenic viral titers during CPX infection in intraperitoneally infected mice.

Female WT B6 mice (black) or NKG2D mice (white) were infected with $2x10^6$ pfu of WT CPX (circles), ΔV018 CPX (squares), or D132R CPX (triangles). Spleens were harvested on day 6 p.i., and titered by standard plaque assay on BSC-1 cells. Line represents the median value. Data are aggregated from four independent experiments with 4-5 mice per group.

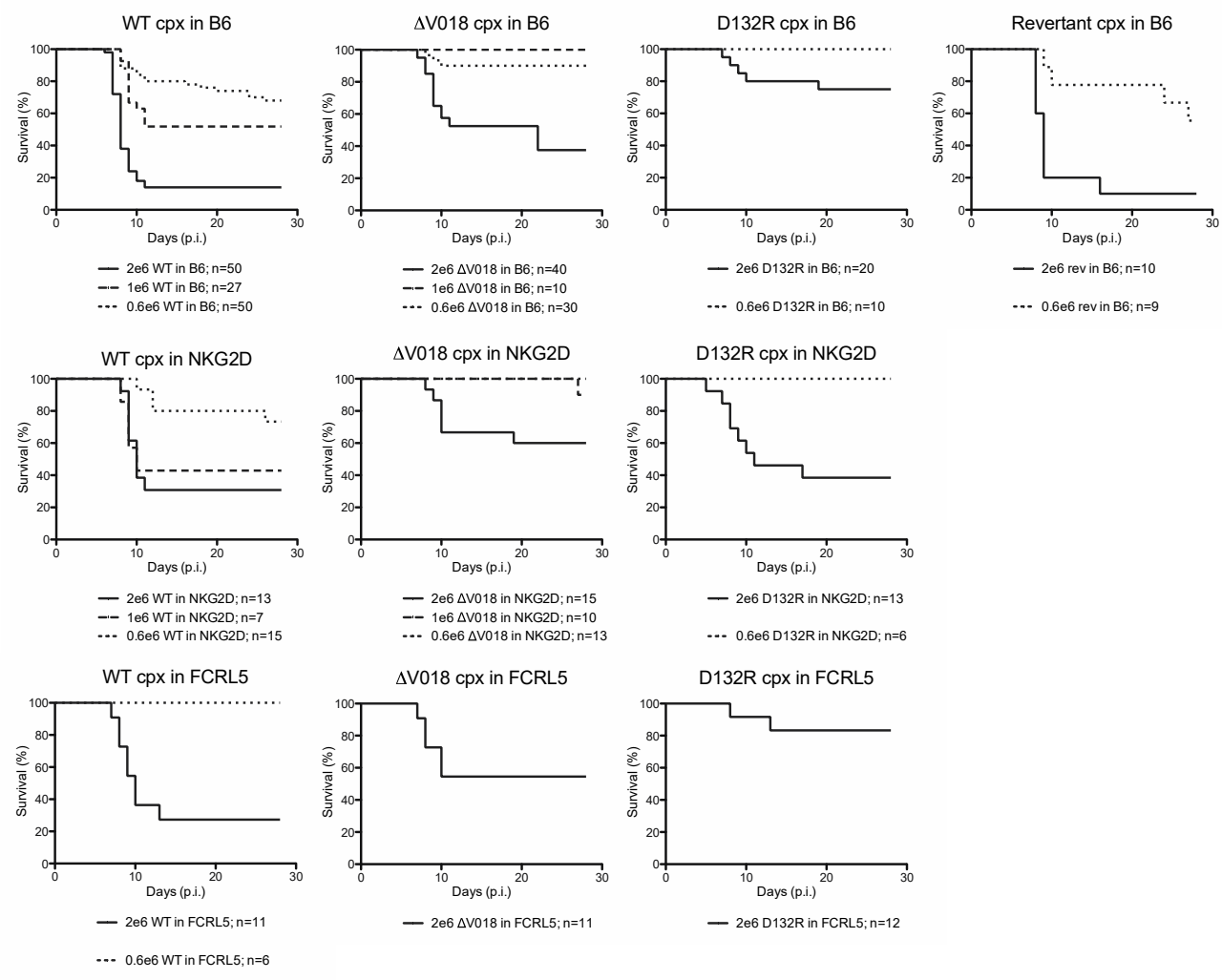

Figure 12: Intraperitoneal survival curves at 3 doses.

WT CPX**,** ΔV018 CPX, D132R expressing CPX, or revertant CPX infected via the intraperitoneal route differentially impact survival in WT B6, NKG2D-deficeint, and FCRL5-deficient mice. Kaplan-Meier analysis shows survival of female mice following intraperitoneal infection with 0.6 x10^6 pfu (dotted line), 1 x10^6 pfu (dashed line), or 2x10^6 pfu (solid line) of the designated CPX strain. Data are aggregated from greater than 10 independent experiments with 4-10 mice per group.

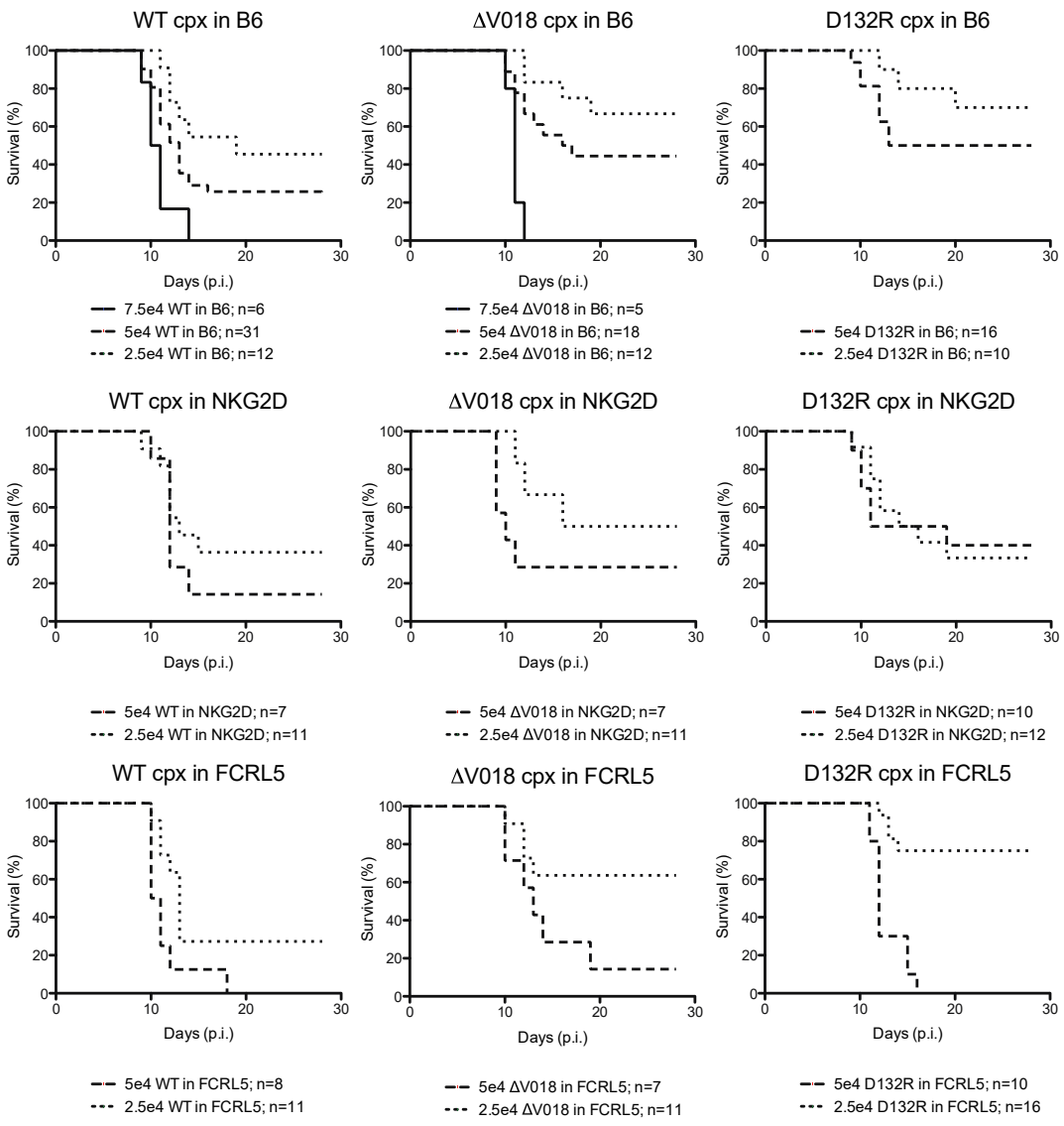

Figure 13: Intranasal survival curves at 2-3 doses.

WT CPX**,** ΔV018 CPX, D132R expressing CPX, or revertant CPX infected via the intranasal route differentially impact survival in WT B6, NKG2D-deficeint, and FCRL5-deficient mice. Kaplan-Meier analysis shows survival of female mice following intranasal infection with 2.5 x10^4 pfu (dotted line), 5 x10^4 pfu (dashed line), or 7.5 x10^4 pfu (solid line) of the designated CPX strain. Data are aggregated from greater than 10 independent experiments with 4-10 mice per group

CHAPTER 3: Assessment of OMCP crosslinking

Introduction:

OMCP blocked with recombinant NKG2D does not bind NK cells but retains the ability to bind to B cells and macrophages [4], suggesting that OMCP binds to NKG2D and the other receptors via distinct binding sites on separate interfaces. This observation raised the hypothesis that OMCP may act during viral infection to link NK cells and B cells or macrophages together via simultaneous binding to these independent receptors. If this is the case, it may be possible that OMCP serves to divert NK cell lysis away from CPX infected cells (that are actively secreting OMCP to protect infected cells from NKG2D recognition), and redirect NK cell lysis towards innate B cells or macrophages that constitutively express an OMCP binding receptor. We wished to address whether OMCP held on a cell surface by FCRL5 or a macrophage receptor would act as a pseudo-NKG2D stress ligand and be sufficient to activate NKG2D mediated NK cell killing.

During a typical viral infection, infected cells experience “cellular stress,” resulting in induction of a number of MHC class I like surface glycoproteins (MICA, MICB, ULBP family, and Rae1 family in humans; H60, Mult1, and Rae1 family in mice [45]). NK cells expressing the NKG2D receptor use this as a surveillance mechanism to identify cells that have been perturbed by pathogen infection, tumorigenesis, heat shock, or similar stresses. Engagement of NKG2D by stress ligands on virally infected cells results in subsequent killing of these target cells. We have previously determined that soluble

OMCP blocks NKG2D mediated killing because soluble monomeric OMCP is unable to crosslink and activate NKG2D. We now wished to test whether immobilized OMCP held on a cell surface is sufficient to induce NKG2D signaling and stimulate NK cell killing (Fig 14). Yac-1 targets, a murine T cell lymphoma line highly sensitive to NK cell killing due to low or no surface expression of MHC class I, were used as a positive control in all assays. Surface bound OMCP was expressed using an OMCP-Thy1.1 fusion, but similar surface presentation of OMCP *in vivo* could be envisioned for a cell presenting OMCP bound via the surface receptors FCRL5 or FcγRI. Our experiment demonstrated that Ba/F3 cells that had OMCP presented on the cell surface were killed to a comparable extent as cells expressing the canonical NKG2D ligands Mult1 and Rae1δ (Fig 14). This gave support that redirected NK cell lysis towards OMCP presenting cells is possible. A series of NK cell killing assays were performed to further test this hypothesis.

Experimental Methods:

In vitro Killing Assay

NK cell effectors: Splenocytes were harvested from naïve B6 mouse, and incubated in 200 U IL-2 overnight to activate NK cells for effective killing. Splenocytes were washed with R10 x2, counted, resuspended at $2x10^7$ c/mL, and plated with target cells at defined E:T ratios.

PBMC effectors: Fresh blood is drawn from a healthy donor the day of the experiment. Blood is diluted 1:1 with room temperature HBSS. The blood/HBSS mixture is added

slowly over a ficoll layer at a 2:1 blood mix:ficoll ratio. The cells are spun over a ficoll gradient at 2500 rpm for 30 min at 25^{o}C with no brake. The mononuclear cell layer is isolated and washed with R10 x2. Cells are counted, then resuspended at 2x10^{7} c/mL and plated with target cells.

Target cells: Ba/F3 or Yac-1 target cells are CFSE labeled fresh the day of the experiment. Cells are washed and resuspended in PBS at 3 x10^{6} c/ml. 0.5 uM CFSE diluted in PBS is added in a 1:1 ratio, and cells are incubated at 37^{o}C for 8 min. The Cells are then washed with R10 and incubated with fresh R10 at 37^{o}C for 20 min. Target cells are then counted, resuspended at 5x10^{5} c/mL and plated with target cells at defined E:T ratios.

Targets and effectors are plated at E:T ratios of 10:1, 20:1, and 40:1 in triplicate in 96 well plates. Cells are incubated at 37^{o}C, 5% CO_2 for 4 hours. Cells are then harvested and killing percentage determined by flow cytometry with the dead cell exclusion dye 7AAD. 7AAD is a fluorescent cell viability stain that intercalates into dsDNA, but does not readily pass intact cell membranes. Dead cells stain positive for 7AAD

Killing is analyzed by gating on CFSE+ target cells and determining percent of 7AAD+ (killed) targets. Values are normalized to the percentage of dead cells at baseline in target only control wells. Percent killed is calculated as = (% dead with splenocytes - % dead at baseline) / (% live at baseline)

OMCP incubations: Killing assays testing OMCP killing were performed in several ways. 1.) Effector cells (splenocytes or PBMCs) were incubated with 20 ug OMCP monomer at 37^{o}C for 30 min prior to plating. Cells were then washed x1 with R10, counted, and plated with target cells that were not preincubated with OMCP. 2.) Target cells were incubated with 20 ug OMCP monomer at 37^{o}C for 30 min. Cells were then washed x1 with R10, counted, and plated with effector cells that were not preincubated with OMCP. 3.) Both Effector cells and Target cells were incubated with 20 ug OMCP monomer, and cells were counted and plated together. 4.) Effector cells and Target cells were not preincubated with OMCP, but rather plated normally, then free OMCP monomer was added to the media prior to the full 4 hour incubation. Serial dilutions of 10 ug, 5 ug, 2.5ug, 1.25ug, 0.625ug, 0.3125ug, 0.156ug, and 0.78ug OMCP were added to the effector and target cell wells. All experiments were performed at E:T ratios of 10:1, 20:1, and 40:1 in triplicate, with the exception of the serial dilutions of free OMCP, which were performed at 20:1 in triplicate.

Combined CD107a and IFNγ Degranulation Assay

Splenocytes are harvested, washed, counted, and plated in wells of a 24 well plate. 10 ug, 5 ug, or 2.5 ug of monomeric or tetrameric OMCP is added to the media, or no protein control. Cells stimulated with plate bound anti-NK1.1, plate bound anti-NKG2D, or a cytokine cocktail (10 ng/mL IL-12, 50 ng/mL IL-18, 10 ng/mL IL-15) were included as positive controls. A647-CD107a antibody is added to each well, and cells are incubated for 1 hour at 37^{o}C, 5% CO_2. After 1 hour, Golgiplug and GolgiStop (monensin and brefeldin A) are added to each well, and the cells are incubated for a further 6 hours

at 37^{o}C 5% CO_2. Cells are then harvested and stained for additional cell surface markers, incubate 30 min at 4^{o}C in the dark. Intracellular staining for IFNγ is performed using BD CytoFix/CytoPerm solution with 2uL of PE-IFNγ per sample. Cells are then analyzed by flow cytometry for intensity of A647-CD107a and PE-IFNγ.

Results:

Multimeric OMCP is not sufficient to activate NK cells through NKG2D

Our proposed OMCP bridging and NK cell redirecting hypothesis would require OMCP to sufficiently activate NK cells through the NKG2D receptor to trigger NK cell mediated killing. We have previously shown that soluble monomeric OMCP does not cause NKG2D receptor downregulation or activation, and rather soluble monomeric OMCP binding to the NKG2D receptor is inhibitory. Here, we sought to test whether multimeric OMCP is sufficient for activation through NKG2D. NK cells were enriched using Miltenyi negative selection kits and incubated with either monomeric OMCP or tetrameric OMCP for 7 hours (initial 1 hour incubation, then 6 hours after addition of monensin & brefeldin A). Cells stimulated with plate bound anti-NK1.1, plate bound anti-NKG2D, or a cytokine cocktail (10 ng/mL IL-12, 50 ng/mL IL-18, 10 ng/mL IL-15) were included as controls. We did not observe any activation of NK cells using tetrameric OMCP, as determined by IFNγ or CD107a staining (Fig 15). Additionally, there was no upregulation of the activation markers CD69 or CD71 using multimeric OMCP (data not shown). These results suggest that soluble tetrameric OMCP is not sufficient to cluster NKG2D and activate NK cells *in vitro*, however it remained possible that OMCP on a cell surface may allow enough crosslinking for signaling.

NK cell Killing Assays

We developed a killing assay to further test the possibility of OMCP acting as a bridging ligand to activate NKG2D. Splenocytes harvested from naïve B6 mice were incubated overnight in 1000 U/mL IL-2 to prime NK cells for more effective killing. Ba/F3 transgenic targets or Yac-1 positive controls were then CFSE labeled, and incubated with IL-2 activated splenocytes for 4 hours at several E:T ratios (40:1, 20:1, 10:1). Cells were harvested after 4 hours, and dead cells identified with 7AAD cell viability stain to determine percentage of target cells killed. Untransduced Ba/F3 targets were used as a negative control. Control experiments were performed to confirm that soluble OMCP can block killing of BaF/Mult1 in this system, as was previously established.

A series of experiments were performed to assess the possibility of OMCP bridging between NKG2D and FCRL5 receptors. For these killing assays, OMCP was titrated in an attempt to achieve optimal effect. Too little protein would have no effect, whereas too much protein would saturate both the NKG2D and FCRL5 receptors, preventing crosslinking. Therefore we expected that a bridging effect resulting in increased target killing would be seen at some optimal concentration of OMCP. A range of protein concentrations were tested for each experiment to accommodate this fact. Additionally, scenarios were tested in which only NK effectors were preincubated with OMCP, only FCRL5 expressing targets were preincubated with OMCP, or both effectors and targets were preincubated with OMCP to identify any combination that would allow us to see increased killing in the presence of OMCP.

OMCP does not redirect killing towards FCRL5 expressing targets

Killing assays were performed with two independent BaF/FCRL5 transductants (Fig 16 and 17), a C1498/FCRL5 transductant (data not shown), and the WEHI231 cell line (Fig 18). Assays with each cell line were performed 1-2 times, with two independently produced lots of OMCP protein. In all cases, addition of OMCP did not result in increased killing at any of the tested doses (Fig 16, 18). If anything, there is a slight downward trend in killing at high OMCP concentrations, suggesting that OMCP is functioning only as a high affinity inhibitor of NKG2D. Despite extensive investigation, these results provide no clear evidence to support the hypothesis that OMCP functions by "bridging" $NKG2D^+$ NK cells and $FCRL5^+$ B cells thereby facilitating NK cell killing.

OMCP does not redirect killing towards mouse BMDMs

All experiments thus far have suggested that OMCP does not crosslink NK cells and B cells to result in activation and redirected lysis of B cells by NK cells. Subsequent assays were performed to test the possibility of OMCP crosslinking of NKG2D and the putative macrophage receptor. Our initial experiment used primary bone marrow derived macrophages (BMDMs) obtained through long term culture of WT bone marrow cells in M-CSF. BMDMs have previously been shown to bind to OMCP tetramers in the unstimulated state. We incubated WT BMDM targets with IL-2 activated splenocyte effectors, however our assay showed no evidence of receptor bridging (Fig 19). In fact, BMDMs appeared to be highly resistant to killing. It may be possible that other macrophage or monocyte subtypes would be more optimal for these killing assays.

Further experiments using primary mouse macrophage or human monocyte derived macrophage targets can also be performed to confirm these findings.

Future Experiments:

The most likely reasons we were not able to see OMCP crosslinking of these separate receptors are due to low affinity binding or short half-lives of interaction. A bridging effect is only possible if OMCP binding to NKG2D and OMCP binding to FCRL5 or the macrophage receptor are both stable for long enough to allow bridging to occur followed by clustering of receptors and initiation of downstream activating signals. The OMCP-murine NKG2D interaction has a short half life on the order of seconds (k_{off} = 1.8 x 10^{-2} s^{-1}), while OMCP's interaction with human NKG2D has a strikingly longer half life on the order of minutes (k_{off} = 1.23 × 10^{-4} s^{-1}) [4]. Given this difference, we plan to repeat these bridging killing assays using human PBMCs and human monocyte targets.

We plan to use the Thp1 cell line as the human monocyte target. Thp1 is a human monocyte cell line derived from an acute monocytic leukemia patient. These cells have previously been shown to stain positive for OMCP tetramer binding, and were the cell line used in our immunoprecipitation pull-down approach to try to identify the OMCP binding receptor on macrophages and monocytes (Appendix 1).

Due to the magnitude of our experiment, we plan to use human PBMCs obtained from a leukocyte reduction system (LRS) chamber, rather than PBMCs from fresh blood as our effector cells. Leukocyte reduction is the removal of white blood cells from blood or

blood components used for blood transfusion. The leukocytes are separated by size using counterflow centrifugation elutriation and are trapped in the LRS chamber. These LRS cones are a source of viable human white blood cells that can be used in research applications. We will ficoll purify cells obtained from the LRS chambers, then freeze the cells with 10% DMSO in smaller aliquots for use.

In our killing assay, we will use CFSE labeled human Thp1 cells as targets and frozen human PBMCs from an LRS cone source as effectors. Effectors will not be preactivated. OMCP should have a higher binding affinity and longer half life with human NKG2D as compared to murine NKG2D. However, OMCP binding kinetics to the human or mouse macrophage receptor have not been determined. Our results will show if there is any effect of OMCP on Thp1 cell killing by human PBMC effectors under any of the conditions tested (effectors preincubated with OMCP, targets preincubated with OMCP, both effectors and targets preincubated with OMCP, and titration of OMCP directly in wells with effectors and targets).

Discussion:

We have extensively investigated the possibility of OMCP crosslinking of NKG2D bearing NK cells with FCRL5 expressing cells. Killing assays performed with two independent BaF/FCRL5 transductants, a C1498/FCRL5 transductant, and the WEHI231 cell line targets did not show increased killing in the presence of soluble OMCP under any contition. Additionally, we did not see any evidence of increased killing with murine splenocytes against murine BMDMs. This might suggest that soluble

OMCP is not sufficient to crosslink NKG2D bearing cells and FCRL5 or macrophage receptor bearing cells.

However, we have yet to thoroughly test human PBMC effectors against human cell line targets. We might expect better success using human PBMCs, due to the higher affinity of human NKG2D for cowpox OMCP. We plan to investigate killing of human PBMCs against the Thp1 monocyte cell line first, as we consider it more likely that OMCP may be acting on monocytes in preference to FCRL5 bearing innate B cells.

The binding affinities and kinetics of OMCP-FCRL5 and the unidentified macrophage receptor have yet to be determined by SPR. Once these values are obtained, a theoretical half life for the bridged species can be calculated, and the feasibility of such a species occurring at high enough a density to result in clustering and crosslinking of the NKG2D receptor can be assessed. Given our lack of success in validating this hypothesis with killing assay data using murine splenocytes with an array of cell lines expressing FCRL5 or macrophage cell line targets, we suspect that crosslinking and activation of NK cells in this manner is unlikely *in vivo*. However, crosslinking of human NK cells has yet to be determined.

Alternatively, cell bound OMCP may not be sufficient to activate through the NKG2D receptor, but may be able to activate through FCRL5 or the macrophage receptor if those receptors have a lower threshold for activation. Similar experiments can be performed to look at receptor activation on macrophages using tetrameric OMCP, plate

bound OMCP, or BaF/OMCP-Thy1.1 to crosslink receptors on macrophages. We can also incubate BaF/OMCP-Thy1.1 cells with receptor expressing macrophages and assay for phagocytic and ADCC activity against BaF/OMCP-Thy1.1 targets. Finally, NKG2D expressing NK cells could be incubated with BMDMs in a range of OMCP concentrations similar to the previous experiment, instead assaying for phagocytosis of NK cell targets rather than NK cell mediated killing. Unfortunately similar experiments investigating FCRL5 activation will be complicated by the lack of knowledge of FCRL5's endogenous function. Although the hypothesis of macrophage or FCRL5 activation via OMCP binding is possible, it suffers from the same requirement for the sustained existence of an NKG2D-OMCP-macrophage receptor bridged species that may be only present transiently *in vivo*.

Figures:

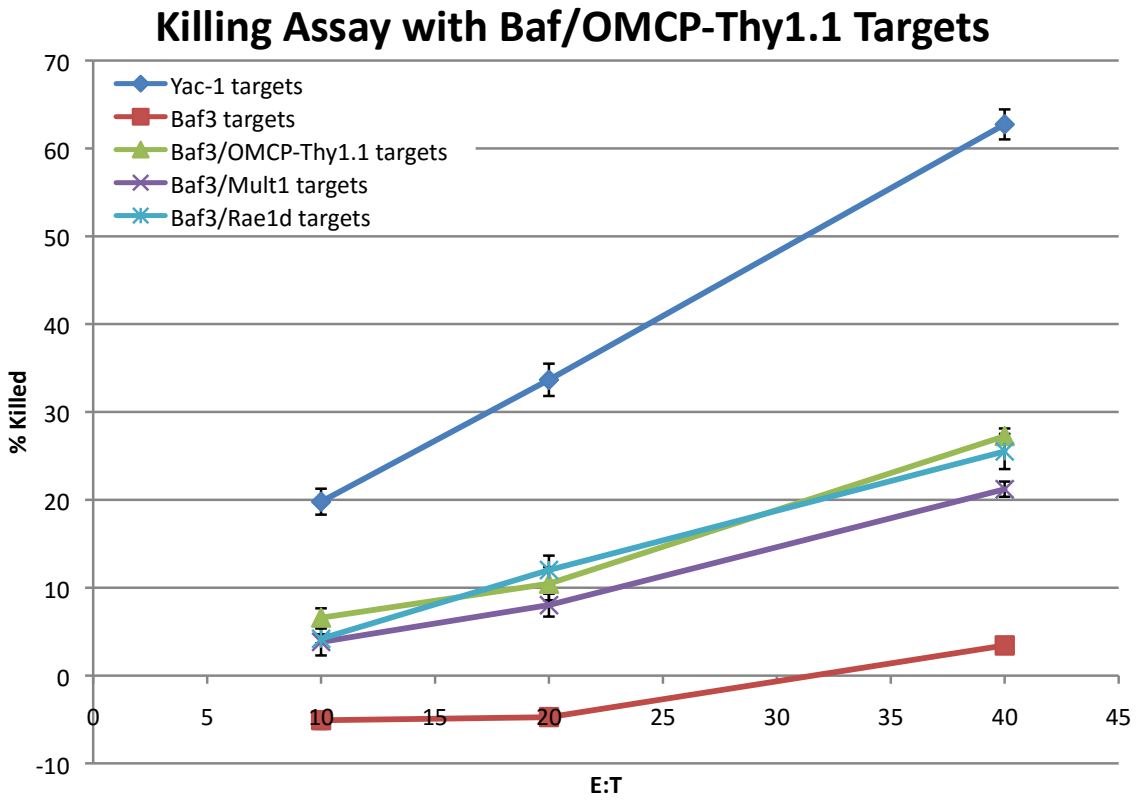

Figure 14: Cell surface OMCP is sufficient to crosslink NKG2D and stimulate NK cell killing.

Splenocytes harvested from naïve B6 mice were incubated in 1000 U/mL IL-2 overnight to activate NK cells for effective killing. Yac-1 or Ba/F3 transgenic targets were CFSE labeled and incubated with IL-2 activated splenocytes at 10:1, 20:1, and 40:1 effector:target ratios for 4 hours at 37^{o}C, 5% CO_2. Cells were harvested after 4 hours and percentage of CFSE+ dead cells identified using 7AAD cell viability stain. Yac-1 targets are a positive control; untransduced Ba/F3 targets are negative control. Note that BaF/OMCP-Thy1.1 cells show comparable killing to BaF/Rae1δ and BaF/Mult1 cells that express known NKG2D ligands on the surface.

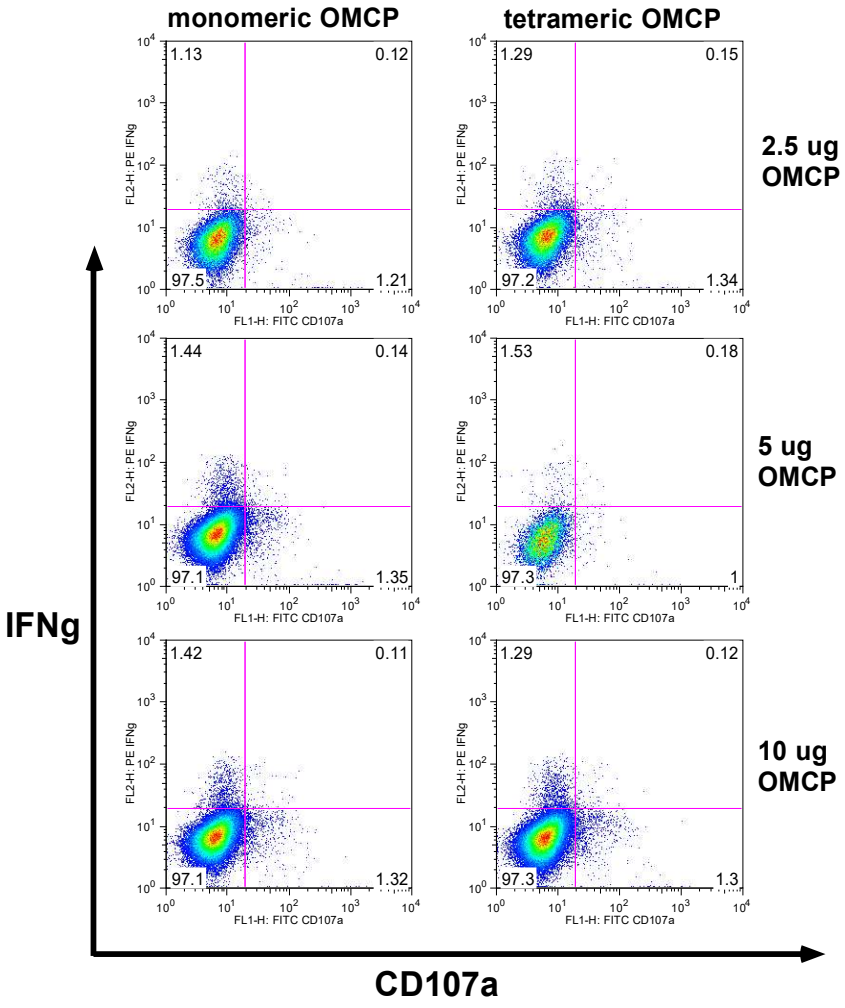

Figure 15: Tetrameric OMCP is not sufficient to activate NKG2D.

Negatively enriched NK cells were incubated with several doses of monomeric or tetrameric OMCP for 7 hours, with addition of golgiplug & golgistop after the first hour. Cells were stained for CD107a and intracellular IFNγ

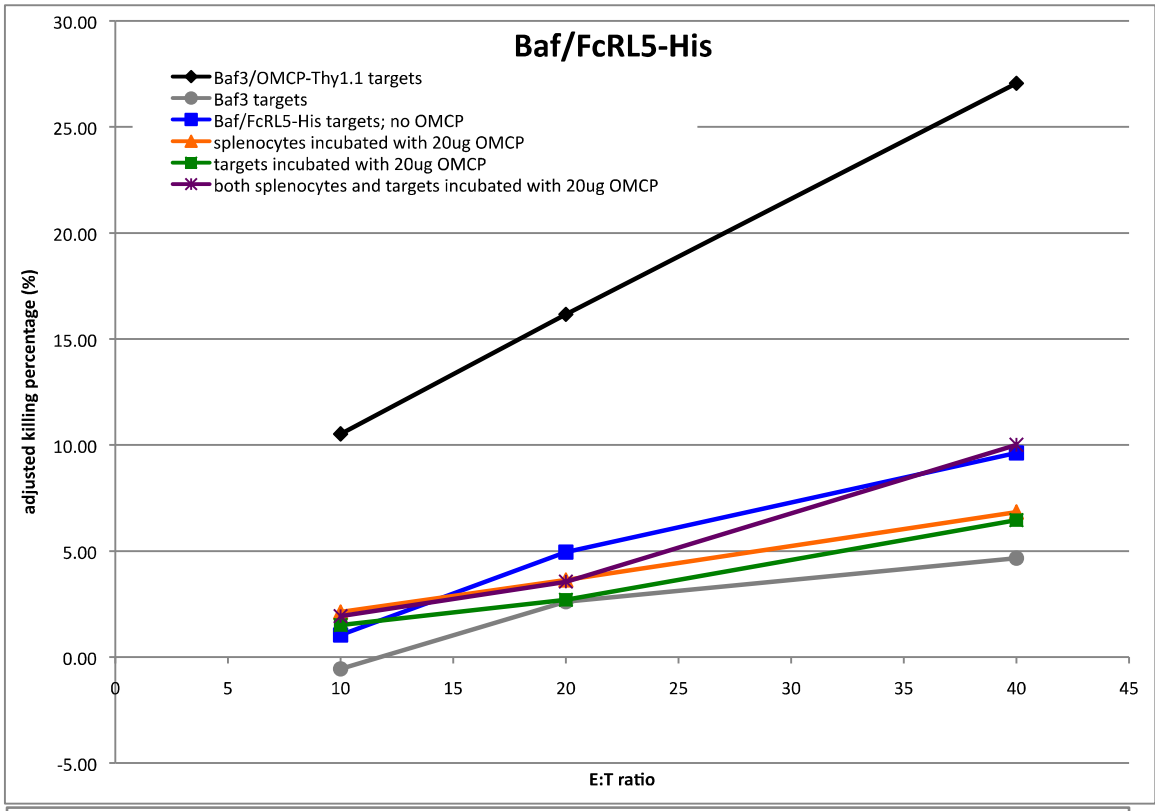
Baf/FcRL5-His
Baf3/OMCP-Thy1.1 targets
Baf3 targets
Baf/FcRL5-His targets; no OMCP
splenocytes incubated with 20ug OMCP
targets incubated with 20ug OMCP
both splenocytes and targets incubated with 20ug OMCP
adjusted killing percentage (%)
E:T ratio
30.00
25.00
20.00
15.00
10.00
5.00
0.00
-5.00
0
5
10
15
20
25
30
35
40
45

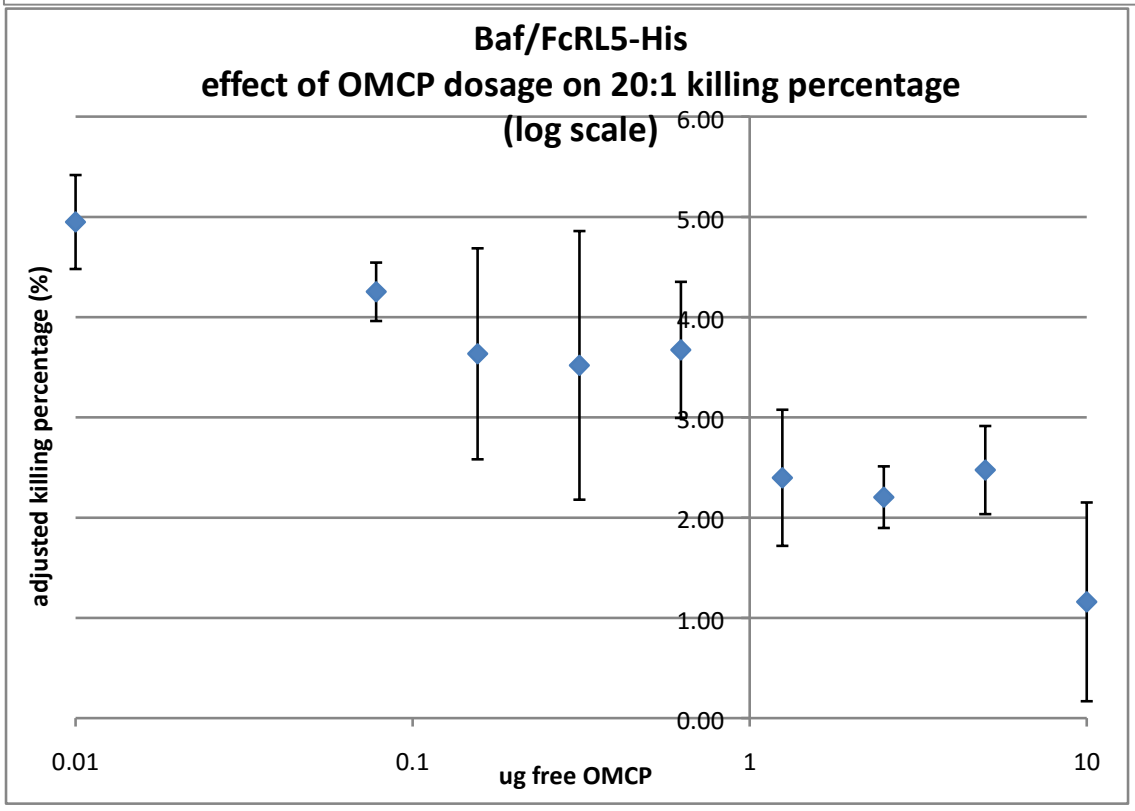
Baf/FcRL5-His
effect of OMCP dosage on 20:1 killing percentage
(log scale)
adjusted killing percentage (%)
ug free OMCP
6.00
5.00
4.00
3.00
2.00
1.00
0.00
0.01
0.1
1
10

Figure 16: Representative killing assay with BaF/FCRL5-His transductants.

Target cells, IL-2 activated splenocytes, or both were incubated with a saturating amount of OMCP (20ug), washed, then plated together for a 4 hour killing assay (top panel). Alternatively, known concentrations of OMCP (10ug to 0 ug) were titrated in with targets and splenocytes (bottom panel). At no dose of OMCP did we observe increased NK mediated killing. Killing assay with each cell line was performed 1-2 times with two batches of OMCP protein.

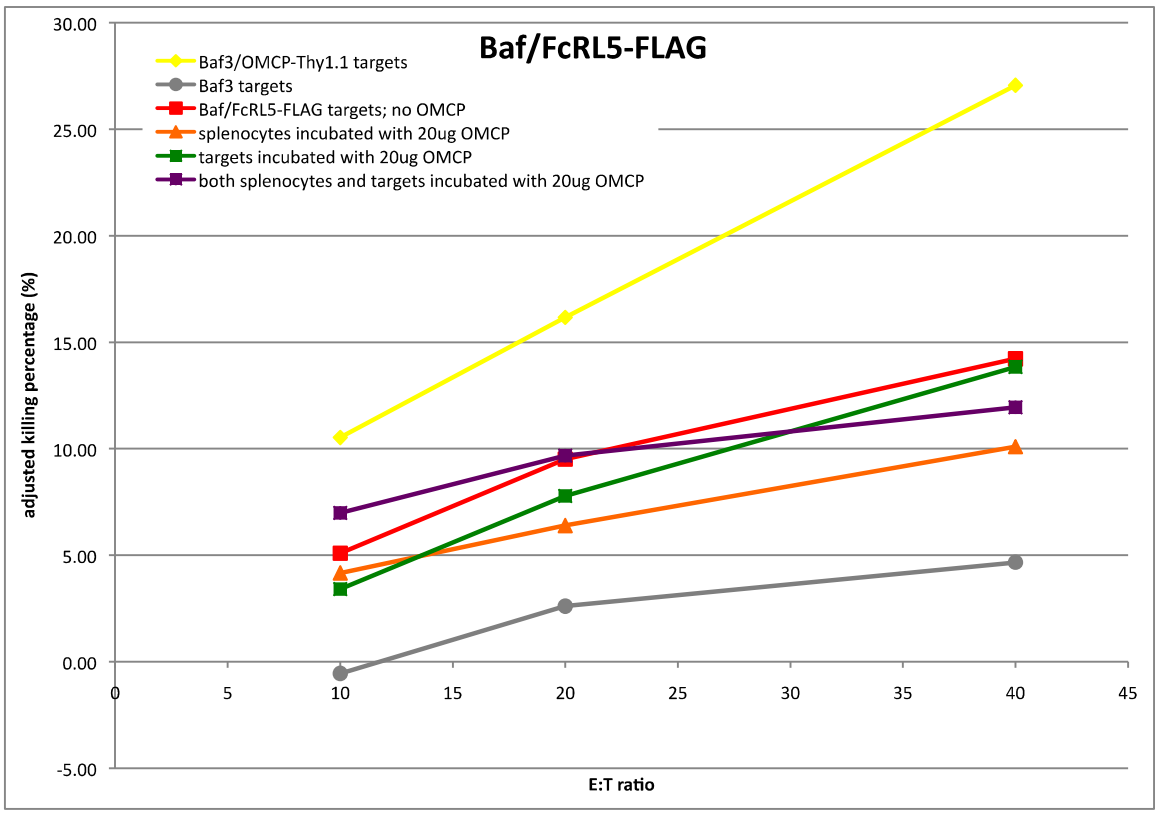

Figure 17: Representative killing assay with an independently generated BaF/FCRL5-FLAG transductant.

Target cells, IL-2 activated splenocytes, or both were incubated with a saturating amount of OMCP (20ug), washed, then plated together for a 4 hour killing assay (top panel). Alternatively, known concentrations of OMCP (10ug to 0 ug) were titrated in with targets and splenocytes (not shown). At no dose of OMCP did we observe increased NK mediated killing. Killing assay was performed once.

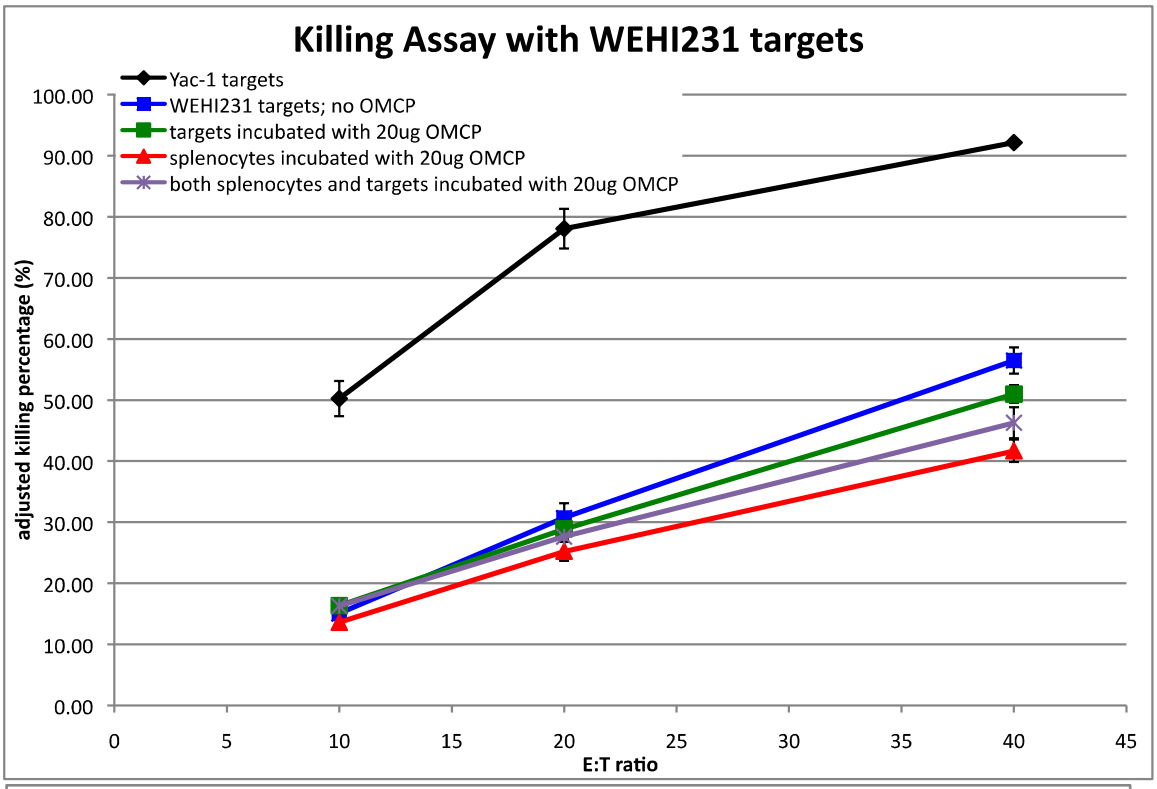
Killing Assay with WEHI231 targets
Yac-1 targets
WEHI231 targets; no OMCP
targets incubated with 20ug OMCP
splenocytes incubated with 20ug OMCP
both splenocytes and targets incubated with 20ug OMCP
adjusted killing percentage (%)
100.00
90.00
80.00
70.00
60.00
50.00
40.00
30.00
20.00
10.00
0.00
0
5
10
15
20
25
30
35
40
45
E:T ratio

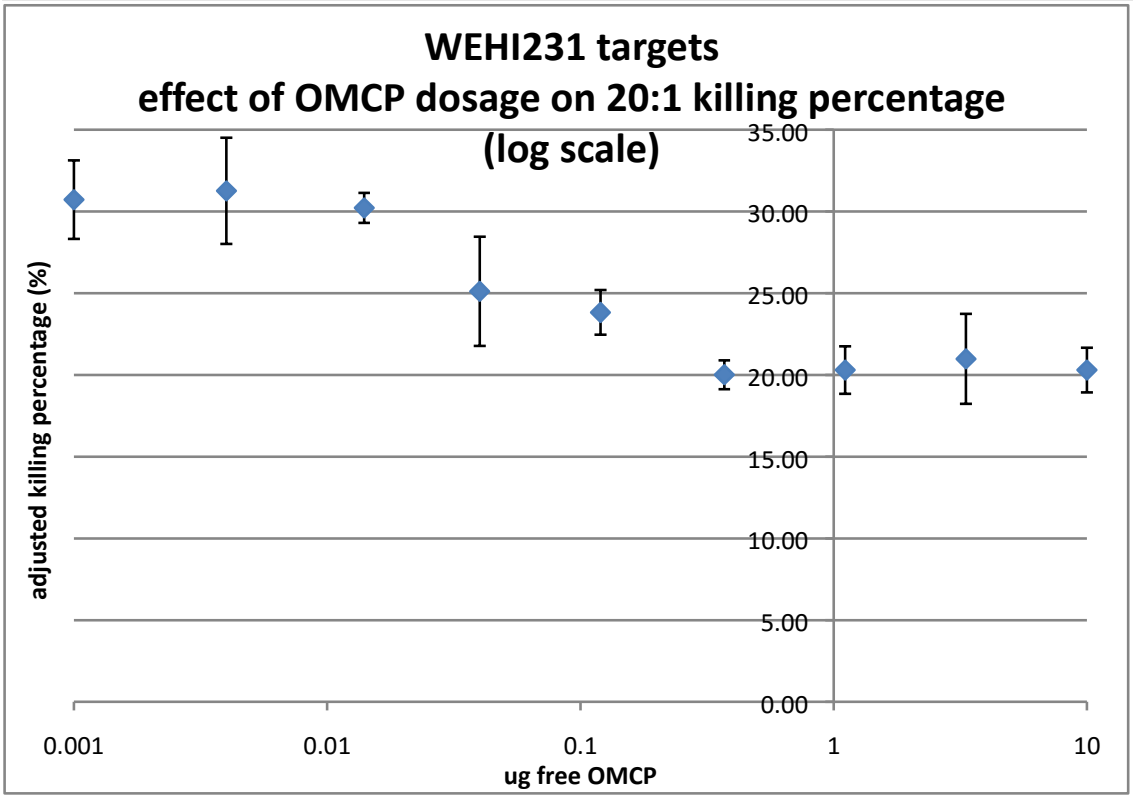
WEHI231 targets
effect of OMCP dosage on 20:1 killing percentage
(log scale)
adjusted killing percentage (%)
35.00
30.00
25.00
20.00
15.00
10.00
5.00
0.00
0.001
0.01
0.1
1
10
ug free OMCP

Figure 18: Representative killing assay with the OMCP binding, FCRL5 expressing WEHI231 cell line.

Target cells, IL-2 activated splenocytes, or both were incubated with a saturating amount of OMCP (20ug), washed, then plated together for a 4 hour killing assay (top panel). Alternatively, known concentrations of OMCP (10ug to 0 ug) were titrated in with targets and splenocytes (bottom panel). At no dose of OMCP did we observe increased NK mediated killing. Killing assay was performed 1-2 times with two batches of OMCP protein.

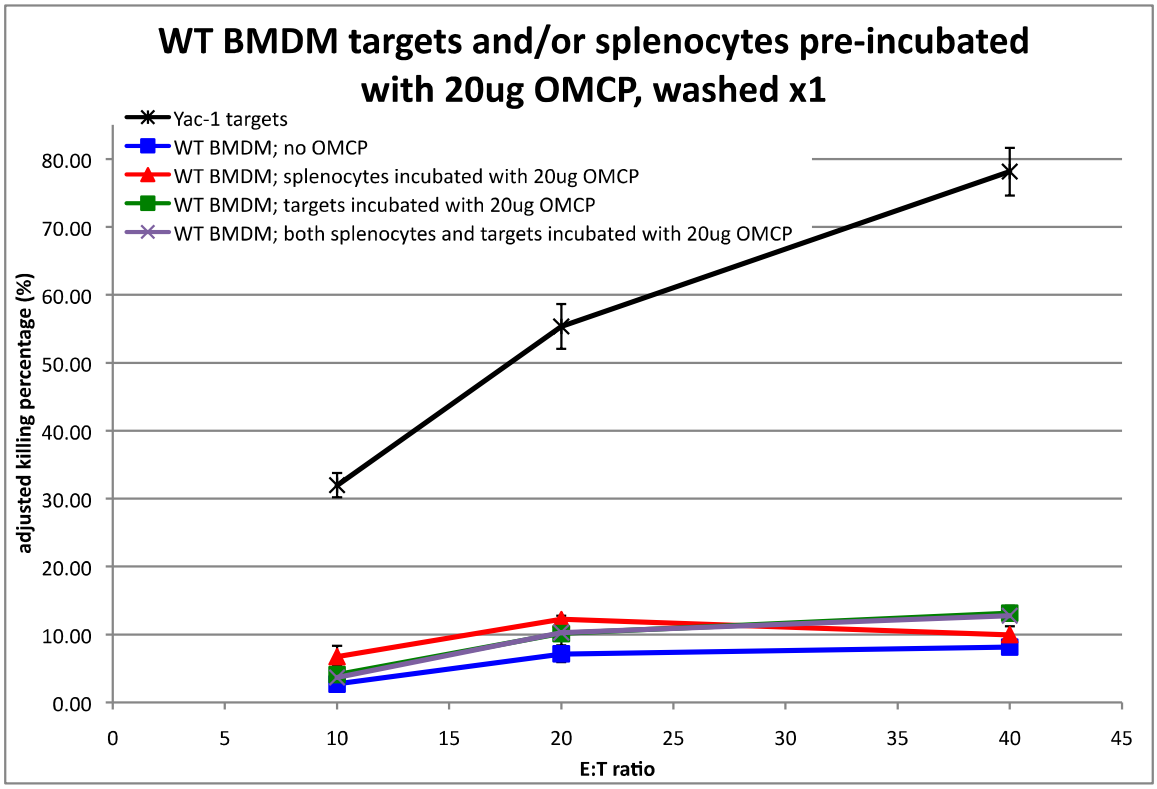

Figure 19: Representative killing assay with BMDMs cultured from WT B6 mouse bone marrow to test OMCP crosslinking of macrophage targets.

Target cells, IL-2 activated splenocytes, or both were incubated with a saturating amount of OMCP (20ug), washed, then plated together for a 4 hour killing assay. Alternatively, known concentrations of OMCP (10ug to 0 ug) were titrated in with targets and splenocytes (not shown). At no dose of OMCP did we observe increased NK mediated killing. Killing assay was performed once.

CHAPTER 4: Future Experiments

NKG2D binding activity

Previous work has clarified the role of OMCP on NKG2D expressing NK cells both *in vitro* [4], and *in vivo* (Sun M., manuscript submitted). Data indicating OMCP's importance as an NKG2D antagonist in the context of viral infection is conclusive, and work on this avenue is finalized.

FCRL5 binding activity

Despite extensive investigation, we have not identified a clear role for OMCP binding to the immune receptor FCRL5 on innate B cells. *In vivo* data indicates that FCRL5$^{-/-}$ mice respond identically to CPX infection as wildtype C57BL/6 mice via all routes of infection tested, suggesting that OMCP binding to FCRL5 is not crucial for survival, weight loss, or organ titers. Any effect of OMCP binding to FCRL5 is therefore likely to have minimal impact on CPX virulence. Additionally, FCRL5 is an orphan receptor, and its endogenous ligand is unknown. As such, the regulation and endogenous activity of this receptor is not clear. I therefore propose that follow-up of FCRL5 binding activity be postponed secondary to investigation of OMCP's macrophage binding activity, which may be more relevant biologically as well as easier to probe with assays on known macrophage functions.

It is possible that OMCP may also bind to FCRLA and FCRLB, intracellular FCRL family members that have three domains homologous to the domains responsible for OMCP

binding to FCRL5. However, we thought this was unlikely, since OMCP has been definitively shown to be secreted in large numbers from a virally infected cell, and is more likely to be acting on cell surface receptors of immune cells as they approach the infected cell. Additionally, due to the presence of the signal peptide, directing OMCP to the secretory pathway of the ER, OMCP produced within infected cells does not have an opportunity to interact with cytoplasmic receptors such as FCRLA and FCRLB. For these reasons, OMCP binding to intracellular FCRL family members was not evaluated. However, more extensive investigation of FCRL receptor binding may be pursued if desired.

Macrophage binding activity

Definitive identification of an OMCP binding receptor on macrophages has yet to be determined. Macrophages are an extremely important cell subset involved in many facets of innate immunity. Their primary roles include phagocytosis of pathogens, processing of antigen, and acting as specialized antigen presenting cells to stimulate T cells and other immune cells. In addition to their endocytic and phagocytotic activity, they are also responsible for producing oxidative bursts which create reactive oxygen or reactive nitrogen species to destroy pathogens directly. Furthermore, they can secrete a variety of cytokines and chemokines to alter the overall inflammatory milieu [46]. Macrophages are not homogenous, and distinct populations of macrophages with different roles in host defense, wound healing, and immune regulation have been described [47-49].

Initial attempts to identify a change in macrophage activity in the presence of OMCP were unsuccessful. These experiments involved measuring TNF production by ELISA, nitric oxide production using the colorimetric Greiss reagent assay, induction of iNOS by ELISA, assay for reactive oxygen species using DCF fluorescence, and a bulk phagocytosis assay by ingestion of fluorescently labeled *E. coli* particles (data not shown). No difference was seen in the presence of OMCP in this broad panel of assays.

Attempts to identify the receptor responsible for OMCP binding to macrophages were performed using an immunoprecipitation approach where tagged OMCP was incubated with human Thp1 cell lysate. The initial protein of interest identified in this method was the high affinity Fc receptor FcγRI. Although subsequent experiments have called this particular hit into question (see Appendix 1), this immunoprecipitation pull-down coupled with mass spec identification approach can be repeated to identify additional putative receptor binding partners. Other methods to identify the putative macrophage receptor might include a cDNA library approach using total RNA from Thp1 cells or BMDMs similar to the approach used to identify FCRL5. The BMDM cDNA library would be amplified and cloned into plasmids for expression into C1498 cells. Transduced cells can then be sorted for high OMCP tetramer staining, subject to limit dilution cloning and genomic DNA extraction to identify OMCP tetramer positive clones.

Identification of the receptor responsible for OMCP binding on macrophages would make characterization of OMCP's impact on macrophage function more tractable. However, gross macrophage function assays can be performed in the absence of an

identified receptor, as macrophage functions are fairly limited in scope and well established functional assays exist.

We hypothesize that OMCP inhibits a function performed through activation of a macrophage receptor, analogous to its inhibition of NKG2D mediated killing. Macrophages are highly adept at recognizing and internalizing foreign material including complement or antibody opsonized pathogens. Following internalization of an opsonized pathogen, foreign peptides are presented to T cells via standard processing and presentation pathways. Macrophages can also mediate ADCC during processes such as *in vivo* tumor rejection [50], and antibody therapy [51]. Therefore, we propose to focus on a few of the main activities performed by macrophages, namely phagocytosis and antigen presentation.

Combined Phagocytosis & ADCC assay by flow: To further probe the effect of OMCP on macrophage function, we would like to assay for phagocytosis and ADCC activity by flow cytometry. In this experiment, Raji cells, a Burkitt's lymphoma cell line, will be CFSE labeled and opsonized with a panel of antibodies that have the rituximab variable region (anti-CD20) fused to various mouse (mIgG1, mIgG2a, mIgA) and human (huIgG1, huIgG2, huIgG3, huIgG4) constant regions (Invivogen). This panel will be a helpful tool in identifying effects of OMCP that may be isotype or FcR specific. The rituximab variable region is identical within this panel of mAbs and is very well characterized. We can then analyze antibody mediated phagocytosis and ADCC by bone marrow macrophages. The CFSE labeled Raji cells will be opsonized, then incubated with

BMDMs for up to 72 hours in the presence or absence of OMCP or a control protein. Following incubation, BMDMs will be labeled with PE-CD115, and cells will be analyzed by flow cytometry with the dead cell exclusion dye 7AAD. On analysis, PE-CD115 cells represent macrophages, CFSE+ cells represent Raji cells, while the PE-CD115+ CFSE+ double positive cells will represent cells that have been phagocytosed or surface bound doublets, as has previously been published [52]. Additionally, Raji cells that are killed externally by ADCC will be identified as the CFSE+ 7AAD+ subset. The percent phagocytosed and the percent killed will be obtained for each condition in the presence or absence of OMCP. An unopsonized sample will be included to ensure that cell death is due to antibody mediated phagocytosis or ADCC rather than another nonspecific process.

Rituximab is used clinically to treat Burkitt's lymphoma, so use of rituximab antibodies to opsonize CD20+ Raji cells should work well. Rituximab is known to mediate ADCC in monoclonal antibody mediated cancer therapy [51, 53] via macrophages and neutrophils [50]. Our planned assay is adapted from the flow cytometic imaging and quantification of ADCC that was introduced by Helguera et al. [52] using the anti-CD20 antibody rituximab to target CFSE labeled Ramos human Burkitt's lymphoma cells to labeled human monocyte effectors. The protocol is straightforward, and no problems are expected in adapting it for our use. Antibody mediated phagocytosis has readily been observed using similar flow cytometric and plate reader based readouts using fluorescently labeled bacteria or particles [54, 55]. One caveat with using large Raji B cells, however, is that complete phagocytosis of a Raji cell will likely be a rare event,

and one macrophage would be expected to ingest at most one or two cells. Compared to other macrophage phagocytosis assays using much smaller bacteria or yeast particles that show high percentage of double positive phagocytosed cells, the percentage of double positive cells using opsonized Raji cells will likely be closer to the 1.5-2% seen in [52]. However, the advantages of using a panel of rituximab antibodies of different isotypes outweigh the anticipated decrease in absolute phagocytosis numbers when using the larger CD20+ B cell lines.

A preliminary phagocytosis and ADCC experiment was completed to assess the feasibility of this experiment as proposed (Fig 20). In this experiment using naïve BMDMs and unopsonized Raji cells, we observed approximately 0.5% of double positive phagocytosed cells and approximately 2% externally killed Raji cells. Activation of BMDMs with LPS and/or IFNγ or opsonization of Raji target cells would be expected to increase the phagocytosis and ADCC percentage.

Fc mediated RBC phagocytosis: An alternative phagocytosis assay will be performed using more easily phagocytosed RBCs. This assay can be adapted for either flow cytometry or fluorescent plate reader. Human RBCs from healthy donors will be FITC labeled and opsonized with mouse anti-human RBC antibodies. The opsonized RBCs will be incubated with unlabeled mouse BMDMs in the presence or absence of OMCP. At various time points, the extracellular fluorescence of uningested RBCs will be quenched with trypan blue allowing phagocytosed cells to be assessed with a fluorescent plate reader. Alternatively, we can use human D^+ RBCs from an Rh^+ donor,

FITC label, and opsonize with human anti-D mAbs and incubate with unlabeled human PBMCs in the presence or absence of OMCP to test the effect in both mouse and human.

The adherence and rosetting of these opsonized RITC labeled RBCs around Fc bearing macrophages will concurrently be examined by fluorescence microscopy. Macrophages will be labeled a complementary color to facilitate identification of cells. We would expect to see numerous RBCs in rosette formation around each macrophage. In the presence of OMCP, the rosetting might be expected to be disturbed, with fewer RBCs clustering per macrophage. The numbers of RBCs attached to each macrophage may be quantified and analyzed.

We can readily obtain human polyclonal anti-D from pooled donors that is the standard treatment for Rh^- mothers [56, 57]. Both phagocytosis and ADCC have been determined to be among the mechanisms for anti-D antibody mediated clearance of D^+ RBCs [58], suggesting that the use of anti-D antibodies in our RBC phagocytosis assays should result in adequate ingestion of donor RBCs. We may expect to see reduced phagocytosis in the presence of OMCP, as shown by reduced fluorescence intensity of macrophages after quenching. Adapting a phagocytosis experiment for analysis by plate reader is advantageous because the faster readout allows more control over time, so the kinetics of phagocytosis in the presence and absence of OMCP can be parsed out more thoroughly.

Antigen presentation to T cells: Human RBCs (or alternatively sheep RBCs) will be covalently labeled with ovalbumin [59]. The RBC-OVA will then be opsonized with mouse anti-human RBC IgG and incubated with mouse BMDMs in the presence or absence of OMCP as described previously. After incubation for various times to allow for adequate internalization of the RBC-OVA, the BMDMs will be washed to remove uninternalized RBCs. The BMDMs will then be incubated with OVA-specific T cells, and antigen presentation will be assessed by assaying for T cell proliferation by thymidine incorporation, CFSE dilution, or IL-2 production (by ELISA).

RBCs are easily conjugated to small haptens or proteins, so the production of RBC-OVA is not expected to be difficult. We choose to use RBC-OVA rather than unconjugated RBCs in these antigen presentation assays due to the fact that OVA-specific T cells are readily available and will allow a more specific readout. If phagocytosis experiments suggest a reduction in RBC internalization in the presence of OMCP, then it would follow that fewer peptides will be presented to T cells, resulting in less IL-2 production and less T cell proliferation. If the previous phagocytosis experiments are inconclusive or suggest no difference in phagocytic ability, it is still possible that internalized OMCP alters signaling in some way to reduce antigen presentation. Based on the function that OMCP has on NKG2D, we hypothesize that OMCP blocks activation of macrophages through an activating receptor, and expect that all downstream effects such as internalization and antigen presentation will be reduced.

It is possible that the outlined approaches will not delineate a functional consequence of OMCP binding to macrophages. We will then pursue tests of other macrophage functions including cytokine production, reactive oxygen production, and related activities. A negative outcome could suggest that OMCP binding to macrophages may be simply an epiphenomenon of NKG2D or FCRL5 binding. However, we postulate that OMCP is independently targeting NKG2D, FCRL5, and a macrophage receptor, and possibly has unique functional effects on each receptor.

Figures:

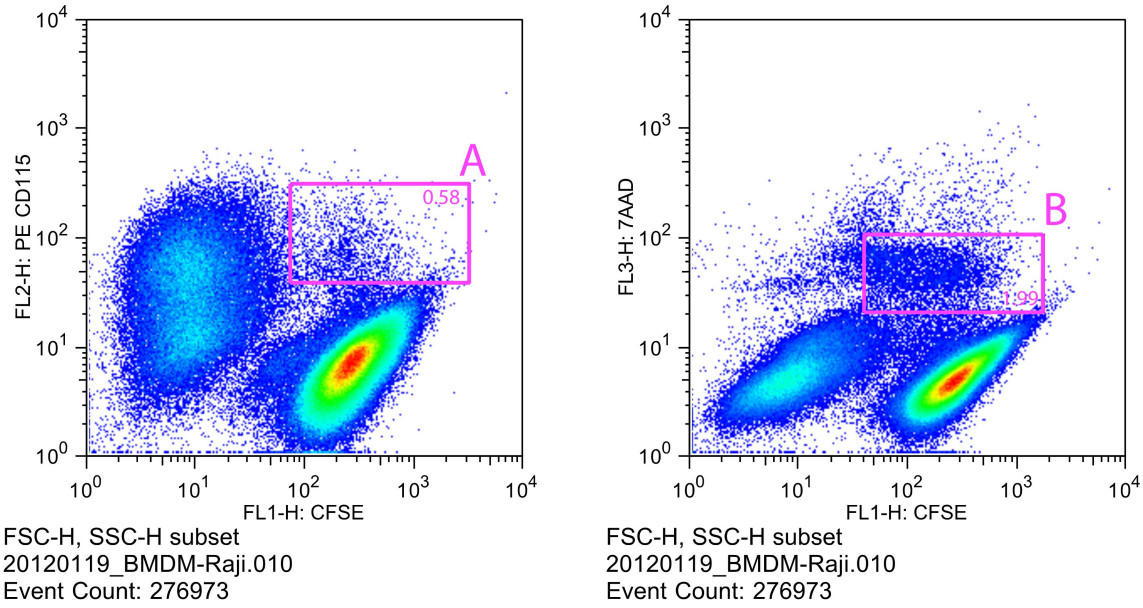

Figure 20: Phagocytosis & ADCC assay Gating Scheme.

Anticipated gating scheme using CFSE labeled Raji cells and CD115 labeled primary BMDMs. PE-CD115 cells represent macrophages, CFSE+ cells represent Raji cells, while the PE-CD115+ CFSE+ double positive cells (population A) will represent cells that have been phagocytosed or surface bound doublets, as has previously been published [52]. Additionally, Raji cells that are killed externally by ADCC will be identified as the CFSE+ 7AAD+ subset (population B).

APPENDIX 1: Investigation of FcγRI as a putative OMCP binding receptor

Introduction:

The FCRL5 receptor is not expressed on macrophages, and although activated murine macrophages have been reported to express NKG2D [60], experimental evidence showed that preincubation with anti-NKG2D antibodies or the recombinant NKG2D ligand MULT1 does not inhibit OMCP tetramer binding to monocytes/macrophages, suggesting that macrophages express an additional receptor distinct from both FCRL5 and NKG2D [7]. An immunoprecipitation pull down method was used to identify FcγRI (CD64) as a putative OMCP-binding receptor expressed on macrophages. An OMCP-human IgG(Fc) fusion protein and a Mult1-human IgG(Fc) control were generated and used to pull down protein lysate from a human monocyte cell line previously shown to bind OMCP (Thp1 cells). Mass spectrometry sequencing results identified FcγRI as a receptor of interest. OMCP binding to FcγRI was initially confirmed by OMCP tetramer staining to stable BaF/human FcγRI transductants. Specificity of the interaction was validated by blockade with anti-FcγRI polyclonal antibodies, anti-FcγRI $F(ab')^2$ fragments, and cold OMCP tetramers (Fig 21). OMCP binding was also confirmed on BaF/mouse FcγRI transductants (Fig 22).

The high affinity FcγRI receptor

FcγRI is part of a large family of Fc receptors that contains both activating and inhibitory members that have different affinities for the various subclasses of immunoglobulins.

FcγRI is the only high affinity IgG receptor (with near nanomolar affinity for IgG subclasses). It is constitutively expressed on monocytes and macrophages, and it is inducible on activated granulocytes by IFNγ [61]. Macrophages express all classes of activating Fcγ receptors, and there is significant redundancy between the functions of these receptors, as all activating Fc receptors use the same ITAM bearing gamma signaling chain [61]. However, there is evidence that the FcγRI alpha chain can elicit functions independently of the gamma chain, making it possible that FcγRI may have unique functions that can not be compensated for by the other activating Fc receptors present on macrophages [62].

Fc receptors bind antibodies at their invariant Fc region, allowing cells bearing Fc receptors to bind to opsonized pathogens, immune complexes, or in some cases monomeric Ig. FcγRI is the highest affinity IgG receptor that preferentially binds mouse IgG2a and IgG2b (or human IgG1 and IgG3) [63, 64]. The high affinity interaction between FcγRI and serum IgG is also unique among Fcγ receptors. FcγRI's affinity for IgG is higher than the concentration of IgG in serum (20 nM for mouse FcγRI binding to mouse IgG2a [65]; 15-40 nM for human FcγRI binding to human IgG1, IgG3, IgG4 [66]), making FcγRI capable of binding monomeric serum IgG. The receptor is thought to be prearmed with IgG similar to mast cell FcεRI with IgE [61].

The high affinity IgG receptor FcγRI is known to facilitate phagocytosis and antibody dependent cellular cytotoxicity. But the involvement of macrophages and monocytes and the role of FcγRI in particular in orthopoxvirus infections has not been well

established, although macrophage dependent clearance of ectromelia [67] and vaccinia [68] viruses has previously been observed.

It is proposed that FcγRI in an unactivated state functions as a type of scavenger receptor, constantly sampling extracellular antigens as the receptor-IgG complex gets internalized and recycled back to the surface. However, at sites of inflammation, cytokine production promotes *de novo* synthesis of FcγRI and accelerates the recycling process, allowing macrophages to internalize more antigen in an inflammatory area [61]. Following internalization of an opsonized pathogen, foreign peptides are presented via standard processing and presentation pathways. Another process involving Fc receptors is antibody dependent cell mediated cytotoxicity (ADCC). ADCC is classically thought of as being mediated by FcγRIII receptors on NK cells, where engagement of FcγRIII by an opsonized target stimulates release of cytotoxic granules. ADCC has also been shown to be mediated by macrophages during processes such as *in vivo* tumor rejection [50], and antibody therapy [51] where lysis of cells is thought to involve release of the cytotoxic mediators TNF-α and IL-1 [69, 70].

Phenotype of FcγRI$^{-/-}$ knockout mouse and human mutations

The FcγRI $^{-/-}$ mouse has been generated independently by two separate labs, both of which described a range of defects involving impaired endocytosis of monomeric IgG, phagocytosis of immune complexes, chemokine release, macrophage based ADCC, reduced hypersensitivity responses, immune complex dependent antigen presentation to primed T cells, and impaired protection from bacterial infection [71, 72]. In contrast,

no defects were appreciated in leukocytes isolated from a human family with a premature stop mutation in human FcγRI [73, 74]. Their monocytes were able to bind and phagocytose aggregated human IgG and coated human RBCs normally through redundancy with FcγRII. This situation illustrates the problem that OMCP inhibition of FcγRI may be masked by the functions of other Fc receptors on macrophages. However, the virus has targeted a receptor that is quite unique in its high affinity nature of binding, so it is unlikely that targeted functions of FcγRI can be completely compensated for by other Fc receptors. If this is the case, then we expected that the FcγRI $^{-/-}$ mouse may exhibit an equal or increased survival advantage compared to WT mouse when both are infected with OMCP-sufficient cowpox, while the FcγRI $^{-/-}$ mouse may be more susceptible to infection than WT mouse due to loss of a critical immune receptor when both are infected with OMCP-deficient cowpox.

The initial discovery that viral OMCP specifically targets FcγRI on immune cells was investigated. Given the near nanomolar affinity that FcγRI has for serum IgG, it would be important to determine whether OMCP has a binding affinity that can successfully compete with IgG or immune complexes. Alternatively, we considered OMCP may have been acting as a non-competitive inhibitor on a site other than the IgG binding site. OMCP may also function by stabilizing either activated or unactivated forms of the receptor or disrupting interactions between the alpha and gamma signaling chain of FcγRI.

Experimental Methods:

Immunoprecipitation pull down/mass spec analysis

FcγRI was identified as a putative OMCP-binding receptor through an immunoprecipitation pull down method. An OMCP-human IgG(Fc) fusion protein and a Mult1-human IgG(Fc) control were generated and incubated with Thp1 (human monocyte cell line) cell lysates and pulled down with Protein G beads. The beads were then reduced and run on SDS-PAGE gel, and a unique band in the OMCP-hu IgG(Fc) fusion protein lane was identified, cut out, and sent for mass spectrometry sequencing, which identified FcγRI as a receptor of interest.

FcR cloning

The FcγRI gene was cloned out of the human Thp1 cell line and M-CSF conditioned mouse BMDMs and ligated into the pMX-IRES-GFP vector. PLAT-E retroviral packaging cells were transfected with human or mouse FcγRI expressing plasmids, and grown to allow packaging of the plasmid material into retroviruses with the Moloney murine leukemia virus capsid. This retroviral supernatant was then used to transduce BaF/3 cells. Stable incorporation of the pMX-IRES-GFP insert was selected for by FACS sorting for GFP positive BaF/3 cells, and expression of FcγRI was confirmed by antibody staining.

We have also completed cloning of all of the murine and human Fc receptors for transduction into BaF3 cell lines. Total RNA was isolated from cultured mouse BMDMs or fresh human PBMCs, and reverse transcribed into total cellular cDNA. Sequences for

mouse FcγRIIb, FcγRIII, and FcγRIV and human FcγRIIa and FcγRIIIa were amplified, restriction digested, and ligated into pMX-IRES-GFP vectors for transformation into ultracompetent cells as described above for FcγRI. Plasmids were grown for transfection into PLAT-E retroviral packaging cells for stable transduction of BaF3 cells. Fc receptor transduced BaF3 cell lines were then used to further evaluate OMCP tetramer binding.

Recombinant protein expression and tetramerization

Recombinant BirA tagged OMCP was expressed in bacterial cells, refolded from inclusion bodies, and purified by size exclusion chromatography. A biotin ligase reaction was performed to site-specifically biotinylate the OMCP protein at the BirA tag, followed by another size exclusion chromatography purification. Biotinylated OMCP was tetramerized fresh before each staining experiment by incubation with APC labeled streptavidin at a 4:1 molar ratio for 10 min at RT and used for cell staining same day.

OMCP tetramer binding by flow cytometry

The appropriate cell lines or primary cells for each experiment are stained with 400ng of OMCP tetramer, D132R tetramer, DIII control tetramer, or streptavidin control for 1 hour on ice, in the dark. Tetramers are fluorescently labeled by binding biotinylated protein with APC-streptavidin in a 4:1 molar ratio. All tetramers are made fresh for each experiment. In blockade experiments, the designated protein or antibody blockade is incubated with cells first for 1 hour on ice in the dark, followed by an additional 1 hour incubation with labeled tetramers. Following staining, cells are washed with sorting

buffer x3 to remove unbound tetramer. Data was collected on a FACSCalibur, and analyzed using FlowJo software (TreeStar, Ashland, OR).

In vitro generation of murine bone marrow derived macrophages

Male or female 8 week old mice were sacrificed by CO_2 euthanasia. The long bones (tibia and femur) of the hind leg are harvested and cleaned of muscle and tendons. The ends of each bone are snipped open to access bone marrow. Marrow is flushed or centrifuged out of the bone, and resuspended in DMEM with 20% L929 cell supernatant, 10% FBS, 1% L-glutamine, 1% Na pyruvate, 1% P/S. Marrow from one mouse (4 bones) can be plated in 5x 10 cm tissue culture petri dishes. Incubate at 37^{o}C, 5% CO_2 for 7 days. On Day 5, add fresh L929 supplemented media. BMDMs ready for use between day 7-day 14. Note – L929 cell line produces murine M-CSF. Supernatant from L929 cells in log phase growth is filtered and used for BMDM media. L929 supernatant can be replaced with recombinant murine M-CSF.

Mutant D132R OMCP protein expression

Initial binding assays have identified the D132 residue of OMCP as integral for NKG2D binding. To create a mutant that has exclusively lost NKG2D binding, we sought to introduce a positively charged arginine to disrupt interactions. Primers were designed for a SOE reaction to introduce D132R mutation into VO18 sequence. The product was ligated into p7.5gpt plasmid and transformed into competent cells with selective media, followed by mini-prep and sequencing (PNACL) to verify presence of mutation. BSC-1 cells were infected with cowpox, then transfected with D132R plasmid under gpt

selective pressure. Plaques were picked and plaque purified twice in gpt selective media, then twice in non-selective media. Viral stock was grown and sequenced to confirm presence of the D132R mutation.

Mutant CPX virus generation

An OMCP deficient cowpox virus (V018$^{-/-}$ CPX) was generated using a transient domain selection strategy to introduce mutations into the virus genome. Two tandem stop codons were inserted in the OMCP open reading frame, resulting in loss of functional OMCP with minimal impact on other genes [7]. The virus was propagated in BSC-1 cells, purified through sucrose gradient, titered, and used for i.p. mouse infections at $0.61x10^6$ pfu/mouse and $1.93x10^6$ pfu/mouse. We have established that cowpox virus deficient in OMCP has decreased virulence as determined by lethality in WT C57BL/6 mice.

Results:

Initial Identification of FcγRI

An immunoprecipitation pull down method was used to initially identify FcγRI (CD64) as a putative OMCP-binding receptor expressed on macrophages. Here, an OMCP-human IgG(Fc) fusion protein and a Mult1-human IgG(Fc) control were generated and incubated with Thp1 (human monocyte cell line) cell lysate and pulled down with Protein G beads. The beads were then reduced and run on an SDS-PAGE gel, and a unique band in the OMCP-hu IgG(Fc) fusion protein lane was identified, cut out, and sent for mass spec sequencing. Sequencing results identified FcγRI (CD64) as a receptor of interest.

OMCP binding to FcγRI was confirmed by OMCP tetramer staining to stable BaF/human FcγRI transductants, as well as murine bone marrow derived macrophages (BMDMs) (Fig 22). OMCP tetramers do not bind untransduced Ba/F3 cells, and an irrelevant WNV DIII protein was used as a negative control in all staining experiments. Specificity of the interaction was validated by blockade with anti-huFcγRI polyclonal antibodies and cold OMCP tetramers on BaF/huFcγRI transductants (Fig 21). We found that preincubation of cells with cold OMCP tetramers (Fig 21C) or anti-huFcγRI F(ab)2 fragments (Fig 21D) greatly decreased labeled OMCP tetramer binding, supporting our initial hypothesis that OMCP specifically targets the FcγRI receptor on macrophages and monoctyes. We believed this experiment addressed the possibility that the OMCP-Fc used in our initial pull down was binding to FcγRI via its Fc, as our purified OMCP protein should not have contained Fc binding domains.

Characterization of FcγRI binding

We showed that cells that express the human FcγRI receptor had a correspondingly high level of OMCP tetramer binding, although BaF cells transduced with murine FcγRI appeared to have lower affinity binding. Inconsistently, we saw that OMCP binding was strong on murine BMDMs, despite the apparent low binding on the BaF/muFcγRI cell line (Fig 22). This may have suggested additional factors responsible for OMCP binding on primary murine macrophages. To determine whether NKG2D binding may be playing a role, we tested binding of the D132R mutant on cells expressing NKG2D, FCRL5, or FcγRI. As expected, the D132R mutant lost all binding to NKG2D expressing cells, with

no decreased binding to the FCRL5 expressing cells (BaF/FCRL5 or WEHI cells) (Fig 23). Additionally, there was no reduced binding of the D132R mutant to BaF/huFcγRI cells. However, binding of D132R was reduced, but not completely abrogated on murine BMDMs (Fig 23). This finding was inconsistent with previous published results that showed no reduction in OMCP binding when murine macrophages are preincubated with anti-NKG2D antibodies [8].

Further experiments showed repeatable dose dependent OMCP tetramer binding to murine BMDMs and human CD14+ monocytes isolated from fresh PBMCs (Fig 24). Bone marrow derived macrophages (BMDMs) exhibit high FcγRI expression in the unactivated state, with a 3 fold increase in expression after overnight stimulation with interferon gamma (IFNγ) and bacterial lipopolysaccharide (LPS) (data not shown). OMCP tetramers demonstrated robust binding to WT BMDMs even in the unactivated state (Fig 24). Here we demonstrate that OMCP tetramers from the Brighton Red strain of CPX bind both human PBMCs and murine primary BMDMs.

OMCP retains binding to FcγRI ko BMDMs

After initially confirming binding to mouse bone marrow derived macrophages (BMDMs), human PBMCs, as well as specific binding to BaF/muFcγRI and BaF/huFcγRI transductants, we obtained FcγRI $^{-/-}$ mice for our studies. Unexpectedly, we found that OMCP tetramer binding was retained on FcγRI $^{-/-}$ BMDMs, with no apparent reduction in staining intensity (Fig 25). This has been repeated with BMDMs from multiple FcγRI $^{-/-}$ mice, and lack of expression of FcγRI on their cells has been confirmed. Additionally,

although anti-FcγRI polyclonal F(ab')2 blockade is sufficient to block OMCP tetramer staining on BaF/FcγRI transductants, it is not sufficient to block OMCP binding on WT mouse BMDMs or human CD14+ monocytes (Fig 26). Additional blockade using the anti-FcγRI polyclonal F(ab')2 fragments with 2.4G2 sup (anti-FcγRII/FcγRIII monoclonal) showed no reduction in OMCP tetramer binding compared to unblocked controls. This data may implicate other murine FcRs or some unrelated receptor as being responsible for OMCP binding on FcγRI ko BMDMs.

It is possible that OMCP binds to multiple Fc receptors. This is not a novel strategy in poxviruses, as the immunoevasin CrmD has been demonstrated to promiscuously bind all tested Fc receptors (M. Epperson, unpublished data). Based on anti-FcγRI and 2.4G2 blocking data, as well as analysis of expression patterns of each of the Fc receptors in mouse, we suspected OMCP may be binding to both FcγRI and FcγRIV on murine macrophages. The FcγRI and FcγRIV receptors are both gamma chain dependent activating Fc receptors that display selectivity for the most potent mouse IgG subclasses, IgG2a and IgG2b [75]. FcγRI is uniquely expressed on monocytes, macrophages, and a subset of monocyte derived DCs [76], while FcγRIV expression is detected on monocytes, macrophages, neutrophils, and DCs, but notably not T cells, B cells or NK cells [77], consistent with earlier results in our laboratory. Although FcγRI is the high affinity IgG receptor, FcγRIV has an intermediate affinity ($3x10^7\ M^{-1}$) for IgG2a and IgG2b, and there is convincing evidence that FcγRIV plays a central role in IgG2a and IgG2b activity [75-77].

Possible OMCP binding to multiple FcRs

We subsequently tested OMCP binding to all murine and human Fc receptors (mFcγRI, mFcγRIIb, mFcγRIII, mFcγRIV, huFcγRI, huFcγRIIa, huFcγRIIIa). We have cloned all of the murine and human Fc receptors for transduction into Ba/F3 cell lines. Total RNA was isolated from M-CSF cultured mouse BMDMs or fresh human PBMCs, and reverse transcribed into total cellular cDNA. Sequences for mouse FcγRIIb, FcγRIII, and FcγRIV and human FcγRIIa and FcγRIIIa have been amplified, restriction digested, and ligated into pMX-IRES-GFP vectors for transformation into ultracompetent cells. Plasmids were grown for transfection into PLAT-E retroviral packaging cells for stable transduction of Ba/F3 cells. Fc receptor transduced Ba/F3 cell lines were then be used to further evaluate OMCP tetramer binding.

When we tested OMCP binding to Ba/F3 cells expressing mouse FcγRIIb, FcγRIII, and FcγRIV and human FcγRIIa and FcγRIIIa, we saw that in addition to binding to mouse FcγRI and human FcγRI, we saw consistent binding to murine FcγRII (CD32) (Fig 27). We did not see binding of OMCP tetramers to any of the other murine and human FcRs. Contrary to our initial hypothesis, we did not see OMCP binding to mouse FcγRIV. We noted that OMCP binding to FcγRIIb strangely showed a pattern of multiple peaks, which was inconsistent with the uniform expression of the FcγRIIb receptor as determined by staining using the 2.4G2 (anti-FcγRII/FcγRIII) antibody (Fig 28). This unexpected pattern is repeatable, but remains unexplained.

These experiments in aggregate suggested that OMCP may bind to additional Fc receptors, namely murine FcγRIIb, which may explain the retained tetramer binding in the FcγRI ko mouse BMDM cells. However, there were several abnormalities observed in this data, which complicates the interpretation of these findings. For example, OMCP binding to FcγRIIb is inconsistent with our previous observations that combined anti-mFcγRI and anti-mFcγRIIb blockade does not block OMCP binding to WT BMDMs (data not shown).

OMCP binding to BMDMs does not require Dap10, Dap12, or FcRγ

To further investigate possible OMCP binding to Fc receptors, we tested OMCP binding to BMDMs derived from FcR gamma chain ko mice and Dap10/Dap12 double ko mice. The FcRγ$^{-/-}$ mice do not express the activating Fc receptors FcεRI, FcγRIII, FcγRIV that require the signaling gamma chain for surface expression. Although the FcR gamma chain ko mice has been reported to have 1/5 the normal level of FcγRI expression, the residual FcRs were found to be deficient in activity [71]. Dap10 and Dap12 are signaling adaptors are required for expression of numerous immune receptors, including NKG2D, Ly49D, and Ly49H on NK cells; Clec5a, Trem1, and Trem2 on macrophages; Siglec-H, pDC-Trem, and DlgR1 on myeloid cells, as well as many other important receptors [78]. Contrary to expectations, we found that OMCP binding to murine BMDMs did not appear to require expression of any of the adaptor molecules Dap10, Dap12, or FcRγ (Fig 29). Strangely, there was no reduction in OMCP binding to FcRγ $^{-/-}$ BMDM, despite our evidence of OMCP binding to mFcγRI and mFcγRII. This inconsistency might indicate that OMCP is binding a receptor that is completely FcRγ independent, ruling

out all of the known Fc receptors. If true, the binding observed to BaF/mFcγRI, BaF/mFcγRII, and BaF/huFcγRI may be artifactual.

OMCP does not bind human FcγRI by SPR

Independent analysis performed by Eric Lazear (Fremont Lab) demonstrated that OMCP monomer indeed does not bind to human FcγRI by SPR (data not shown). Controls demonstrated strong OMCP binding to mNKG2D, and strong IgG2c binding to FcγRI as expected. This independent assessment strengthens the idea that presumed OMCP binding to FcγRI was in fact artifactual.

New batches of OMCP protein does not bind FcγRI

Additional experiments using new batches of inclusion body derived OMCP protein that was refolded and purified at later times did not reproduce our initial findings (Fig 30). Also, binding assays using mammalian derived OMCP produced from 293F cells did not show FcγRI or any FcR binding (Fig 31). We performed two additional IP-mass spec pulldowns with biotinylated OMCP (instead of OMCP-Fc fusion protein) on lysate from RAW264.7 and IC21 mouse macrophage cell lines (instead of the human Thp1 monocyte cell line). These experiments did not pull down any FcRs, and no promising hits were identified (data not shown). These later experiments are all consistent, and strongly imply that our initial conclusions were incorrect, and may be attributed to contaminated protein stocks.

Summary of evidence that OMCP may not bind to FcγRI

Following the initial positive results suggesting OMCP binding to the high affinity Fc receptor FcγRI, came a series of disappointing results that subsequently shed doubt on our initial conclusions.

- OMCP still binds to FcγRI$^{-/-}$ BMDMs.
- Anti-mFcγRI polyclonal blockade does not block OMCP binding to WT BMDMs.
- Combined anti-mFcγRI and anti-mFcγRIIb blockade does not block OMCP binding to WT BMDMs.
- Most recent batch of inclusion body derived OMCP does not replicate binding to BaF/huFcγRI, BaF/mFcγRI or BaF/mFcγRIIb by flow cytometry. Staining with old OMCP in parallel with most recent OMCP batch demonstrated binding in the old batch of protein only.
- Mammalian 293F derived fully glycosylated OMCP does not bind to BaF/huFcγRI, BaF/mFcγRI or BaF/mFcγRIIb by flow cytometry or SPR.
- Independent SPR analysis suggests OMCP does not bind any mouse or human FcRs
- Two subsequent IP-mass spec pulldowns with biotinylated OMCP (instead of OMCP-Fc fusion protein) on lysate from RAW264.7 and IC21 mouse macrophage cell lines did not pull down any FcRs.

Together, these independent results suggest that the original strong binding of OMCP to FcγRI may have been an artifact.

Discussion:

The viral immunoevasin Orthopoxvirus MHC Class I-like Protein (OMCP) binds with high affinity to the NK cell activating receptor, NKG2D. OMCP acts as a competitive antagonist of NKG2D, preventing interactions with cellular stress ligands and inhibiting NK killing. OMCP also engages the orphan receptor FCRL5 on splenic marginal zone and peritoneal B-1a B cells, but the functional consequence of this interaction is unknown. We had evidence that implicated the high affinity IgG receptor FcγRI (CD64) on macrophages as a putative third receptor for OMCP. However this finding has recently been called into question.

Original hypotheses

Our initial hypothesis was that OMCP acts as a competitive inhibitor, blocking IgG binding to FcγRI and subsequent macrophage activation. This would require a very high (at least nanomolar) affinity to the receptor to overcome the high affinity that FcγRI has for monomeric IgG and even higher affinity for immune complexes. A high nanomolar to picomolar binding affinity is plausible, as OMCP has previously been demonstrated to have a K_D of 37 ± 6 nM for muNKG2D, and K_D of 168 ± 33 pM for huNKG2D [4]. Alternatively, OMCP might act as a noncompetitive inhibitor at a site unique from the IgG binding site. In this event, OMCP may have inhibitory effects on the receptor with a more modest binding affinity. Another possibility was that OMCP is acting within infected cells and binding FcγRI internally, possibly when both molecules are synthesized in the ER and golgi, before the receptor has opportunity to get transported to the cell surface to bind free IgG. In this scenario, OMCP has the chance to bind FcγRI

in infected cells without competing with its endogenous ligand, IgG. Poxviruses have been demonstrated to preferentially infect monocytes/macrophages, B cells, and DCs [79], suggesting that intracellular binding is a plausible possibility.

An additional hypothesis that we initially pursued is the possibility that OMCP was selectively targeting FcγRI and crossreacting with FCRL5 due to homology, or vice versa. Comparison of affinity and avidity data for the FCRL5 receptor and FcγRI receptor with OMCP would be useful in determining if OMCP is truly targeting one receptor and only incidentally binding the other. We might expect to see higher affinity binding to the targeted receptor compared to the incidental receptor.

Structural similarity between FCRL5 and FcγRI

Classical Fc receptors have not been reported to bind NKG2D ligands. Additionally FCRL5 and other Fc-like receptors have not been reported to bind other NKG2D ligands [7]. However, we expected that these binding interactions were unique to viral OMCP, and did not originally consider these distinct binding partners unusual. In fact, it appeared appropriate that OMCP would bind to two receptors in closely related families that were composed of similar immunoglobulin domains.

FCRL5 is the largest of the FCRL family of proteins, consisting of 5 extracellular Ig domains, a transmembrane domain, and a cytoplasmic domain with a noncanonical ITAM and two canonical ITIMs (Fig 32) [80]. To determine which domains of FCRL5 were responsible for OMCP binding, a series of domain truncation mutants of FCRL5

fused to the GPI linked Thy1.1 were previously created. A library of each individual domain and combinations of consecutive domains were generated and tested for OMCP tetramer binding. These experiments demonstrated that domains 1, 2, and 3 were necessary and sufficient for OMCP binding, while domains 4 and 5 were superfluous (Fig 33) [8].

The FcγRI α chain consists of 3 ligand binding Ig domains, a transmembrane domain, and a cytoplasmic domain that associates with the ITAM bearing FcR γ chain for signaling (Fig 32) [61]. Interestingly, FcγRI is the only classical IgG receptor with 3 Ig domains (all others have only 2 domains) [66, 81], and the 3 Ig domains of FcγRI share significant homology to the 3 N-terminal Ig domains of FCRL5 that were identified as necessary for OMCP tetramer binding. The full length FcγRI has approximately 24% amino acid identity compared to full length FCRL5, and each Ig domain has 28-32% amino acid identity between receptors [82]. The homology between two receptors raised the possibility that OMCP is targeting one of these closely related receptors, and is binding the other incidentally. This seemed likely given the high homology between the 3 Ig domains that compose FcγRI and the N-terminal 3 Ig domains in FCRL5 (Fig 32).

Furthermore, the closely related monkeypox version of OMCP ($OMCP_{mpx}$), although capable of binding to BaF/NKG2D, does not bind BaF/mouse FCRL5 [7]. The homology between mouse FCRL5 and FcγRI (Fig 32), as well as the unexpected lack of conservation of $OMCP_{br}$-FCRL interaction in the human species and between OMCP from different orthopoxvirus species prompted the initial hypothesis that viral OMCP

may be specifically targeting FcγRI, and incidentally binding mouse FCRL5. This might suggest that OMCP has two specific targets – NKG2D on NK cells and a receptor on monocytes and macrophages – rather than three targets. These extensive structural similarities also seemed to validate our initial pull down of FcγRI as a putative OMCP binding macrophage receptor, since a protein would be more likely to bind to members of related families with moderate to high sequence homology.

However, in retrospect, the structural similarities between FCRL5 and FcγRI may simply be coincidental. Although we originally interpreted this as theoretical validation for our pull-down of FcγRI, it is very likely that the use of an Fc fusion protein was responsible for the identification of an FcR. The relationship between the FcR and FCRL families may have been due to chance, but unfortunately misguided our investigations.

Problems with Identification of FcγRI

The putative OMCP binding receptor on macrophages was initially identified using an immunoprecipitation-mass spec approach, where an OMCP-huIgG(Fc) fusion protein or Mult1-huIgG(Fc) control was incubated with lysate from a human Thp1 cell line and pulled down with Protein G beads. Binding to FcγRI was validated using labeled OMCP tetramers (with no Fc) on Ba/F3 cells transduced with human FcγRI, mouse FcγRI, and primary mouse BMDMs. This binding could be specifically blocked with cold OMCP tetramers and anti FcγRI F(ab)2 fragments. OMCP was also subsequently shown to bind to mouse FcγRIIb transduced Ba/F3 cells, but none of the other mouse or human FcRs.

The fact that a high affinity Fc receptor was pulled down by an IgG(Fc) fusion protein initially generated concern. This result may have been due to binding of the FcR directly to the IgG domain, rather than the OMCP domain of the fusion protein. However, this should have been controlled for with the Mult1-human IgG(Fc) control that was generated in parallel with the OMCP fusion protein. In retrospect, it is possible that the Mult1 fusion protein had misfolded IgG domains that rendered it incapable of pulling down the FcR, whereas the OMCP-IgG fusion protein was successfully folded and presented. The Mult1 fusion protein was never tested for proper folding, whereas the OMCP protein was only tested for NKG2D binding ability.

When later IP-mass spec pulldowns were performed, we used biotinylated OMCP as bait instead of an OMCP-Fc fusion protein, to attempt to minimize the role of the Fc domain. We incubated biotinylated OMCP with lysate from RAW264.7 and IC21 mouse macrophage cell lines instead of the human Thp1 monocyte cell line used in our first experiment. These later pull downs did not identify any FcRs as potential binding partners for OMCP. This again suggests that the use of the OMCP-Fc fusion protein in our initial pull down was responsible for our erroneous FcR identification.

Possible explanations for protein binding artifacts

In order to rule out artifact binding due to the presence of the IgG domain in the OMCP-IgG fusion protein, subsequent binding experiments were performed with what was thought to be pure refolded OMCP. These subsequent experiments with OMCP binding

suggested true binding to FcγRI, including successful blockade with anti-FcγRI antibodies. In retrospect, it is possible that our initial stocks of OMCP were contaminated with small amounts of the OMCP-IgG fusion protein that strongly bound to FcRs. This may be plausible, as batches of inclusion body derived OMCP protein produced years later, as well as batches of OMCP protein produced independently in mammalian 293F cells did not replicate the initial FcR binding phenotype. However, this explanation is not completely satisfactory, as any OMCP-IgG fusion protein contaminant present should not have been biotinylated, and therefore should not have generated productive fluorescently labeled tetramers when incubated with APC-streptavidin.

Other possibilities to explain this incongruous binding artifact include contamination, misfolding of protein, degradation of protein, or the creation of higher order oligomers. Artifactual binding may have been due to a contaminating protein that interacts with OMCP-b. For example an OMCP-Fc fusion protein contaminant could oligimerize with OMCP-b through OMCP-OMCP dimer or multimer formation. Although OMCP has been determined to be secreted as a monomer, OMCP was crystallized as a trimer in the asymmetric unit. If strong OMCP-OMCP interactions are possible in solution, this would allow FcR binding to the Fc fusion protein, while remaining labeled by APC-streptavidin interactions with the biotinylated OMCP partner, however this interaction is highly unlikely.

Another more likely possibility may be contamination with a biotinylated protein that is inappropriately binding FcR bearing cells and capable of being labeled by APC-

streptavidin independently of OMCP-b. An example of this type of contaminant could be a biotinylated full length antibody that may have been used as a primary antibody for other experiments in the lab. These biotinylated antibody reagents are commonplace and used by all members of the lab, and it is possible that despite meticulous care, contamination of protein stocks may have occurred. Given the simplicity of this explanation, we think that contamination of our OMCP-b stocks with biotinylated antibody is possible. Contamination with biotinylated antibody would also explain the observation that binding was specifically blocked with anti-FcγRI antibodies.

Alternatively, inappropriate binding may be due to misfolded OMCP-b protein in the initial protein batches. When protein is overexpressed in E. coli, aggregation of partially folded protein in inclusion bodies results. Our protein purification protocol used standard arginine refolding methods to solubilize and slowly refold the overexpressed OMCP. It is possible that some misfolded OMCP remained that had inappropriate FcR binding.

Another possibility is that our OMCP batches contained degradation products that bound to FcRs erroneously. There may have been a mix of full length and degraded OMCP in our initial protein batches. This may be possible if bacterial proteases were not purified out appropriately. We consider this unlikely, as all protein batches were purified by size exclusion chromatography and purity confirmed by SDS-PAGE gel. Additionally, abnormal binding due to degradation product formation would be expected to increase over time, whereas we observed abnormal FcR binding with fresh batches of protein, and there did not appear to be a change in FcR binding intensity over time.

One final consideration is that higher order oligomers may have been involved in inappropriate FcR association. OMCP may have formed covalent or noncovalent interactions with other molecules of full lenth/degraded/misfolded OMCP. These larger complex oligomers would have properties that differ from monomeric OMCP, and may abnormally bind to FcRs.

Reviewing our results in aggregate, we are inclined to believe that binding of OMCP to FcγRI does not truly occur, and our pursuit to identify a receptor responsible for OMCP binding to macrophages was unsuccessful. Recent evidence from several independent sources calls into question our original hypothesis that OMCP binds to FcRs. All OMCP binding seen previously may be artifact of misfolded/contaminated/otherwise altered OMCP-b. However, OMCP may indeed be binding to a receptor on macrophages, as that observation has been consistent across many years, but that receptor remains to be identified.

Figures:

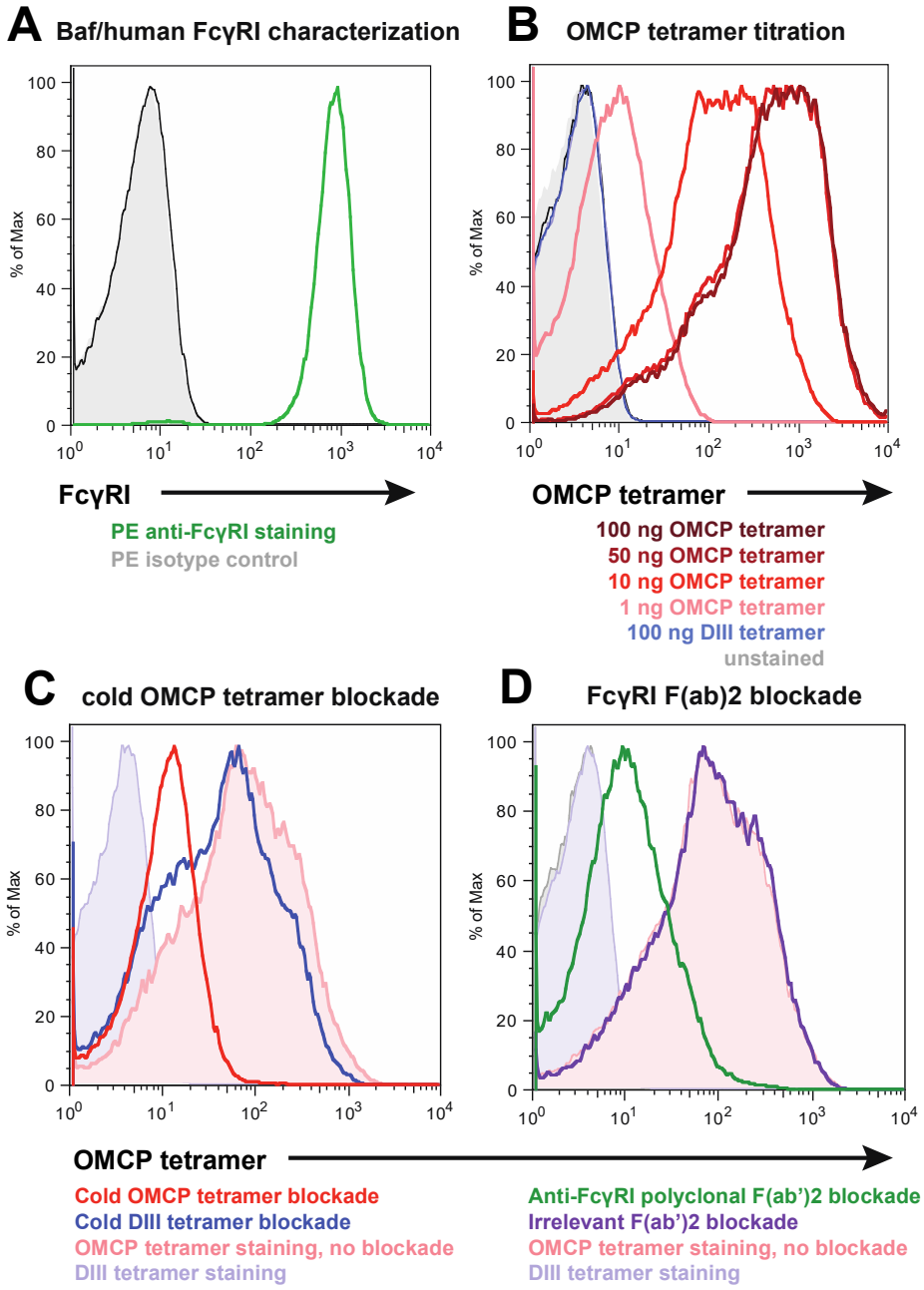
A Baf/human FcγRI characterization
% of Max
FcγRI
PE anti-FcγRI staining
PE isotype control
B OMCP tetramer titration
% of Max
OMCP tetramer
100 ng OMCP tetramer
50 ng OMCP tetramer
10 ng OMCP tetramer
1 ng OMCP tetramer
100 ng DIII tetramer
unstained
C cold OMCP tetramer blockade
% of Max
OMCP tetramer
Cold OMCP tetramer blockade
Cold DIII tetramer blockade
OMCP tetramer staining, no blockade
DIII tetramer staining
D FcγRI F(ab)2 blockade
% of Max
Anti-FcγRI polyclonal F(ab')2 blockade
Irrelevant F(ab')2 blockade
OMCP tetramer staining, no blockade
DIII tetramer staining

Figure 21: OMCP tetramer blockade and anti-FcγRI blockade on BaF/huFcγRI cells

(A) stable BaF/huFcγRI transductants were stained with PE anti-FcγRI (green line), isotype control (black line), or left unstained (gray shading) (B) BaF/huFcγRI transductants were stained with OMCP tetramers labeled with APC (100, 50, 10, or 1 ng titration, red lines), WNV-DIII control tetramer labeled with APC (10 ng and 1 ng, blue lines) or streptavidin-APC alone (gray shading). (C) BaF/huFcγRI transductants were pre-incubated with 5000 ng of cold OMCP-neutravidin tetramers (red line) or DIII-neutravidin control tetramers (blue line), then stained with 10 ng of OMCP-APC labeled tetramers. BaF/huFcγRI stained with 10 ng OMCP tetramers without blockade shown in red shading, control stained with 10 ng DIII tetramers in blue shading. (D) BaF/huFcγRI cells preincubated with polyclonal anti-FcγRI $F(ab')^2$ antibody mix (green line) or $F(ab')^2$ mouse gamma globulin (blue line), then stained with OMCP tetramers. BaF/huFcγRI stained with 400 ng OMCP tetramers without blockade shown in red shading, control stained with 400 ng DIII tets in blue shading. Representative histograms from 3 independent experiments.

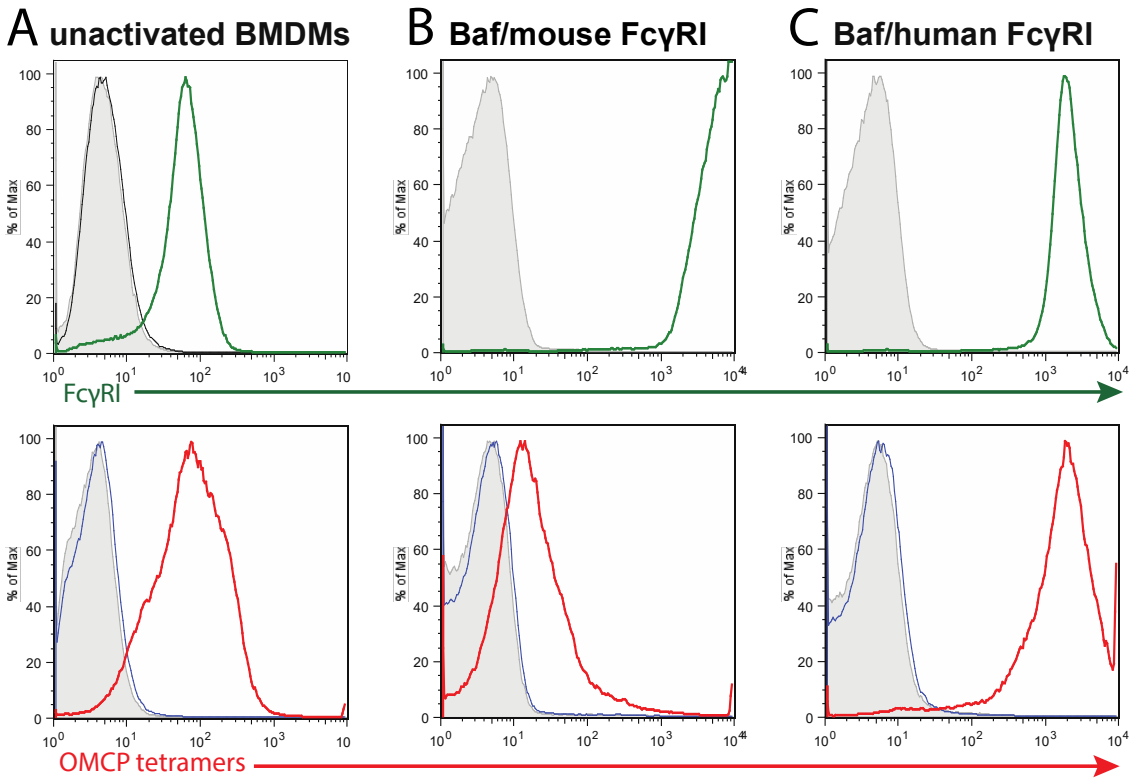

Figure 22: WT B6 BMDMs, BaF/muFcγRI, and BaF/huFcγRI express FcγRI and bind OMCP tetramers.

(A) Bone marrow isolated from C56BL/6 femurs were cultured for 7 days in M-CSF containing media. Unactivated bone marrow derived macrophages were then stained for FcγRI expression (top panel, green line). (Bottom panel) Unactivated BMDMs were stained with 400 ng of OMCP labeled tetramers (red line), a WNV-DIII labeled control tetramer (blue line) and streptavidin only control (gray shading). For comparison see results from similar experiments with BaF/muFcγRI (B) and BaF/huFcγRI (C)

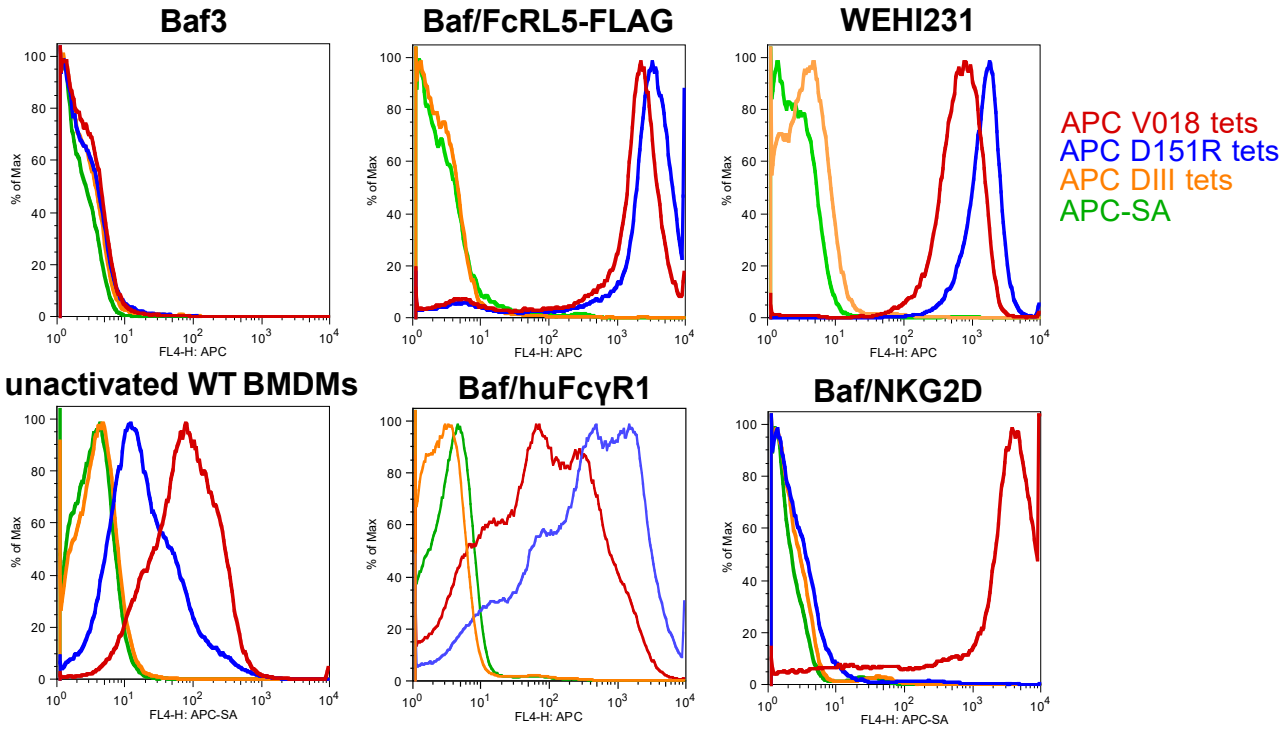

Figure 23: OMCP vs D132R staining on NKG2D, FCRL5, and FcγRI expressing cells.

The appropriate cell lines or primary cells were stained with 400ng of fluorescent OMCP tetramers (red line), D132R tetramers (blue line), DIII tetramers (orange line), or streptavidin control (green line). Note that NKG2D binding is completely lost with the D132R mutation, while binding to FCRL5 expressing cells (BaF/FCRL5 and WEHI231) and BaF/huFcγRI is retained. There is a moderate loss of binding of D132R to murine BMDMs.

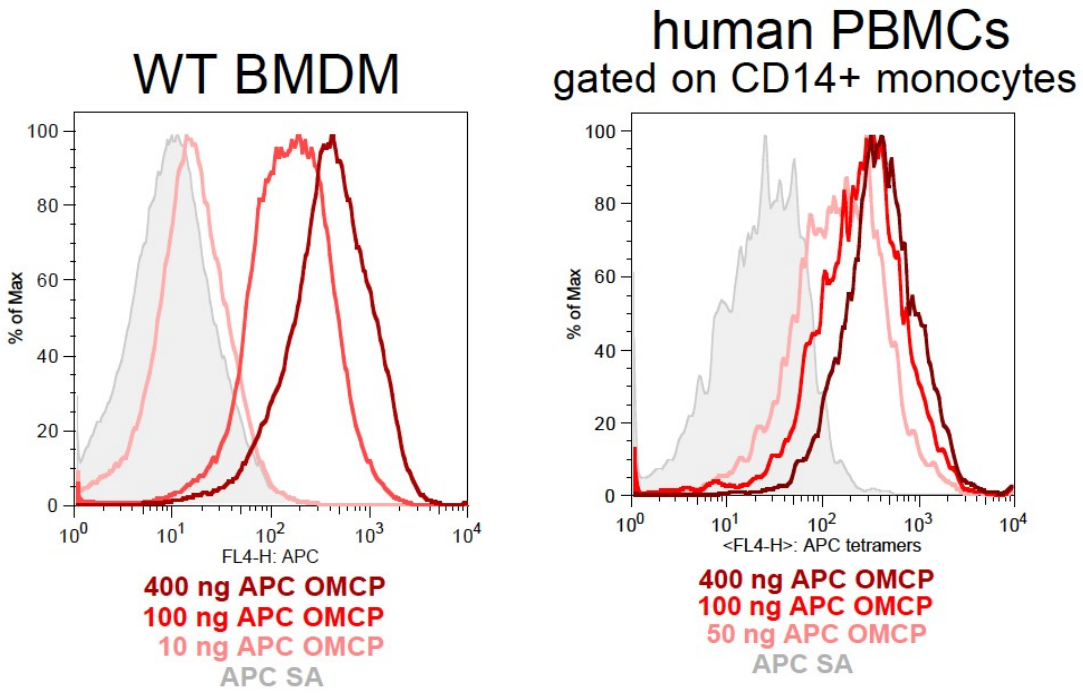

Figure 24: OMCP titration on WT BMDMs and human CD14+ monocytes

Bone marrow isolated from C56BL/6 femurs were cultured for 7 days in M-CSF containing media to generate bone marrow derived macrophages. Unactivated bone marrow derived macrophages were then stained for OMCP binding ability. Human blood was drawn from a healthy donor, and leukocytes were ficoll purified. M-CSF cultured BMDMs or fresh human PBMCs were stained with the indicated concentrations of labeled OMCP tetramer. There is a dose dependent increase in OMCP binding in both mouse macrophage and human monocyte subsets.

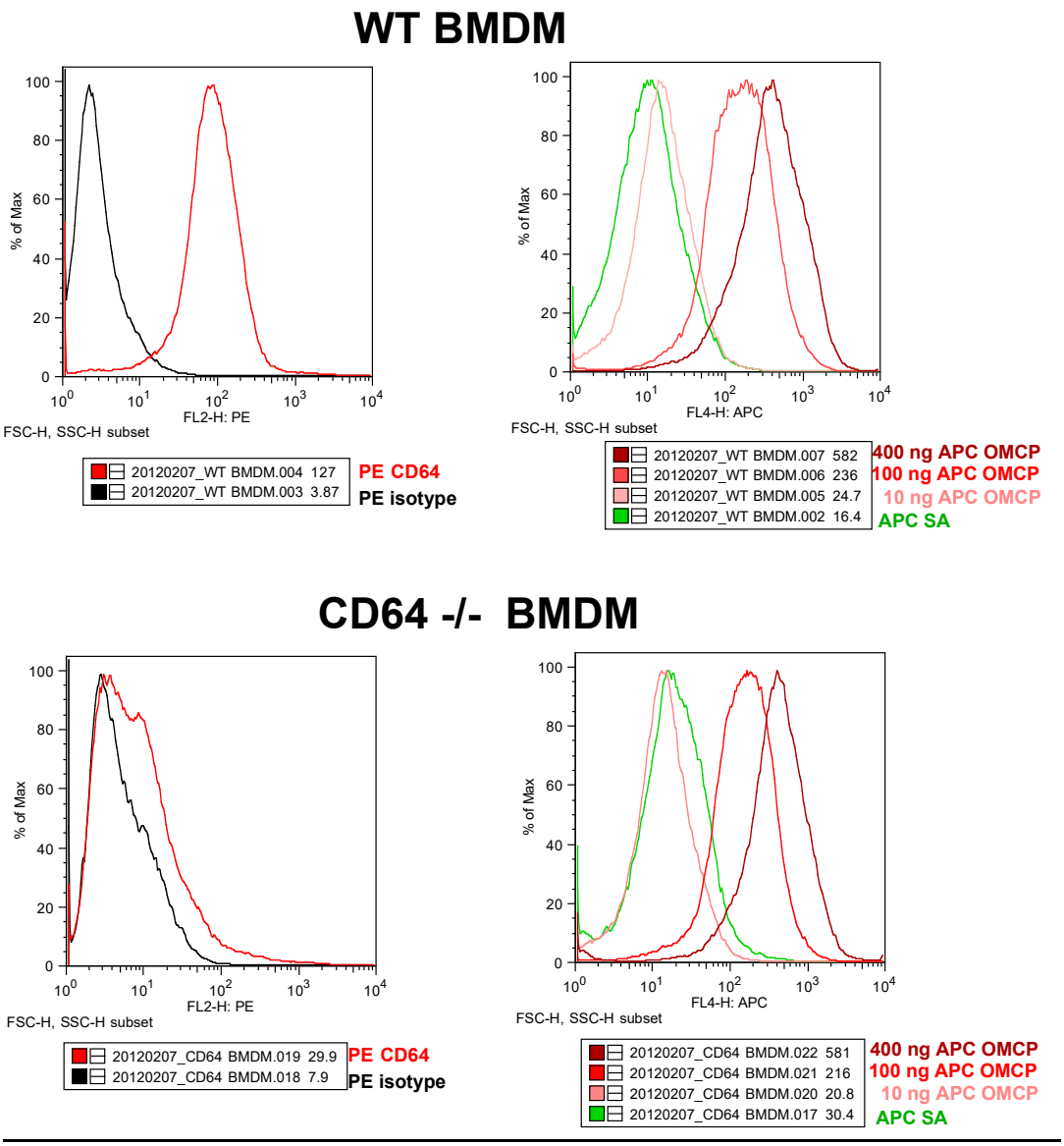

Figure 25: OMCP still binds to FcγRI (CD64) knockout mice

Bone marrow was isolated from wildtype C56BL/6 mice or FcγRI (CD64) knockout mice. Bone marrow was cultured for 7 days in M-CSF containing media. Unactivated bone marrow derived macrophages were then stained for FcγRI (CD64) expression and OMCP tetramer binding. Note that OMCP tetramer binding is unaffected in FcγRI knockout mice, despite the loss of FcγRI receptor expression.

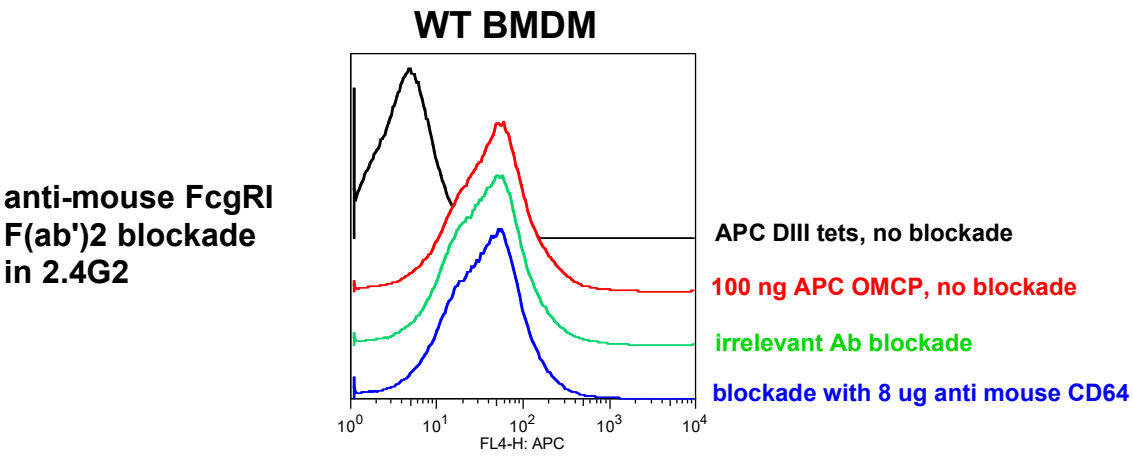

Figure 26: Anti-mFcγRI antibody blockade does not block OMCP binding to BMDMs

Murine BMDMs obtained from a wildtype C57BL/6 mouse were stained with 100 ng of APC OMCP or DIII control tetramers, or preincubated with a large excess of unlabeled anti-mFcγRI antibody or control antibody for 1 hour on ice prior to staining with 100 ng APC OMCP tetramers. The anti-mFcγRI antibody blockade was performed in the presence of 2.4G2 (anti-mFcγRII/ anti-mFcγRIII) supernatant from antibody producing hybridomas. Note that combined blockade with anti-mFcγRI, anti-mFcγRII, and anti-mFcγRIII antibodies does not reduce OMCP tetramer binding.

Baf/mouse FcgRI

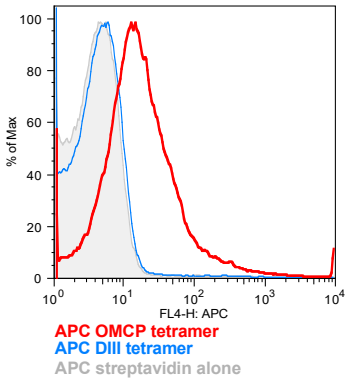

Baf/mouse FcgRIIb

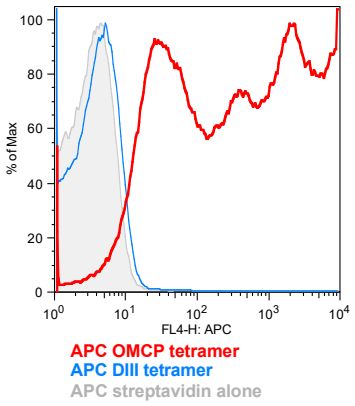

Baf/mouse FcgRIII

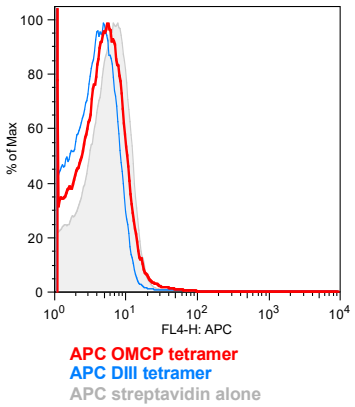

Baf/mouse FcgRIV

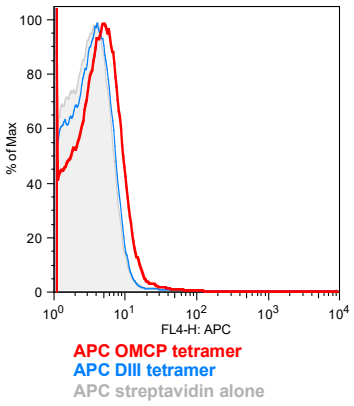

Baf/human FcγRI

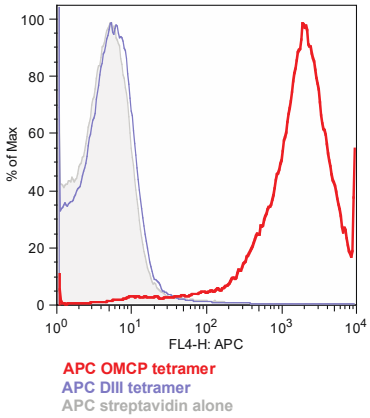

Baf/human FcγRIIa

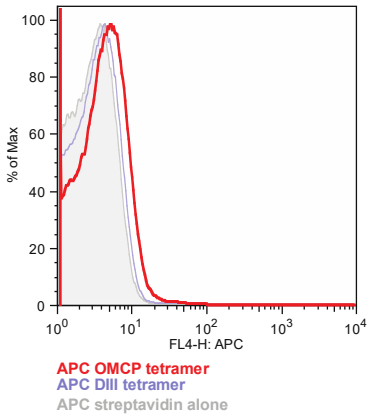

Baf/human FcγRIIIa

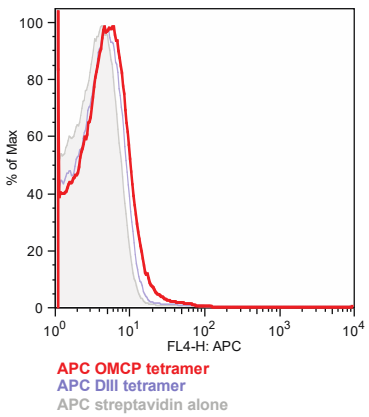

Figure 27: OMCP binds to murine FcγRI (CD64), murine FcγRII (CD32), and human FcγRI (CD64)

Mouse FcγRI, FcγRIIb, FcγRIII, and FcγRIV and human FcγRI, FcγRIIa and FcγRIIIa were cloned and retrovirally transduced into BaF/3 cell lines. Clones with highest receptor expression were sorted and expanded. Each receptor expressing cell line was tested for binding to 800ng APC labeled OMCP tetramer or DIII control. Binding of OMCP tetramers was observed in only the BaF/mFcγRI, BaF/mFcγRII, and BaF/huFcγRI cell lines.

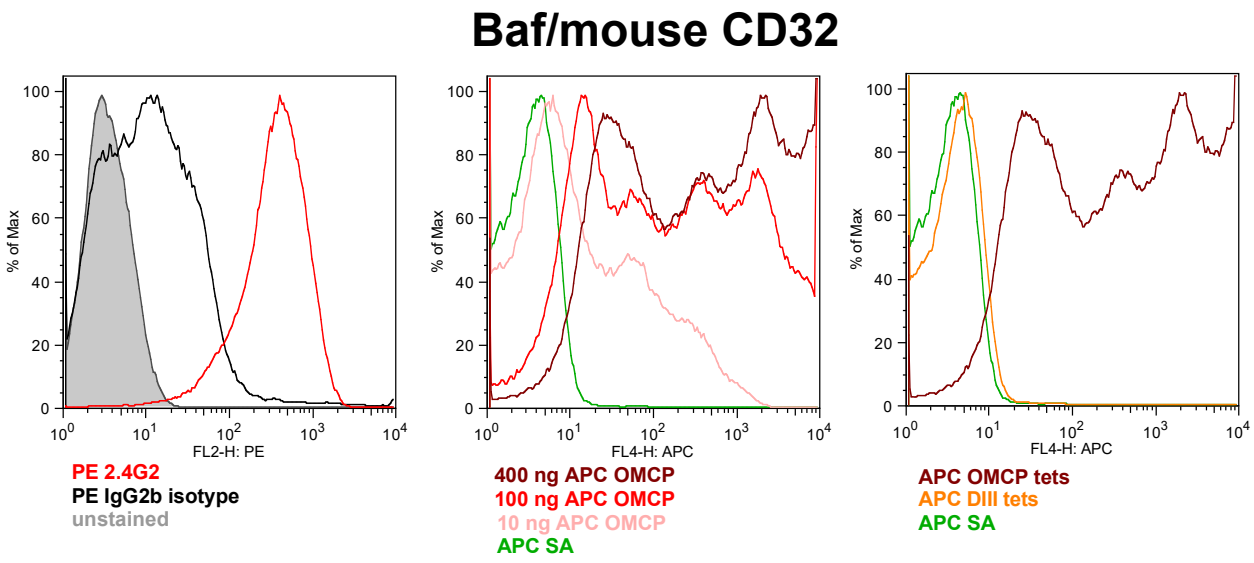

Figure 28: OMCP binding to mCD32 displays multiple peaks, despite uniform expression of the CD32 receptor

BaF/mFcγRII (CD32) was stained for expression of the FcγRII receptor using the PE 2.4G2 antibody. Note there is a uniform distribution of FcγRII expression in the polyclonal cell line. BaF/mFcγRII was stained for binding of the indicated concentrations of labeled OMCP tetramer. Note the unusual, reproducible multi-peaked binding pattern.

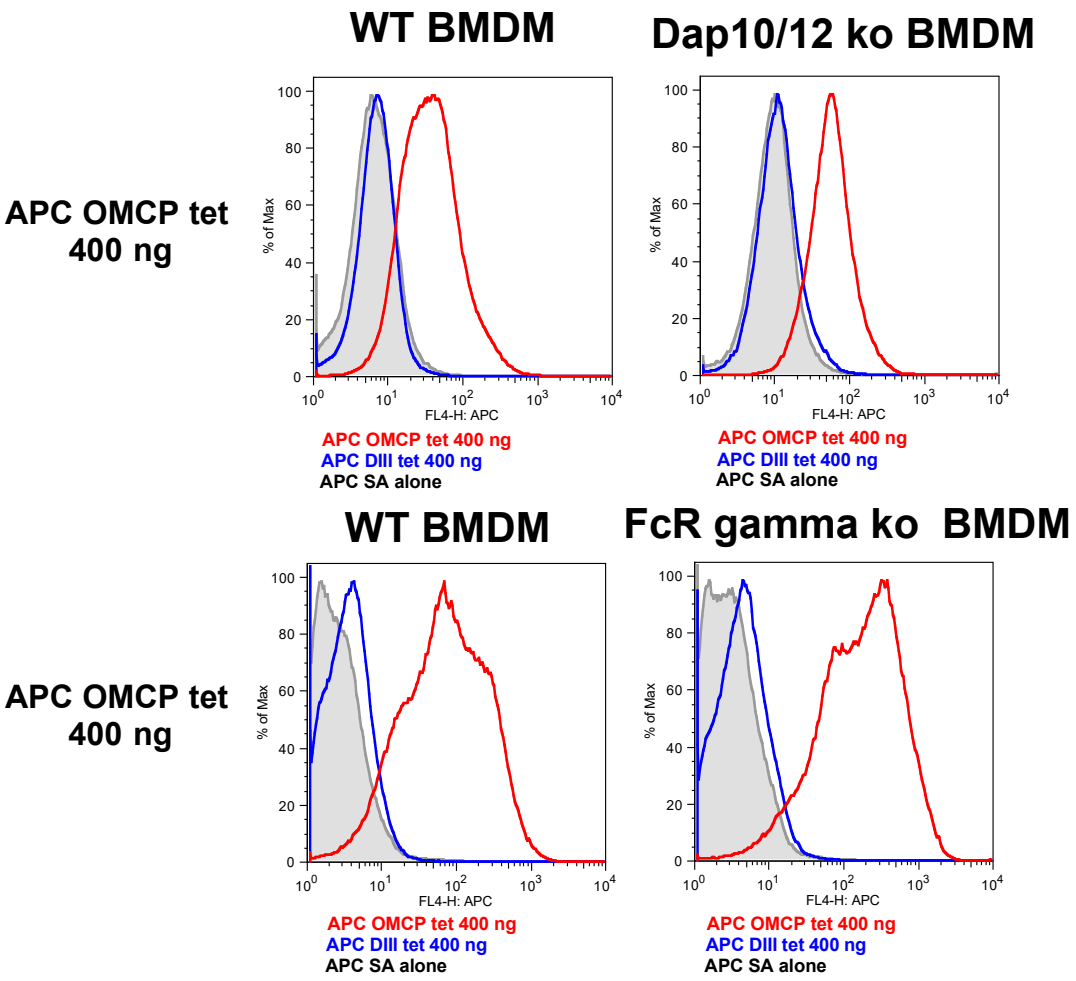

Figure 29: OMCP binding to murine BMDMs does not require expression of the adaptor molecules Dap10, Dap12, or FcRγ

BMDMs were generated from wildtype C57BL/6 mice, Dap10/Dap12 double knockout mice, or FcR gamma chain knockout mice. Cells were stained for binding to OMCP tetramers or DIII control. Note that there is unreduced binding of OMCP tetramers to the Dap10/Dap12 double knockout mice and FcR gamma chain knockout mice compared to wildtype. Experiments were performed independently, each wildtype control is presented.

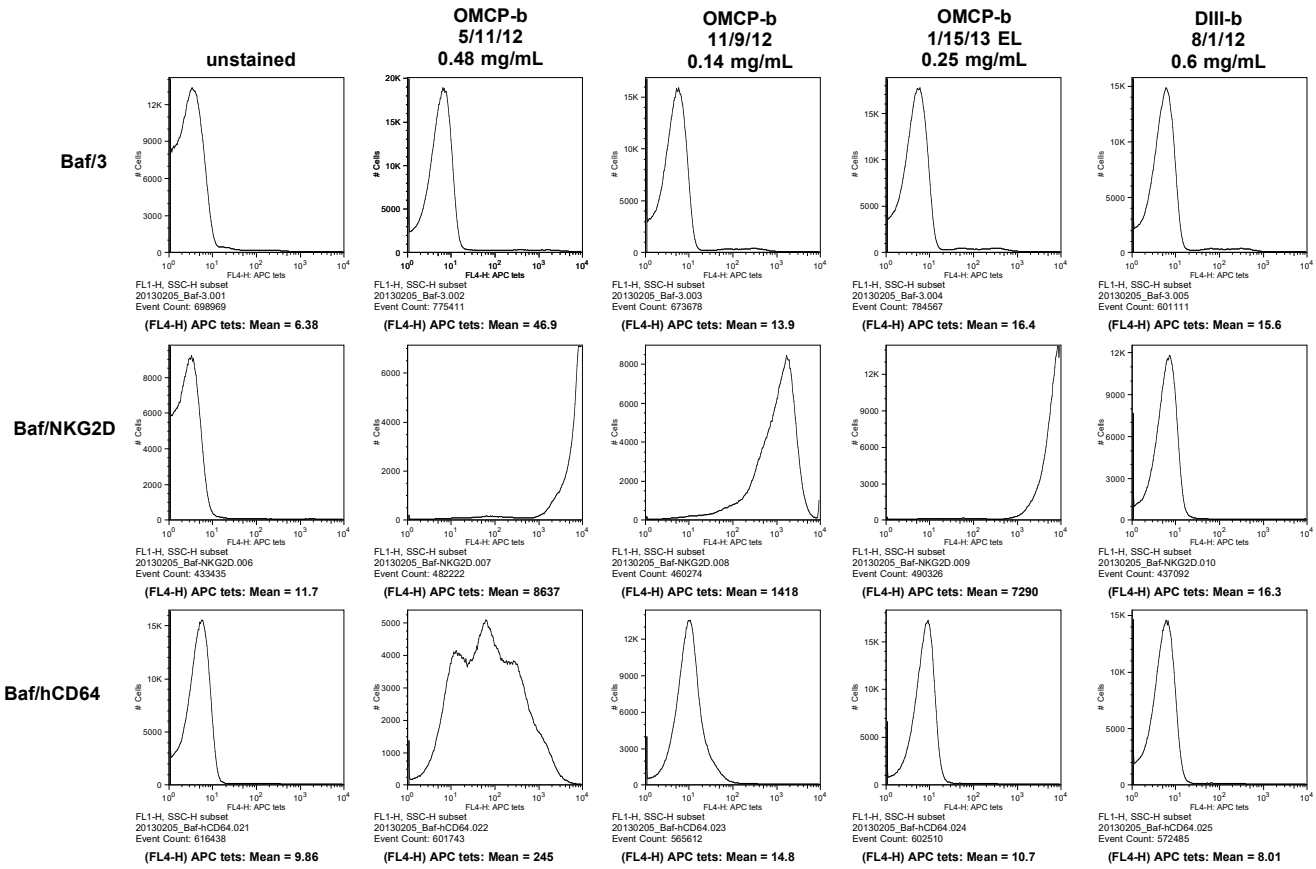

Figure 30: New batches of OMCP protein do not bind BaF/huFcγRI

Three separate OMCP inclusion body preparations (11/8/11 at 0.74 mg/mL, 11/23/11 at 0.37 mg/mL, and 5/1/12 at 0.48 mg/mL) have consistently bound to NKG2D and huFcγRI expressing cells (2nd column). A new batch of protein generated in our lab (11/9/12 at 0.14 mg/mL, 3rd column) was refolded and purified from inclusion bodies, and demonstrated binding to NKG2D, but not huFcγRI. An independently generated fully glycosylated OMCP batch made from mammalian 293F cells (1/15/13 EL at 0.25 mg/mL, 4th column) binds to NKG2D, but not huFcγRI by flow cytometry or SPR (Eric Lazear). Initial FcR binding was not reproduced with protein batches purified after 5/11/12.

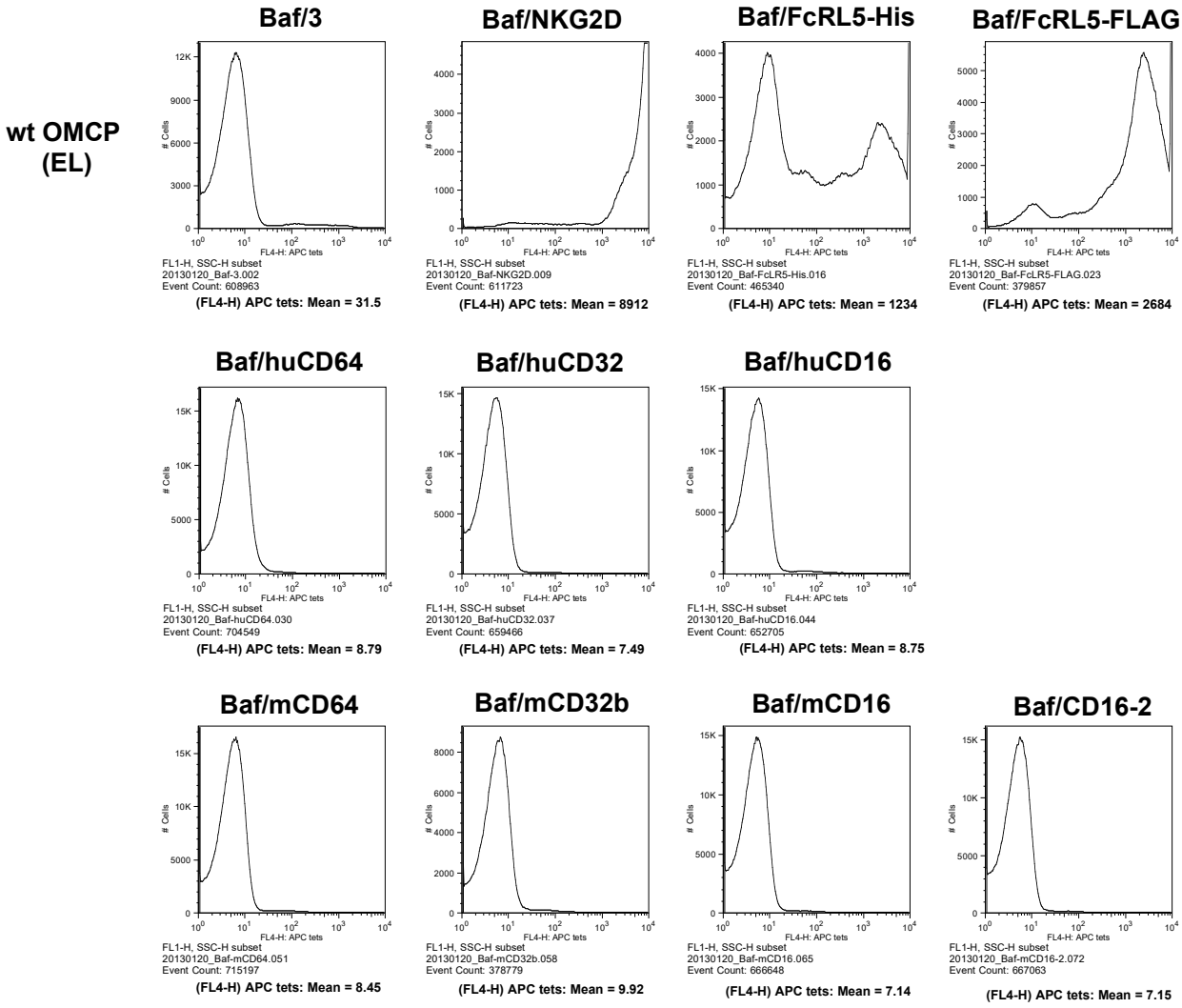

Figure 31: Characterization of OMCP binding using 293F derived protein

Mammalian derived OMCP protein produced by expression in 293F cells does not show binding to huFcγRI or any FcR tested. This batch of OMCP does demonstrate consistently high binding to NKG2D and FCRL5 expressing cells. Protein generated by Eric Lazear (Fremont lab).

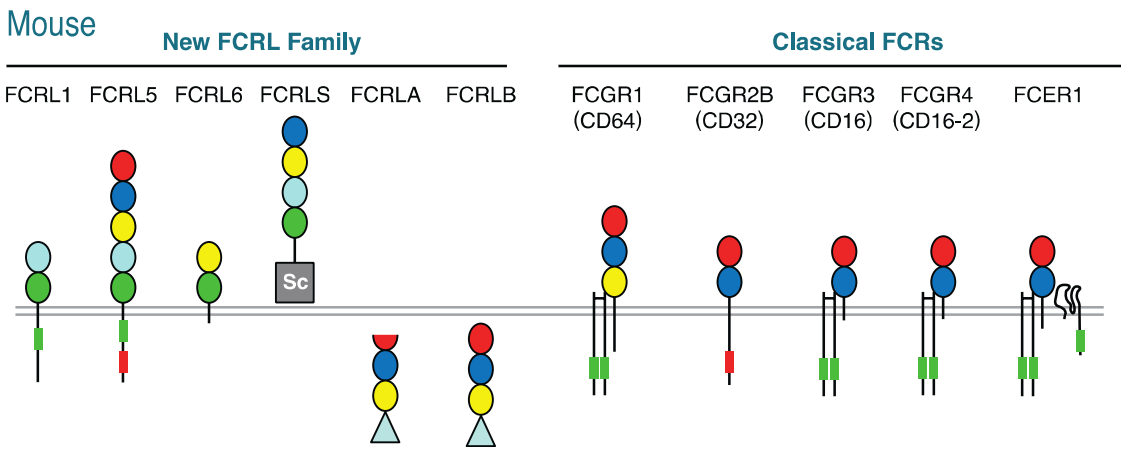

Figure 32: Comparison of mouse FCRL and FcR family members.

Extraceullular Ig domains are color-coded according to phylogenetic relationships as determined by Ig domain amino acid sequence alignments. Cytoplasmic ITIMs or ITAMs are represented by red or green boxes, respectively. Activating FcR family members are shown in complex with the FcεRg1 adaptor subunit. FcεR1a is also shown associated with FcεR1b/MS4A2. (Note the domain homology between FCRL5 and FcγR1). Figure from [13]

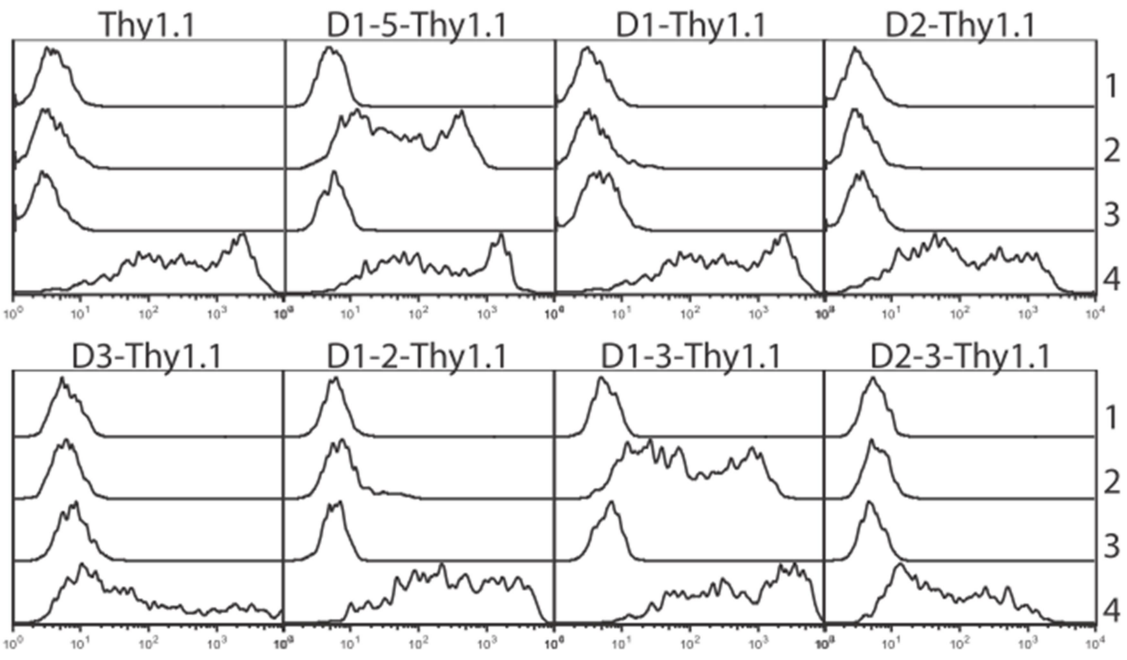

Figure 33: The three N-terminal Ig domains of FCRL5 are necessary and sufficient for OMCP binding.

293T cells transfected with Thy1.1 or the indicated FCRL5-Thy1.1 fusion construct domain truncations were stained with negative control DIII tetramers (line 1), OMCP tetramers (line 2), isotype control mAb (line 3), or anti-Thy1.1 mAb (line 4). Results are representative of three independent experiments. Figure from [8]):

APPENDIX 2: CrmD binding to FcRs

Introduction:

Cowpox virus has evolved an arsenal of immunomodulatory proteins with specificities for virtually all known innate and adaptive immune pathways. In addition to OMCP, cowpox encodes a family of chemokine binding proteins known as the cytokine response modifying (Crm) family (CrmA, CrmB, CrmC, CrmD, and CrmE). CrmA is a viral caspase inhibitor developed to inhibit apoptosis of infected cells [83]. The members CrmB, CrmC, CrmD, and CrmE have been identified as viral TNF receptor homologs [84]. CrmB and CrmD also have additional anti-chemokine activity. Here we focus on the multifunctional cowpox immunevasin CrmD.

CrmD is a 46 kDa secreted glycoprotein that is composed of a distinct N-terminal domain and C-terminal domain [85]. The N-terminal of CrmD is homologous to the TNF receptor superfamily, and has been shown to bind TNFα. The independent C-terminal domain has been identified to bind to diverse chemokines, and recent investigation has identified binding of the C-terminal domain to Fc receptors. Full length CrmD can bind TNFα and FcRs simultaneously, and can also bind FcRs in the presence of chemokine, suggesting that these three binding sites are independent of each other.

C terminal CrmD is sufficient for FcR binding on macrophages, and this binding is blocked by soluble FcR blockade (M. Epperson, unpublished data). Surface plasmon resonance experiments have determined that CrmD is capable of binding to all tested

human and mouse FcRs, with the highest affinity for FcγRIII (CD16) and the lowest affinity for FcγRI (CD64). Preliminary crystal structure of CrmD in complex with FcγRIII suggests that CrmD is binding at the “elbow” region of the FcR, in close proximity to where endogenous IgG binds (M. Epperson, unpublished data). These observations suggest that CrmD has the capacity to bind to Fc receptors on macrophages, and is positioned in such a way as to block FcR recognition of IgG on opsonized virus.

To test this hypothesis, we used Ba/F3 cell lines that had been transduced to stably express mouse or human Fc receptors on their surface. We tested for CrmD’s ability to block binding of soluble IgG as well as heat aggregated IgG to simulate immune complexes.

Experimental Methods:

Cells and Cell Lines

Ba/F3 cells were retrovirally transduced as described previously in Appendix 1. Ba/F3 cells expressing murine FcγRI (CD64), murine FcγRIIb (CD32), murine FcγRIII (CD16), murine FcγRIV (CD16-2), human FcγRI (CD64), human FcγRIIa (CD32), human FcγRIIIa (CD16), FCRL5-FLAG, and FCRL5-His, as well as a mock transduced Ba/F3 control were used in these experiments.

Staining and Blockade

For protein blockade experiments, Ba/F3 cells were incubated with a vast excess (8ug) of non biotinylated CrmD, OMCP, or DIII control on ice for 1 hr. Cells were stained with

400ng APC labeled OMCP tetramers on ice for 1 hr. Cells were washed x3 with sorting buffer, then analyzed by FACS.

For IgG blockade experiments, Ba/F3 cells were incubated with vast excess (1ug -8ug) of CrmD, OMCP, or DIII control for 30 min on ice. Cells were then incubated with (200ng - 11.2ug) of mouse gamma globulin (Talecris Biotherapeutics, Research Triangle Park, NC), for an additional 30 min on ice. Cells were washed, then stained with either PE goat anti-mouse (BD Pharmingen, San Jose CA) or APC goat anti-mouse F(ab')2 (R&D Systems, Minneapolis MN) secondary antibodies. Cells were washed, then analyzed by FACS.

For dual label experiments, Ba/F3 cells were blocked with excess cold CrmD, OMCP or DIII control for 1 hr, then incubated with APC-labeled OMCP tetramers and mouse gamma globulin for 1 hr on ice. Cells were washed, then stained with PE goat anti-mouse secondary for 30 min on ice.

Heat aggregated IgG

To produce heat aggregated IgG, purified concentrated mouse gamma globulin was heated in water bath at 63^{o}C for 1 hr. Aggregates were diluted prior to use.

Results:

CrmD blocks monomeric IgG from binding FcRs

Because CrmD is expected to bind in close proximity to the IgG binding site on Fc receptors, we were interested to see if CrmD is able to prevent IgG binding on FcR bearing cells. We preincubated cells with 2-8 ug of CrmD, OMCP, or DIII control, then incubated with a vast excess (11.2 ug) of mouse gamma globulin. We stained cells using a PE goat anti-mouse secondary antibody or APC goat anti-mouse F(ab')2 fragments.

Our results showed that excess OMCP is not able to block FcR binding of mouse gamma globulin. However, CrmD clearly is able to block IgG binding to mouse FcγRIIb (CD32) and FcγRIII (CD16) (Fig 34), even at the lowest concentrations of CrmD tested and in the presence of 5x excess of IgG. CrmD can also partially block IgG binding to mouse FcγRI (CD64) under these conditions (Fig 34). This partial blockade is not unexpected, as FcγRI is the high affinity Fc receptor with the highest IgG affinity, yet CrmD has low affinity for FcγRI compared to the other FcRs.

The IgG blocking results were repeated using APC goat anti-mouse F(ab'2) fragments to avoid issues with using Fc bearing antibodies as a secondary stain. These experiments were also repeated using varying concentrations of protein and mouse gamma globulin, and we consistently see very efficient blocking of IgG binding with monomeric CrmD. Monomeric OMCP is unable to block IgG binding to Fc receptors

even in cases of high OMCP concentration (16ug) with much lower mouse gamma globulin (200ng).

CrmD blocks heat aggregated IgG binding to FcRs

Because of these striking results demonstrating complete blockade of IgG binding when cells are preincubated with monomeric CrmD, we subsequently made our experiments more rigorous by challenging CrmD with heat aggregated IgG. Soluble IgG is heated at 63^{o}C for 1 hr to form larger aggregated complexes that mimic immune complexes. We preincubated FcR bearing cells with CrmD for 1 hr, then incubated with soluble mouse gamma globulin or heat aggreagated mouse gamma globulin, and stained with PE goat anti-mouse. Of note, the MFI of heat aggregated IgG binding to FcRs is higher than soluble IgG in all cases, consistent with the increased avidity of the complexed IgG.

Our experiments with heat aggregated IgG demonstrated that CrmD is capable of complete blockade of aggregated IgG on mouse FcγRIIb (CD32) and FcγRIII (CD16) bearing cells (Fig 35). There was a partial blockade on human FcγRI (CD64) and mouse FcγRI (CD64) bearing cells, which is consistent with the very high affinity these FcRs have for IgG. CrmD was unable to block heat aggregated IgG binding to human FcγRIIa (CD32a), but was able to block soluble IgG to huFcγRIIa (CD32a) (Fig 35). This is consistent with the fact that CrmD has low affinity for the FcγRII receptor. These results demonstrate that CrmD is capable of blocking not only monomeric IgG from binding to FcRs, but also the higher avidity aggregated IgG from binding to the tested

Fc receptors, which may be more meaningful in the context of immune complex formation during viral infection.

Determination of EC50 values for CrmD blocking activity on each FcR

The previous experiments clearly showed that CrmD is very effective at blocking IgG and immune complex binding to all of the FcRs tested. To further assess this blocking ability, we sought to determine the EC50 values for CrmD's IgG blocking activity for each FcR.

We preincubated cells with 1ng - 8000ng of CrmD, then incubated with 200ng mouse gamma globulin, and used a PE goat anti-mouse secondary stain to determine the amount of IgG that was able to bind the FcR bearing cells. We tested 1, 10, 25, 50, 125, 250, 500, 1000, and 8000 ng CrmD blockade on BaF3 cells expressing human FcγRI, FcγRIIa and FcγRIIIa, and mouse FcγRI, FcγRIIb, FcγRIII, and FcγRIV. By plotting CrmD concentration vs MFI, we were able to determine the concentration of CrmD at half maximal inhibitory response and extrapolate the EC50 of this binding assay (Fig 36). The EC50 values determined by flow compare well against the KD of the CrmD-FcR affinity as determined by SPR (Table 1). However, the EC50 value determined by this flow assay also takes into account the affinity of each FcR for mouse gamma globulin, which is another factor in determining how easily CrmD is able to displace or prevent IgG binding to the FcRs. The affinity of each FcR for IgG also varies based on isotype of IgG. Here we did not use IgG purified by isotype, but rather mixed mouse gamma globulin from normal mouse serum.

CrmD preincubation successfully blocks OMCP binding FcRs

OMCP had initially been identified to bind to the high affinity FcγRI Fc receptor on both mouse and human cells as well as mouse FcγRIIb (Appendix 1). CrmD is known to bind to all tested Fc receptors with varying affinities. We therefore tested whether CrmD preincubation of Ba/F3 cells expressing FcRs is sufficient to block OMCP binding and determine if OMCP and CrmD bind to the same location on Fc receptors.

In these experiments, we incubated BaF3/FcR cells with a vast excess (8000 ng) of nonbiotinylated CrmD, OMCP, or DIII control monomers, then stained with 400ng of APC labeled OMCP tetramers and analyzed binding by flow cytometry. CrmD preincubation was successful in blocking OMCP binding to mouse FcγRIIb and human FcγRI expressing cells, but not FCRL5 expressing cells (Fig 37). The almost complete abrogation of OMCP tetramer binding on BaF/mFcγRIIb and BaF/huFcγRI by CrmD preincubation suggests that CrmD has a higher affinity for the FcRs than OMCP and can directly compete with OMCP for binding. On the control BaF/FCRL5 cells, CrmD blockade is ineffective, which is as expected since CrmD is not known to bind to FCRL5, whereas OMCP blockade partially blocks OMCP tetramer binding on FCRL5 bearing cells (Fig 37).

The crystal structure of CrmD in complex with the human FcγRIIIa Fc receptor suggests that CrmD is binding in the region of the FcR where IgG binds. This suggests that both viral proteins may be targeting the same region of the Fc receptor, which is likely the

functional Fc binding site. However CrmD appears to bind with higher affinity and is successful in preventing simultaneous IgG binding.

CrmD blocks OMCP tetramer binding and IgG binding simultaneously

Our previous experiments suggested that CrmD binds FcRs at its functional IgG binding site and is sufficient to block IgG and aggregated IgG binding to FcRs. Additionally, we saw that CrmD can effectively block OMCP binding to FcRs, suggesting both viral proteins bind in the same vicinity. Here, we tested whether CrmD can block OMCP tetramer binding and IgG binding simultaneously to further validate our hypothesis that both proteins interact with FcRs at the IgG binding site.

In these experiments, we preincubated BaF3/FcR cells with unlabeled CrmD tetramer, OMCP tetramer, or DIII tetramer. We then dual labeled the cells with APC labeled OMCP tetramers and the PE goat anti-mouse secondary antibody. We saw that OMCP tetramers and mouse IgG are able to bind FcR bearing cells at the same time (Fig 38). The OMCP tetramer block showed that OMCP can block OMCP binding, but not IgG binding. However, CrmD can completely block OMCP binding as well as partially block IgG binding on FcγRI (Fig 38). Blocking with DIII control monomers had no effect on OMCP tetramer binding or IgG binding, as expected. These experiments were repeated on BaF3 cells expressing huFcγRI, mFcγRI, and mFcγRIIb, and confirm that CrmD is very effective in preventing both OMCP and IgG from binding to classical Fc receptors.

Discussion:

CrmD is clearly a multifunctional immunoevasion protein produced by cowpox. In addition to its established roles as a TNFα sink and chemokine sequestration, our results show that CrmD is capable of blocking IgG binding to Fc receptors. The effectiveness of this CrmD blockade depends on both the affinity of CrmD with the FcR, with stronger blockade on FcγRIII and less effective blockade on the FcγRII receptor, as well as the affinity of IgG for the FcR, with less effective blockade on the high affinity FcγRI receptor.

This ability to bind to Fc receptors and prevent IgG and immune complex binding, is a simple yet effective method to avoid immune detection. Viral particles opsonized by antibodies may be unable to be recognized and removed by macrophages and other FcR bearing cells in the context of excess secreted CrmD which bind with high affinity to FcRs, preventing simultaneous binding and recognition of IgG or immune complexes.

Preliminary studies have also demonstrated that CrmD induces internalization of the FcRs on macrophages (M. Epperson). This activity, combined with the TNFα and chemokine sequestration of the N-terminal portion of CrmD, may result in a situation where N-terminal CrmD binds TNFα and chemokines, while C-terminal CrmD binds FcRs at the IgG binding domain. This may trigger internalization of the complex and degradation of inflammatory TNFα and chemokines required for the full activation of the antiviral response. In this context, CrmD binding to FcRs acts as a trigger for

endocytosis, and the exclusion of simultaneous IgG binding was evolved to avoid unwanted immune complex internalization.

Our other staining experiments demonstrated that CrmD binding precludes OMCP tetramer binding. This suggests that CrmD and OMCP are binding to the same site on FcRs, likely the functional IgG binding site. However, CrmD is able to completely abrogate IgG binding to FcRs, whereas even a vast excess of OMCP tetramers is unable to compete with IgG binding. This may be because OMCP binds most strongly to FcγRI, but may be unable to compete with the very high affinity that the FcγRI receptor has for IgG. Conversely, CrmD has highest affinity binding to human FcγRIIIa, which is a weaker affinity IgG receptor, where IgG is more easily displaced.

To supplement the discourse begun in Appendix 1 on the possible source of inappropriate binding of FcR seen in early batches of OMCP protein, we note that in the experiments described above, OMCP behaves similarly to IgG. Namely, CrmD is capable of blocking OMCP binding (Fig 38) as effectively as it can block IgG binding to FcRs (Fig 34). This supports the possibility that inappropriate OMCP binding of FcRs may have be due to contamination of biotinylated antibody.

Figures:

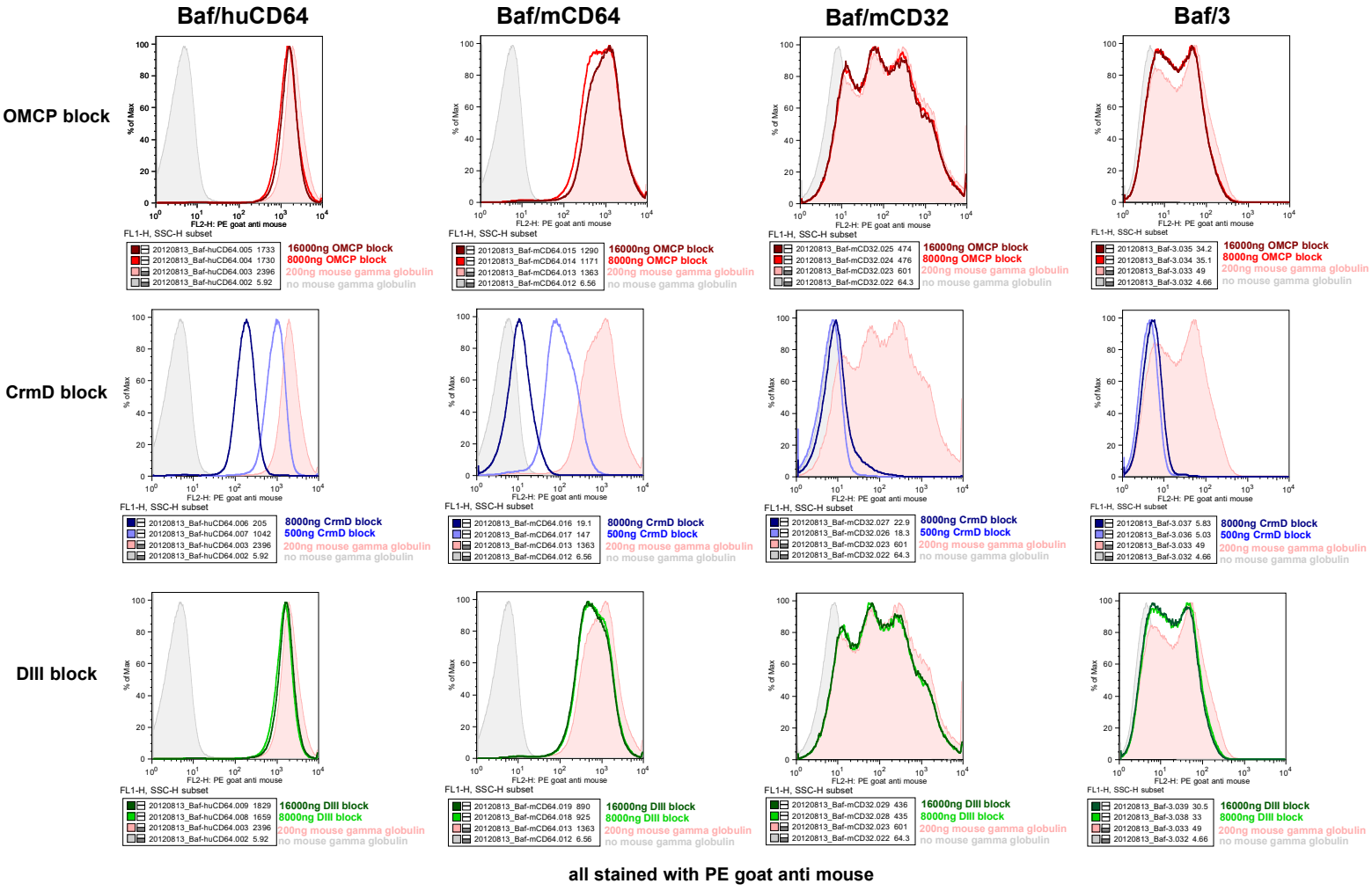

Figure 34: CrmD blocks monomeric IgG from binding FcRs

BaF/3 cells expressing human CD64, mouse CD64, or mouse CD32 (huCD32a, huCD16, muCD16, muCD16-2 not shown) were preincubated with OMCP monomer, CrmD monomer, or DIII monomer for 1 hr on ice. Concentrations of protein used varied from 1000 ng to 16000 ng in independent experiments. After preincubation with blocking protein, cells were incubated with mouse gamma globulin (concentrations tested varied

from 200ng to 11000 ng). Cells were washed, then stained with PE goat anti-mouse secondary antibody or an APC goat anti-mouse F(ab1)2 (not shown) to assess amount of IgG bound to cells. Cells were washed twice and analyzed by flow cytometry. Representative results from three independent experiments.

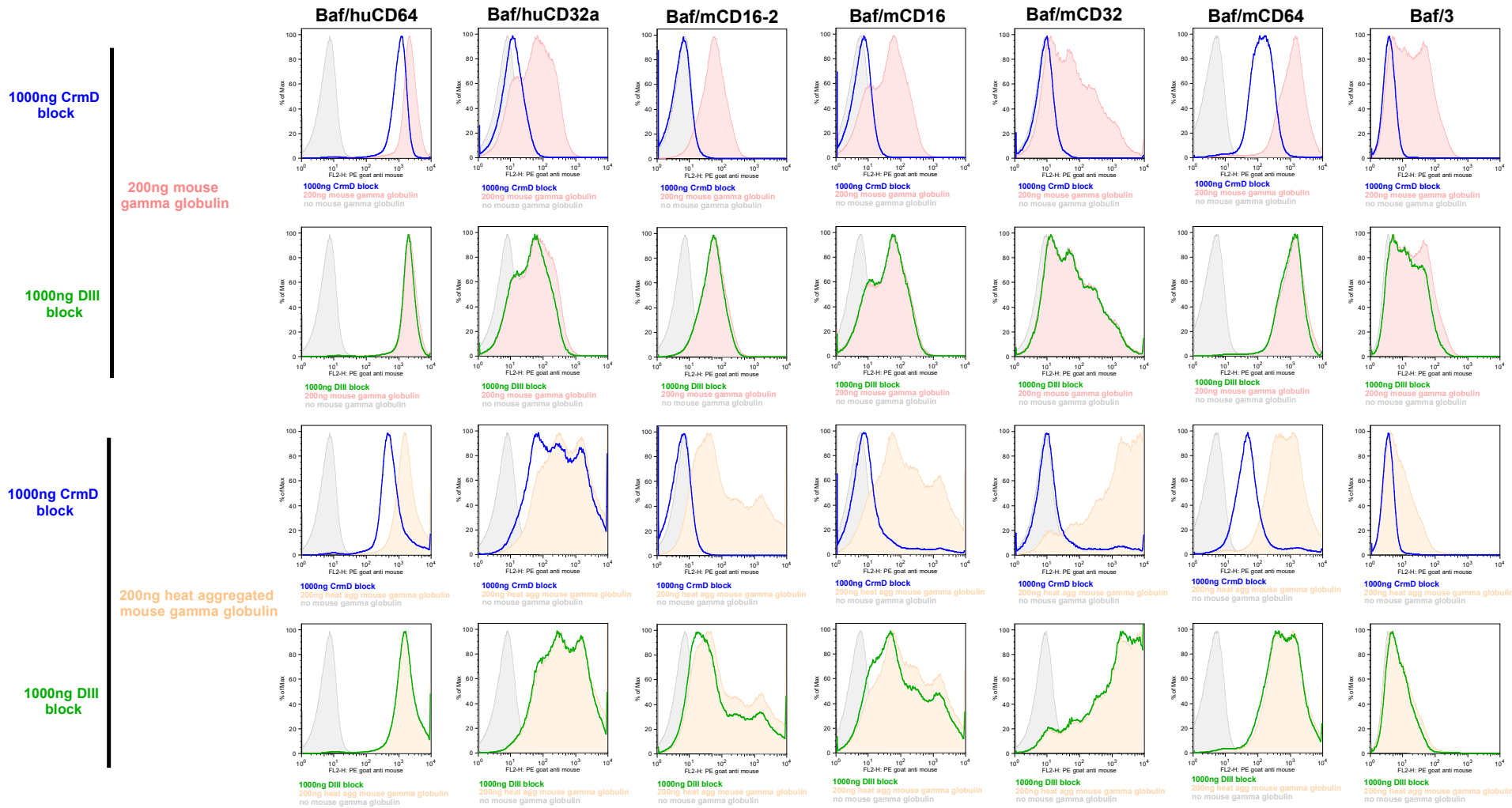
Baf/huCD64
Baf/huCD32a
Baf/mCD16-2
Baf/mCD16
Baf/mCD32
Baf/mCD64
Baf/3
1000ng CrmD block
200ng mouse gamma globulin
1000ng DIII block
1000ng CrmD block
200ng heat aggregated mouse gamma globulin
1000ng DIII block
% of Max
FL2-H: PE goat anti mouse
1000ng CrmD block
200ng mouse gamma globulin
no mouse gamma globulin
1000ng DIII block
200ng mouse gamma globulin
no mouse gamma globulin
1000ng CrmD block
200ng heat agg mouse gamma globulin
no mouse gamma globulin
1000ng DIII block
200ng heat agg mouse gamma globulin
no mouse gamma globulin

Figure 35: CrmD blocks heat aggregated IgG from binding FcRs

BaF/3 cells expressing human CD64, CD32a, CD16, or mouse CD64, CD32, CD16, or CD16-2 were preincubated with 1000 ng CrmD monomer or DIII monomer for 1 hr on ice. After preincubation with blocking protein, cells were incubated with 200ng mouse gamma globulin (top two rows) or 200ng heat aggregated mouse gamma globulin (bottom two rows). Cells were washed, then stained with PE goat anti-mouse secondary antibody to assess amount of IgG bound to cells. Cells were washed twice and analyzed by flow cytometry. Representative results from two independent experiments. Heat aggregated IgG was made the day of each experiment by incubating concentrated monomeric IgG (11.2 mg/mL) at 63^{o}C for 1 hr. Heat aggregated IgG was diluted prior to use in sterile PBS.

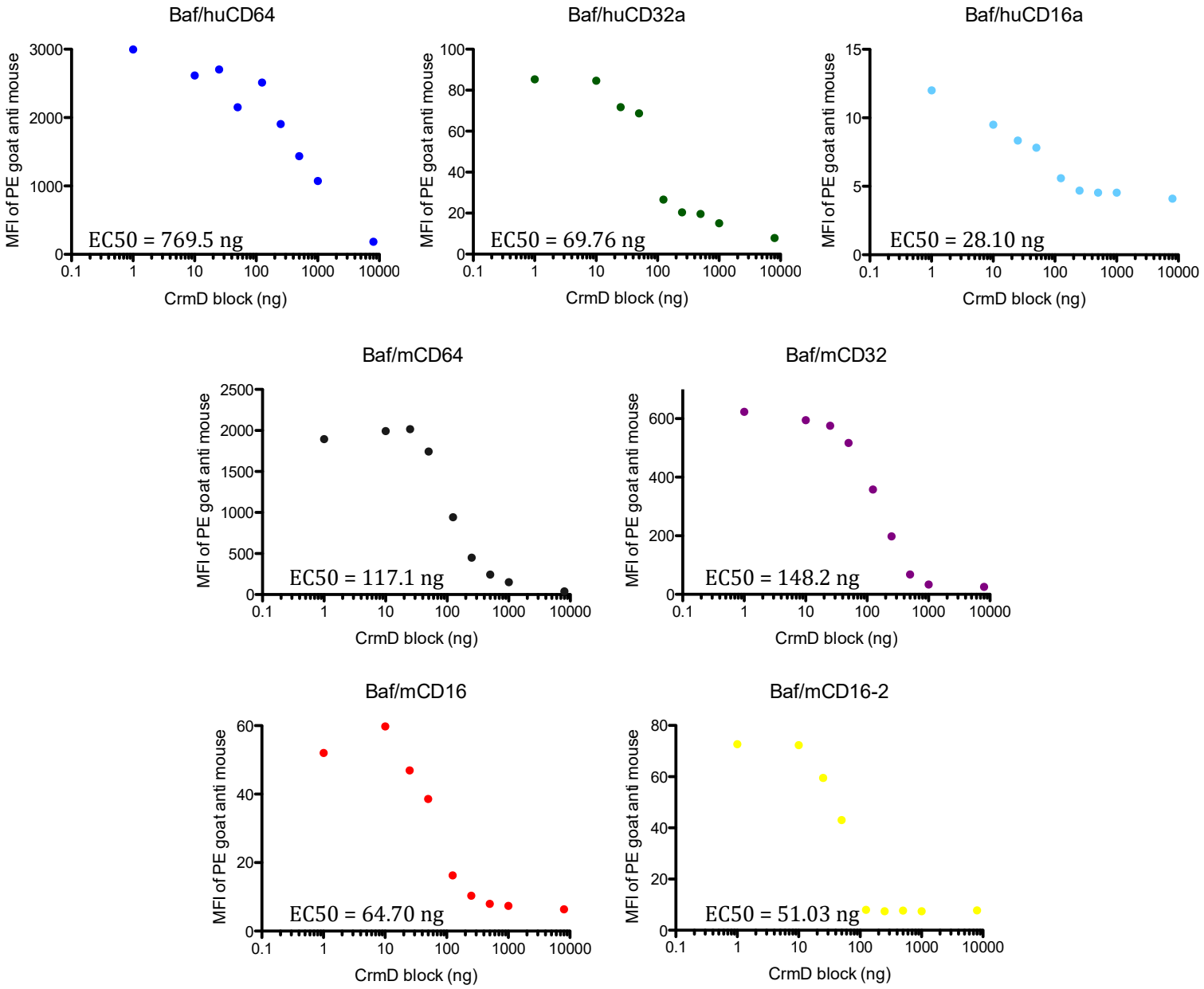
Baf/huCD64
MFI of PE goat anti mouse
3000
2000
1000
0
EC50 = 769.5 ng
0.1
1
10
100
1000
10000
CrmD block (ng)
Baf/huCD32a
MFI of PE goat anti mouse
100
80
60
40
20
0
EC50 = 69.76 ng
0.1
1
10
100
1000
10000
CrmD block (ng)
Baf/huCD16a
MFI of PE goat anti mouse
15
10
5
0
EC50 = 28.10 ng
0.1
1
10
100
1000
10000
CrmD block (ng)
Baf/mCD64
MFI of PE goat anti mouse
2500
2000
1500
1000
500
0
EC50 = 117.1 ng
0.1
1
10
100
1000
10000
CrmD block (ng)
Baf/mCD32
MFI of PE goat anti mouse
600
400
200
0
EC50 = 148.2 ng
0.1
1
10
100
1000
10000
CrmD block (ng)
Baf/mCD16
MFI of PE goat anti mouse
60
40
20
0
EC50 = 64.70 ng
0.1
1
10
100
1000
10000
CrmD block (ng)
Baf/mCD16-2
MFI of PE goat anti mouse
80
60
40
20
0
EC50 = 51.03 ng
0.1
1
10
100
1000
10000
CrmD block (ng)

Figure 36: Determination of EC50 values for CrmD blocking activity on each FcR

BaF/3 cells expressing human CD64, CD32a, CD16a, or mouse CD64, CD32, CD16, or CD16-2 were preincubated with 1ng, 10ng, 25ng, 50ng, 125ng, 250ng, 500ng, 1000 ng, or 8000ng of CrmD monomer for 1 hr on ice. After preincubation with CrmD protein, cells were incubated with 200ng of mouse gamma globulin for 1 hr on ice. Cells were washed, then stained with PE goat anti-mouse secondary antibody to assess amount of IgG bound to cells. Cells were washed and analyzed by flow cytometry and MFI of PE goat anti-mouse was recorded. CrmD concentration was plotted against MFI, and the EC50 concentration at half maximal was extrapolated using Graphpad Prism software.

	EC50 mIgG blockade activity (ng)	K_D CrmD–FcR binding affinity by SPR (nM)
BaF/huCD16a	28.10	3.33
BaF/mCD16-2	51.03	N/A
BaF/mCD16	64.70	3.29
BaF/huCD32a	75.47	8.78
BaF/mCD64	117.1	22
BaF/mCD32	148.2	4.19
BaF/huCD64	769.5	24

Table 1: Comparison of the EC50 by flow against the KD of CrmD-FcR affinity by SPR

CrmD concentration was plotted against MFI of PE goat anti-mouse, and the EC50 concentration at half maximal was extrapolated using Graphpad Prism software as described. This table lists the EC50 values determined by the flow cytometry assay compared to the equilibrium dissociation constant K_D values determined by surface plasmon resonance (Megan Epperson) for each of the human and murine Fc receptors.

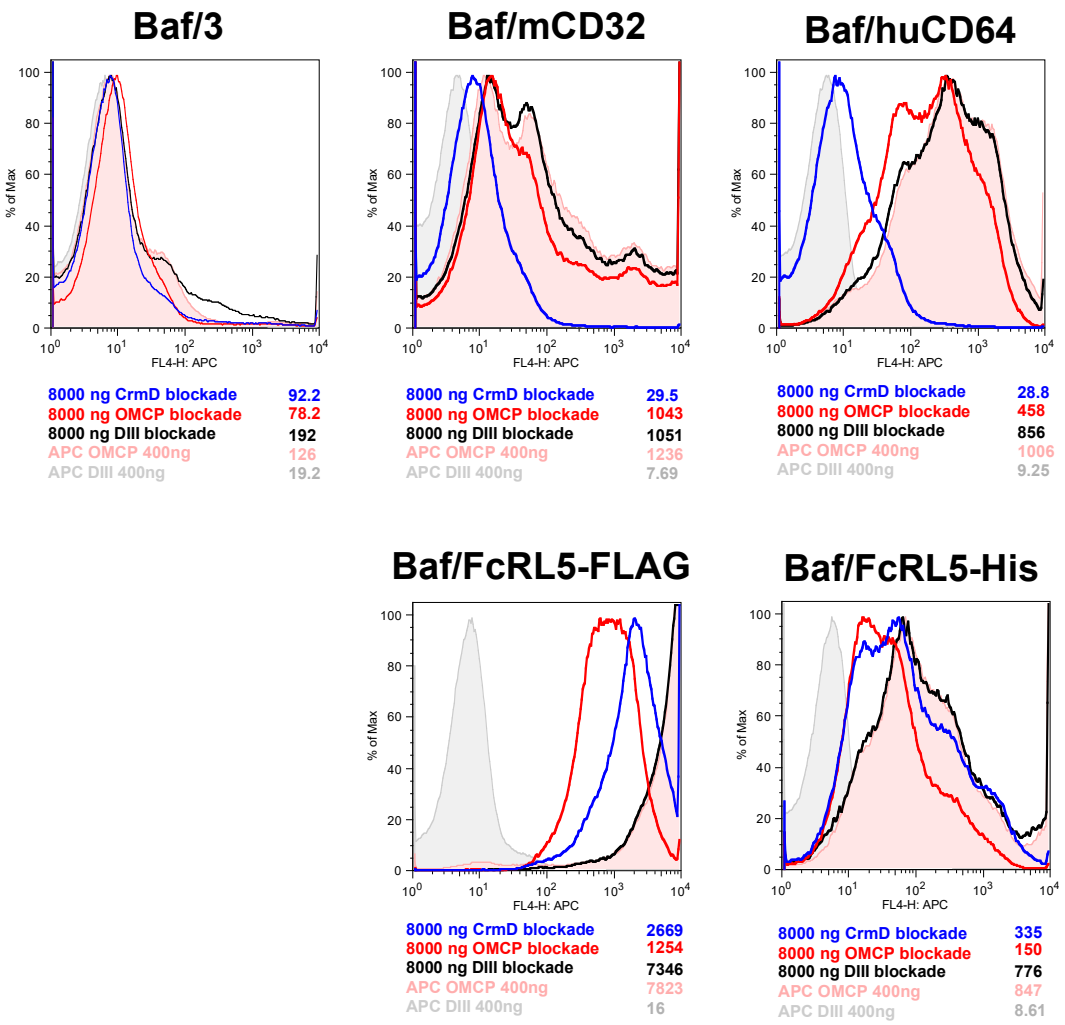

Figure 37: CrmD preincubation successfully blocks OMCP binding FcRs

BaF/3 cells expressing human CD64 or mouse CD32 (human CD32a, CD16a, mouse CD64, CD16, or CD16-2 not shown) were preincubated with 8000ng of CrmD monomer, OMCP monomer, or DIII monomer for 1 hr on ice. After preincubation with protein, cells were incubated with 400ng of APC labeled OMCP tetramers for 1 hr on ice. Cells were washed x3, then analyzed by flow cytometry to assess amount of OMCP binding. Tetramers were made fresh prior to each experiment by incubating 400ng of OMCP-biotin with APC-streptavidin in a 4:1 ratio for 10 min at room temperature prior to dilution for staining.

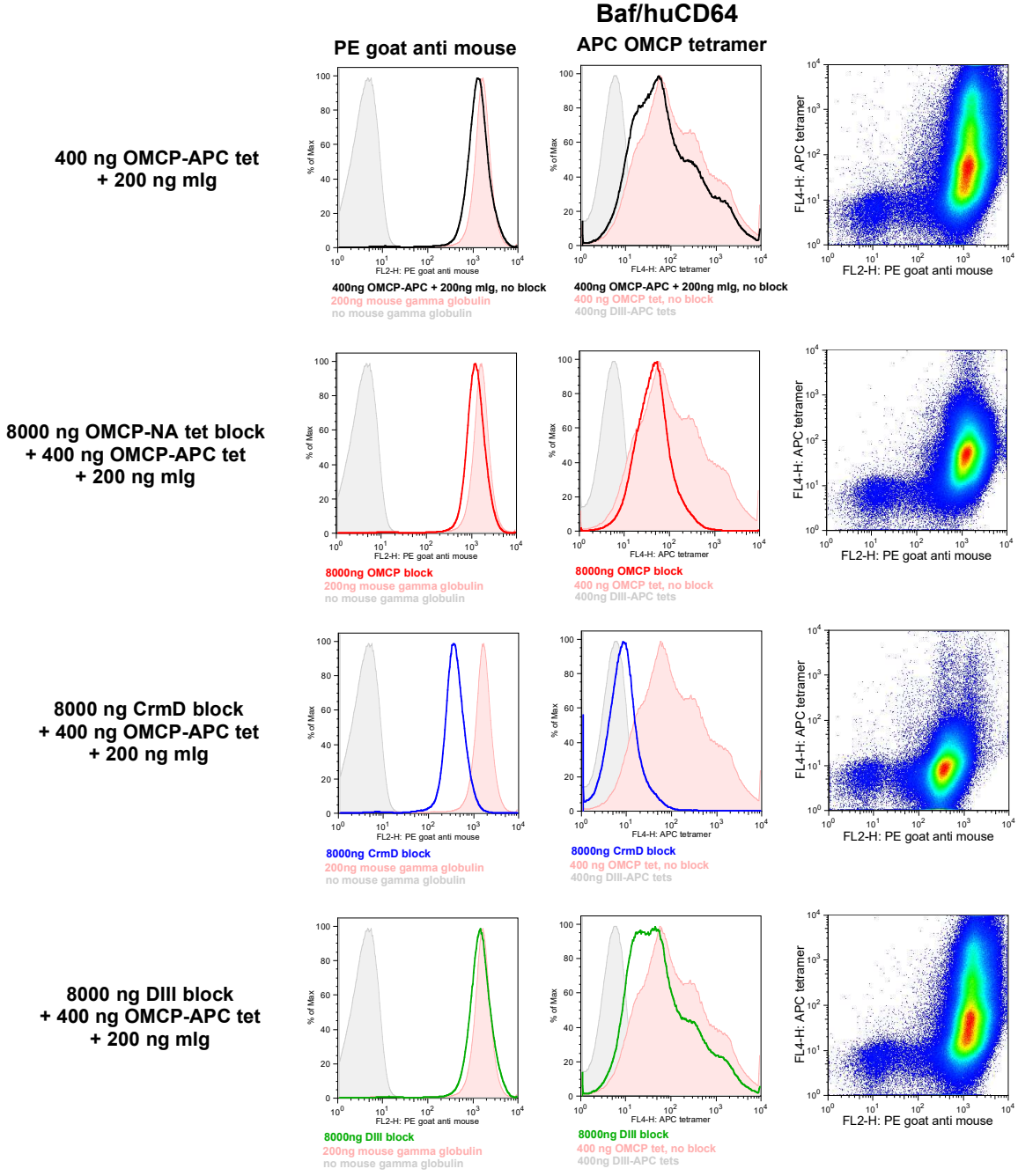
Baf/huCD64
PE goat anti mouse
APC OMCP tetramer
400 ng OMCP-APC tet
+ 200 ng mIg
% of Max
FL2-H: PE goat anti mouse
FL4-H: APC tetramer
400ng OMCP-APC + 200ng mIg, no block
200ng mouse gamma globulin
no mouse gamma globulin
400 ng OMCP tet, no block
400ng DIII-APC tets
8000 ng OMCP-NA tet block
+ 400 ng OMCP-APC tet
+ 200 ng mIg
8000ng OMCP block
8000 ng CrmD block
+ 400 ng OMCP-APC tet
+ 200 ng mIg
8000ng CrmD block
8000 ng DIII block
+ 400 ng OMCP-APC tet
+ 200 ng mIg
8000ng DIII block

Figure 38: CrmD blocks OMCP tetramer binding and IgG binding simultaneously

BaF/3 cells expressing human CD64 (mouse CD64 and mouse CD32 not shown) were preincubated with 8000ng of cold CrmD-neutravidin tetramers, OMCP tetramers, or DIII tetramers for 1 hr on ice. After preincubation with protein, cells were dual stained with 400ng of APC labeled OMCP tetramers and 200ng of mouse IgG for 1 hr on ice. Cells were washed, then incubated with PE goat anti-mouse secondary. Cells were washed x3, then analyzed by flow cytometry to assess amount of OMCP binding and IgG binding. Labeled APC tetramers were made fresh prior to each experiment by incubating 400ng of OMCP-biotin with APC-streptavidin in a 4:1 ratio for 10 min at room temperature prior to dilution for staining. Cold unlabeled tetramers were made the same manner, except using unlabeled neutravidin instead.

APPENDIX 3: Sex Differences in IFN signaling

Introduction:

Sex differences in autoimmune disease and response to infection

There are many well documented examples of sex differences in humans. Autoimmune diseases in general disproportionately affect females, as exemplified by the 9:1 female to male ratio in systemic lupus erythematosus. Females also have notably higher incidences of other autoimmune diseases including rheumatoid arthritis, myasthenia gravis, scleroderma, Sjogren's syndrome, and multiple sclerosis [86, 87]. Additionally, there are well characterized sex differences in adaptive immune responses, some of which have been attributed to the influences of estrogen [88]. Evidence of sexual dimorphism in the innate immune response has been accumulating [89, 90], and there is evidence that men and women differ in their innate and adaptive responses to viral vaccines [91-93]. In general, females respond to infection, vaccination, and trauma with increased antibody production [94, 95]. There are some reports that men are more susceptible to infection, have more severe inflammation, and increased mortality upon infection [96]. In fact, men with sepsis have a significantly higher hospital mortality rate (70%) compared to that of women (26%) matched for age, cause, and severity of sepsis, despite identical surgical and intensive care management in one hospital study [97]. Generally, estrogens appear to increase the immune response whereas testosterone acts to decrease the immune response, however, gender specific susceptibility depends strongly on the identity of the microbe causing the infection [98]. The mechanisms

leading to the sex bias in immune and autoimmune susceptibility are still not fully understood.

Enhanced immunoreactivity in women compared to men is thought to be the basis of this autoimmunity bias, as women appear to mount stronger cellular and humoral immune responses against viral infections [98]. Hypotheses to explain this difference include the effect of sex steroids [99], the roles of X chromosome microRNAs [100] and Y chromosome non-testis determining genes [101], and fetal microchimerism [102]. Some studies have also suggested that the dosage effect of X chromosome genes may impact the differential immune response between sexes [103, 104].

Sex differences in systemic HSV infection

In a model of murine systemic HSV infection, our lab observed a striking difference in mortality between female and male C57BL/6 mice, with a 28 fold higher LD50 in males compared to females [105]. In our model, we saw no sex differences in serum proinflammatory cytokines (IL-1β, IL-2, IFNγ, and TNFα), suggesting that mortality in females was not due to an overwhelming inflammatory response. In fact, these observations suggested that male viral defense may be more effective than female in keeping virus in check. Importantly, the difference in survival between sexes is nearly completely abrogated when we infected IFNαβR deficient mice.

Importance of IFNαβR signaling in mediating sex differences

Infection of IFNαβR haploinsufficient mice demonstrates a strong role for IFNαβR signaling. Survival of IFNαβR haploinsufficient males remained unchanged compared to WT males, indicating that half the amount of receptors is sufficient to protect males from HSV infection. However, IFNαβR haploinsufficient females were substantially more susceptible than WT females. There were no differences in the serum levels of IFNα in males and females, and no difference in the level of IFNαβR on cells following HSV infection [105]. These results together suggest that signaling events downstream of the IFNαβ receptor plays a central role in mediating sex differences in survival in this systemic virus model.

Given that serum Type I IFN levels and IFNαβR receptor levels are the same in male and female mice, we hypothesized that there are differences in Type I IFN pathway downstream signaling or downstream target gene transcription that account for the large sex difference in susceptibility to HSV.

Type I IFN and differential ISG expression in mediating sex differences

It has been shown that the production of IFNα (a type I IFN) by plasmacytoid dendritic cells is significantly higher in women compared to men in response to HIV-1 antigens [106]. Type I IFNs induce the transcription of thousands of interferon-stimulated genes (ISGs), which play crucial roles in the host defense against pathogens. One recent study reported sex-dependent differences in the expression of some ISGs in HIV-1 infected human plasmacytoid dendritic cells (pDCs), after controlling for viral load [107].

This increased IFNα production and ISG expression in females may contribute to the stronger immune response and faster disease progression in chronic HIV female patients compared to males.

Our lab hypothesized that sex-dependent differences in interferon-stimulated gene (ISG) expression following type I IFN stimulation in human macrophages might partially explain this large sexual dimorphism. We are interested in analyzing the sex differences in IFNαβR signaling in males and females and assessing any differential upregulation of downstream interferon stimulated genes. Differences in ISG expression may help explain the large sex differences seen in response to viral infections and autoimmunity. We planned to investigate sex differences in both humans and mouse models.

Experimental Methods:

Cytokines

Type I IFN responses were evaluated using a panel of interferons, including mouse IFN-α1, IFN-α4, IFN-α11, IFN-α13, and IFN-β. Mouse IFN was purchased from PBL Interferon Source (Piscataway, NJ). This would allow us to assess responses to Type I IFNs with high (IFN-β, IFN-α11), intermediate (IFN-α4, IFN-α13), and low (IFN-α1) activity [108].

We have an extensive panel of human interferons including human IFN-α1, IFN-α2, IFN-α5, IFN-α8, IFN-α10, and IFN-β1a. This panel includes several low activity (IFN-α1, IFN-α2), intermediate activity (IFN-α5), and high activity (IFN-α8, IFN-α10, IFN-β1a)

interferons with a broad range of antiviral activity. Human IFN were all purchased from PBL Interferon Source (Piscataway, NJ). Human recombinant IFN-γ was purchased from Novoprotein (Shanghai, China). Human GM-CSF was purchased from Gold Biotechnology (St Louis, MO).

In vitro generation of murine bone marrow derived macrophages

Male or female 8 week old mice were sacrificed by CO_2 euthanasia. The long bones (tibia and femur) of the hind leg are harvested and cleaned of muscle and tendons. The ends of each bone are snipped open to access bone marrow. Marrow is flushed or centrifuged out of the bone, and resuspended in DMEM with 20% L929 cell supernatant, 10% FBS, 1% L-glutamine, 1% Na pyruvate, 1% P/S. Marrow from one mouse (4 bones) can be plated in 5x 10 cm tissue culture petri dishes. Incubate at 37^{o}C, 5% CO_2 for 7 days. On Day 5, add fresh L929 supplemented media. BMDMs ready for use between day 7 to day 14. Note – L929 cell line produces murine M-CSF. Supernatant from L929 cells in log phase growth is filtered and used for BMDM media. L929 supernatant can be replaced with recombinant murine M-CSF.

In vitro generation of monocyte-derived M1 macrophages

The study was approved by the Institutional Review Board at Washington University in St Louis, and subjects gave written, informed consent. We obtained peripheral blood samples from healthy, age- and race-matched male and female donors. Monocytes were purified from buffy coats of four healthy, age and race-matched donors using a Ficoll-Paque density gradient. Platelets were discarded by washing 2X in 10% FBS

media. Monocytes were seeded in DMEM 10% FBS, 1% L-Glutamine, 1% Pen/Strep, 100 ng/ml GM-CSF at a concentration of 5 x 10^5 cells/ml in 12-well tissue culture treated plates for a total of 10 days to drive differentiation of monocytes into macrophages. Media was replaced every 3-4 days, and non-adherent cells were removed on day 6. On day 7, 100 ng/ml LPS and 20 ng/ml HuIFN-γ were added to the media for 24 hours to drive activation to produce M1 polarized macrophages. Monocyte-derived macrophages were then incubated in LPS-free and IFN-γ-free media for 48 hours. On day 10, macrophages were replated on 12-well tissue culture treated plates at a concentration of 6 x 10^4 c/ml to 1.2 x 10^5 c/ml. The polarized M1 macrophages appeared as a mixture of fibroblast-like cells and round cells Changes in cell morphology were assessed by bright field microscopy (Nikon TS100) on day 10.

IFN stimulation and gene expression analysis

Murine BMDMs were used between 7-14 days old. Macrophages were activated with IFN at the specified dose (1000 U/mL or 200 U/mL) for 24 hours.

Human macrophages were used at 10 days old, and were stimulated with 1000 U/ml IFN-αA for 6 hours. IFN stimulation was initiated after a 48 hour rest period following activation by LPS and IFN-γ. This 48 hour delay was intended to minimize changes in gene expression due to downstream responses to LPS and IFN activation, therefore allowing gene upregulation due solely to stimulation by IFN-αA to be adequately assessed.

RNA was isolated from the cells using Trizol (Invitrogen), followed by Qiagen RNeasy kit, according to manufacturers' instructions. RT-PCR was performed on purified RNA using Superscript III RT kit (Invitrogen), according to manufacturer's instructions. Relative quantitation of cDNA levels was performed by qPCR, using beta-actin as a reference gene. Taqman Universal PCR Master Mix (Applied Biosystems) was used, and PrimeTime Standard qPCR assay 5' Nuclease primer-probe combinations were obtained from IDT.

Results:

We attempted to test the hypothesis that sex differences in immune response may be evident at the level of IFN target genes, namely that there is differential upregulation of interferon stimulated genes (ISGs). To address this, we evaluated expression of ISGs in response to Type I Interferon stimulation in male and female primary cells by qPCR. We have identified 7 mouse ISGs and their human analogs of particular interest because they are very highly upregulated following viral infection. We have evaluated expression of these ISG targets (ISG15, ISG54, ISG56, IRF7, MX1, Oas1a, and Viperin) by qRT-PCR using primary BMDMs from male and female mice, followed by stimulation with a mouse IFN panel (eg IFNβ, IFNα4) for 24 hours. Activated cells were harvested, and RNA extracted using Trizol/chloroform extraction. Total RNA was then converted to cDNA using Invitrogen Superscript III reverse transcriptase. Target gene expression was determined using qRT-PCR with TaqMan Universal PCR Master Mix and unique 6-FAM/IBQ probes.

Preliminary experiments have provided evidence of some clear sex differences between female (n=5) and male (n=5) mouse bone marrow derived macrophages (Fig 39). Our results suggest that ISG expression in male C57BL/6 mice is on average higher than expression in female mice across all of the tested ISGs (Fig 39). This difference was higher in BMDMs than in BMDCs when activated with 1000 U IFN-α4 for 24 hours (data not shown). The male dominant expression of ISGs was present when BMDMs were activated with 1000 U IFN-β or 1000 U IFN-α4 for 24 hours. This data suggests that there are indeed sex differences downstream of IFNαβR signaling that is evident at the gene transcript level. This global increase in ISG expression in males is also consistent with our initial observations of significantly enhanced male survival during systemic HSV infection.

There are 13 subtypes of IFN-α and a single subtype of IFN-β in mammals, which may have differential regulation and be secreted by different cell types during different stages of infection in different locations [109]. All of these type I IFN proteins bind to the same IFNαβR receptor with varying affinities. We were interested in determining whether the ISG response in males and females differed with activation by select IFN-α or IFN-β subtypes. We purchased type I IFN subtypes that demonstrated a wide range of IFNαβR binding affinity (highest affinity - IFN-β > IFN-α11 > IFN-α4 > IFN-α13 > IFN-α1 – lowest affinity) [108, 110]. In a preliminary experiment, we assessed the response of two ISGs (ISG15 and ISG56) to stimulation using high or low concentrations of a high affinity interferon IFN-β, a medium affinity IFN-α4, and a low affinity IFN-α1 (Fig 40). Interestingly, there was differential response with stimulation by high or low affinity

interferon. For both ISG15 and ISG56, expression in male cells was higher when cells were stimulated with high affinity IFN-β, while expression in female cells was higher when stimulated with low affinity IFN-α1 (Fig 40). The medium affinity IFN-α4 case was intermediate, with slightly higher expression of ISG15 but lower expression of ISG56 in males. This preliminary data suggests that there is a continuum of stimulation with type I IFNs in the inflammatory milieu, and the amount of activation may determine the magnitude and direction of the sex difference between males and females. This may explain observations that males are more susceptible to certain infections, while females are more susceptible to other pathogens [98], if individual pathogens activate type I IFNs to varying degrees.

To follow up our promising mouse data, we were also interested in assessing sex differences in upregulation of interferon stimulated genes in healthy human donors. We initially selected eight genes which have previously been reported to be highly upregulated upon interferon stimulation [111]. These human ISGs (ISG15, IFIT1, IFIT2, IRF7, OAS1, MX-1, RSAD2) were probed in IFN stimulated human monocyte derived M1 macrophages generated from peripheral blood from healthy male and female donors. We used fully differentiated M1 macrophages for Type I IFN stimulation using a panel of human interferons. Activated cells were harvested, RNA extracted and converted to cDNA similar to the protocol described for mouse. Target gene expression was determined using qRT-PCR with TaqMan Universal PCR Master Mix and 6-FAM/IBQ probes unique for the human homologs of the ISGs of interest. Based on our initial experiments in mouse, we expected to find increased ISG transcription in male

cells compared to female cells under conditions of high stimulation.

Our preliminary experiment used a small sample of two age- and race- matched female and male Chinese-American healthy volunteers. Peripheral blood was drawn, and human monocyte derived macrophages generated by long term culture of peripheral blood monocytes in GM-CSF containing media. Using qRT-PCR, we were able to identify clear differences in upregulation of eight ISGs between the male and female samples. We found that six of the eight ISGs had a higher fold change in gene expression in females than in males upon IFN-A2a stimulation (Fig 41). Of these six genes, MX1 and ISG15 had also been previously reported to be more highly expressed in females compared to males in HIV-infected CD4+ and CD8+ T cells [107]. This preliminary experiment suggests that sex-dependent differences in ISG expression can be detected and could help explain the sex disparities in immune response between males and females in both humans as well as mice. The largest sex differential that we observed was in IFIT1, in which females had on average 10 times higher gene expression than males. This differential ISG upregulation between female and male macrophages may partially contribute to the consistent sex bias in autoimmunity, and may help explain the overall sex bias in immune responses.

In our preliminary human experiment we found that six of the eight ISGs tested (IFIT1, MX1, OAS1, ISG15, RSAD2, IRF7) were significantly more upregulated in females than in males. In this experiment we stimulated with an intermediate strength IFN-A2a in our human macrophage experiments. The mixed results were somewhat consistent with our

experiment using stimulation by the intermediate affinity IFN-α4 in mice which also showed mixed results with higher ISG56 expression in females, and slightly higher ISG15 expression in males. This is in contrary to our findings that stronger stimulation with IFN-β in mice appear to consistently more highly upregulate ISG expression in males. Although the responses of males and females are clearly different from each other in both species, significant inter-species variability may also be present. Additionally, there appears to be very different responses to high, medium, and low affinity type I IFN, as well as strong dose dependence. These factors may explain discrepancies in ISG upregulation trends, and emphasize the need for a large scale systematic investigation of type I IFN responses in this model.

Discussion:

Our results from these qPCR experiments show hundreds- to thousands-fold differences in the expression of certain genes between males and females. However, the sample sizes for each of these experiments is too small to extrapolate meaningful conclusions. Additional murine bone marrow derived macrophages and human peripheral monocyte derived macrophages from additional age matched individuals will need to be tested to confirm our initial studies and conduct statistical tests on the data. Our preliminary experiments investigated only M1 macrophages activated by LPS and IFN-γ, and stimulated by only a few subtypes of interferon. Further experiments may focus on other important cell types known to be involved in a Type I IFN response, including dendritic cells and myeloid cells, and systematically investigate the effect of different subtypes of IFN-α and IFN-β. We suspect that the magnitude and direction of

the sex difference is highly dependent on the strength of activation through the IFNαβR receptor. This hypothesis remains to be tested.

If the expression of certain interferon-stimulated genes proves to be consistently higher in one sex, it would be crucial to establish a connection between gene expression differences and sex disparities in immune response. A thorough review of ISGs may identify certain genes of particular interest. Knockdown experiments may then be conducted to determine the requirement of certain ISGs in establishing the immune sex bias, and knock-in experiments may be conducted to determine their sufficiency.

In addition to the handful of ISGs we have identified through literature review as being highly upregulated following viral infection, we are also interested in performing a non-biased microarray screen of all ISGs to evaluate global differences in expression between sexes. We are particularly interested in assessing differential upregulation of ISGs encoded on the X chromosome. There are 77 identified ISGs encoded on the X chromosome in humans (Table 2). It is possible that incomplete X inactivation in females results in increased expression of some or all of these X chromosome ISGs. If true, this may strongly impact immune regulation in humans and mice. Once a mechanism for sex disparities in immune responses is identified, we may be able to better understand the sex bias in infection and autoimmune disorders.

Future Experiments:

We have obtained some promising initial findings that demonstrate a reproducible sex difference in male and female primary cells following Type I IFN stimulation. Although we investigated only a handful of select ISGs, we have identified a strong sex dependent difference in upregulation in the interferon pathway. These findings deserve future follow up, and here we propose some additional experiments to validate and explore this difference in sensitivity of the Type I IFN pathway.

Assess differential phosphorylation of murine IFNαβR signaling intermediates *in vitro* and *ex vivo*

To further assess the difference in male and female IFNαβR responses, we propose to analyze the activation of signaling intermediates immediately downstream of the IFNα/β receptor. We will focus on phosphorylation of intermediates such as STAT1, STAT2, STAT3, Tyk2, JAK1, and IRF9. The STAT1 pathway has been shown to be important in protection of the CNS from HSV infection [112-114], which may explain the high HSV brainstem titers we have observed in female mice compared to males. We plan to screen bone marrow derived macrophages, bone marrow derived dendritic cells, and murine embryonic fibroblasts for differential Type I IFN responses using a panel of interferons, including mouse IFN-α1, IFN-α4, IFN-α11, IFN-α13, and IFN-β. This will allow us to assess responses to Type I IFNs with high (IFN-β, IFN-α11), intermediate (IFN-α4, IFN-α13), and low (IFN-α1) activity [108]. In this assay, we will generate primary cells from male and female mice, stimulate with our Type I interferon panel for various amounts of time (5, 10, 20, 30, 60 min), then quantify the amount and

phosphorylation status of downstream signaling intermediates by flow cytometry or immunoblot. Stronger signaling in one sex may be possible if there exists a higher basal level of important signaling intermediates. Therefore, it will be important to assess the levels of total STAT1, STAT2, JAK1, etc in males and females as well as the phosphorylation status of each signaling intermediate. Enhanced male survival during HSV infection may be due to enhanced IFNαβR signaling. We expect that this approach will identify differential phosphorylation of signaling intermediates in male and female primary cells in response to Type I IFN stimulation and/or differential basal amounts of regulatory signaling molecules.

Assess differential phosphorylation of human IFNαβR signaling intermediates *in vitro* and *ex vivo*

The IFNαβR signaling pathway in humans is similar to that of mouse. Using phospho-antibodies against the signaling intermediates STAT1, STAT2, JAK1, and TYK2, we will also probe the human Type I IFN pathway by flow or immunoblot. We will generate human monocyte derived macrophages from healthy male and female donors. PBMCs purified by Ficoll centrifugation will be plated on tissue culture treated plates and incubated for 1hr at 37^{o}C, 5% CO_2 to allow adherence of monocytes. Non-αdherent cells will be washed away, and the plates enriched for monocytes will be incubated in media supplemented with 50ng/mL hGM-CSF for 7 days. Media will be replaced on day 3. Cells should be fully differentiated M1 macrophages on day 7 and ready for Type I IFN stimulation [115, 116]. We have an extensive panel of human interferons including human IFN-α1, IFN-α2, IFN-α5, IFN-α8, IFN-α10, and IFN-β1a. This panel includes

several low activity (IFN-α1, IFN-α2), intermediate activity (IFN-α5), and high activity (IFN-α8, IFN-α10, IFN-β1a) interferons with a broad range of antiviral activity tested against HSV, VSV, and SFV [117, 118]. After stimulation with different interferons for a variable amount of time (5, 10, 20, 30, 60 min), we will quantify the amount and phosphorylation status of downstream signaling intermediates by flow cytometry or immunoblot. We expect that this approach will identify differential phosphorylation of signaling intermediates in male and female primary cells in response to Type I IFN stimulation and will correlate with our initial mouse observations.

Assess sensitivities of male and female MEFs to a panel of IFNs by protection from HSV cytopathic effect

Any differences in IFNαβR signaling or differences in ISG gene transcription between male and female mice will manifest as differences in the antiviral, antiproliferative, and immunomodulatory effects in male and female cells. We are most interested in the antiviral role of Type I IFNs, so we plan on examining IFN induced resistance to viral cytopathic effect and IFN induced protection against viral growth. These experiments would allow us to determine whether differences in Type I IFN responses leads to a cell intrinsic resistance to viral challenge.

Our working hypothesis is that male and female cells exhibit different sensitivities to Type I IFN, which manifests as a cell intrinsic difference in resistance to HSV viral challenge.

We would like to assess whether male and female cells are differentially sensitive to the development of the Type I IFN induced antiviral state. We will assay for antiviral state induction by modifying a bioassay developed for detection of interferon activity [119]. In this assay, we will use primary mouse MEFs that are highly susceptible to HSV cytopathic effect [120]. We will sacrifice a pregnant mouse at day 13.5 post coitum and harvest the uterine horns. Each embryo will be processed separately, and part of the embryo saved for sex genotyping. We will preincubate fully cultured MEFs with serial dilutions of IFN for 24 hours, followed by a viral challenge with 0.5 MOI HSV for 48 hours. Cells will be stained with crystal violet to determine cell death. Unprotected MEFs will easily lift off the plate and not be stained by crystal violet. The dye can be solubilized with 70% methanol, and absorbance read using plate reader at 590nm. Using serial dilutions of a panel of Type I IFN, we can determine the amount of each IFN required to protect male and female MEFs from HSV cytopathic effect. We expect that males will be more sensitive to the effects of IFN, needing less IFN stimulation to become resistant to HSV.

Assess permissiveness of male and female cells to HSV viral growth

If male and female cells are differentially sensitive to the induction of an antiviral state by Type I IFN, it follows that they may be differentially permissive to HSV viral growth and replication. We will test this by performing HSV growth curves in male and female BMDMs, BMDCs, or MEFs in the presence and absence of Type I IFN. We will plate $5x10^5$ cells per well in a 12 well plate and harvest in duplicate. Following infection with a low MOI of 0.1 HSV, we will collect the culture supernatant at 6hr, 12hr, 24hr, 48hr, 72hr,

and 96hr post infection. We will determine viral loads in the supernatant using qPCR for the HSV thymidine kinase gene. Given our observations of male resistance to HSV and increased male global ISG levels, as well as increased HSV titer in female brainstems, we might expect to see virus replicate more readily in primary female cells. This would be consistent with papers describing the importance of IFNα and the STAT1 pathway in limiting progression of HSV to the CNS [112, 121], limiting replication in the cornea [113], and controlling the acute replication of HSV [122].

Figures:

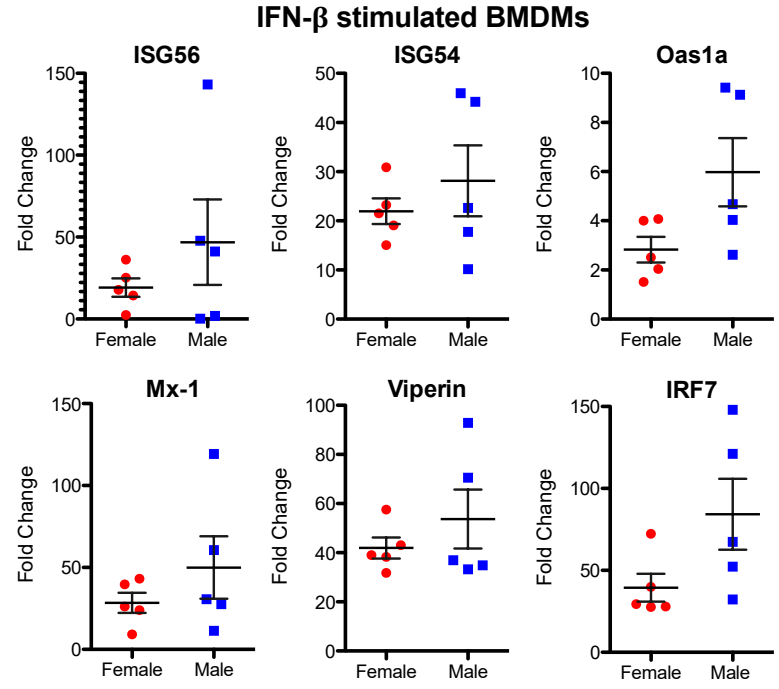
IFN-β stimulated BMDMs
ISG56
ISG54
Oas1a
Mx-1
Viperin
IRF7
Fold Change
Female
Male

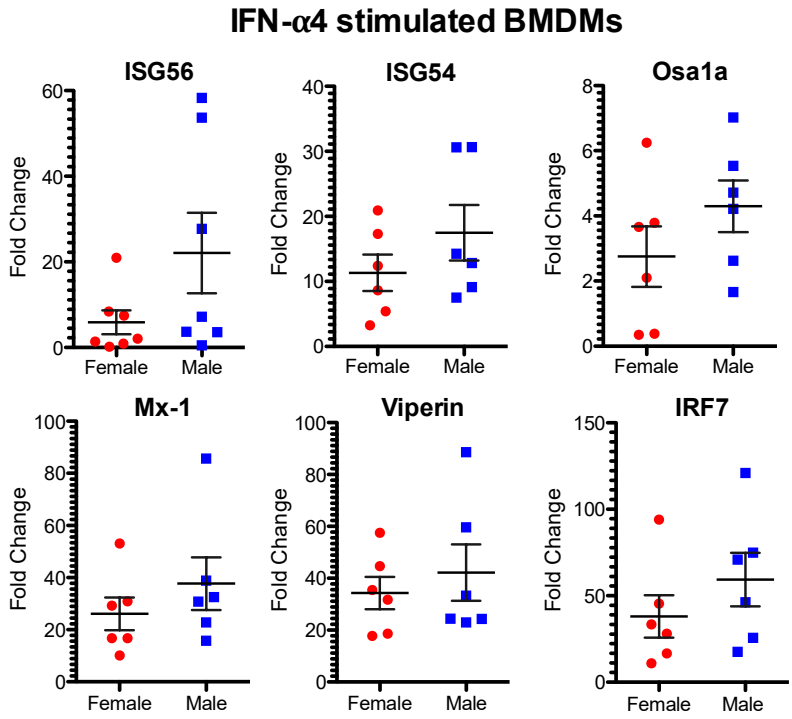
IFN-α4 stimulated BMDMs
ISG56
ISG54
Osa1a
Mx-1
Viperin
IRF7
Fold Change
Female
Male

Figure 39: qRT-PCR of the interferon stimulated genes ISG56, ISG54, Osa1a, Mx-1, Viperin, and IRF7

BMDMs were generated from n=5 male and n=5 female mice. Cells were stimulated with 1000U/mL IFN-β (top Figure) and 1000U/mL IFN-α (bottom Figure) for 24 hours, and qRT-PCR of ISGs performed. Comparisons were made by the comparative Ct method, with β-actin serving as the comparator. Data are presented as fold change relative to naïve unstimulated mice.

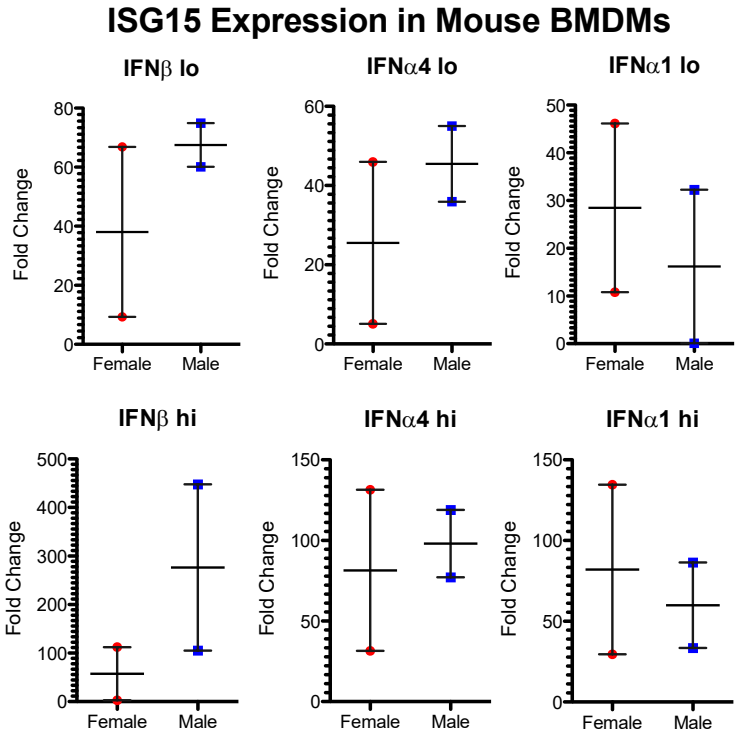
ISG15 Expression in Mouse BMDMs
IFNβ lo
IFNα4 lo
IFNα1 lo
IFNβ hi
IFNα4 hi
IFNα1 hi
Fold Change
Female
Male

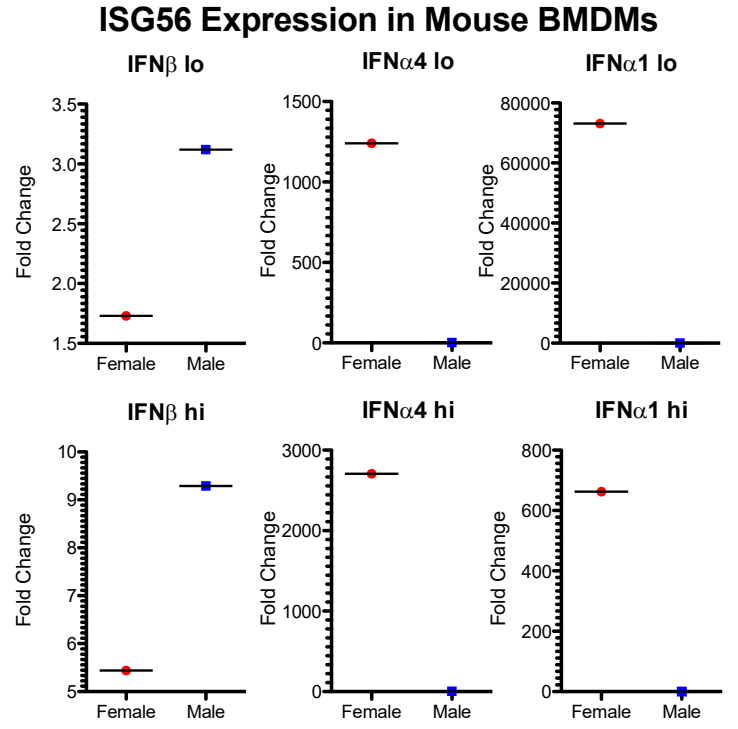
ISG56 Expression in Mouse BMDMs
IFNβ lo
IFNα4 lo
IFNα1 lo
IFNβ hi
IFNα4 hi
IFNα1 hi
Fold Change
Female
Male

Figure 40: Effect of high, medium, and low affinity IFN stimulation of ISG expression

Mouse bone marrow derived macrophages were generated by long term culture in M-CSF. BMDMs were stimulated with 1000U/mL (hi) or 200 U/mL (lo) dose of high affinity IFN-β, medium affinity IFN-α4, or low affinity IFN-α1 for 24 hours. qRT-PCR of the interferon stimulated genes ISG15 (top panel) and ISG56 (bottom panel) in n=2 male and n=2 female mice was performed. Comparisons were made by the comparative Ct method, with β-actin serving as the comparator. Data are presented as fold change relative to naïve unstimulated mice.

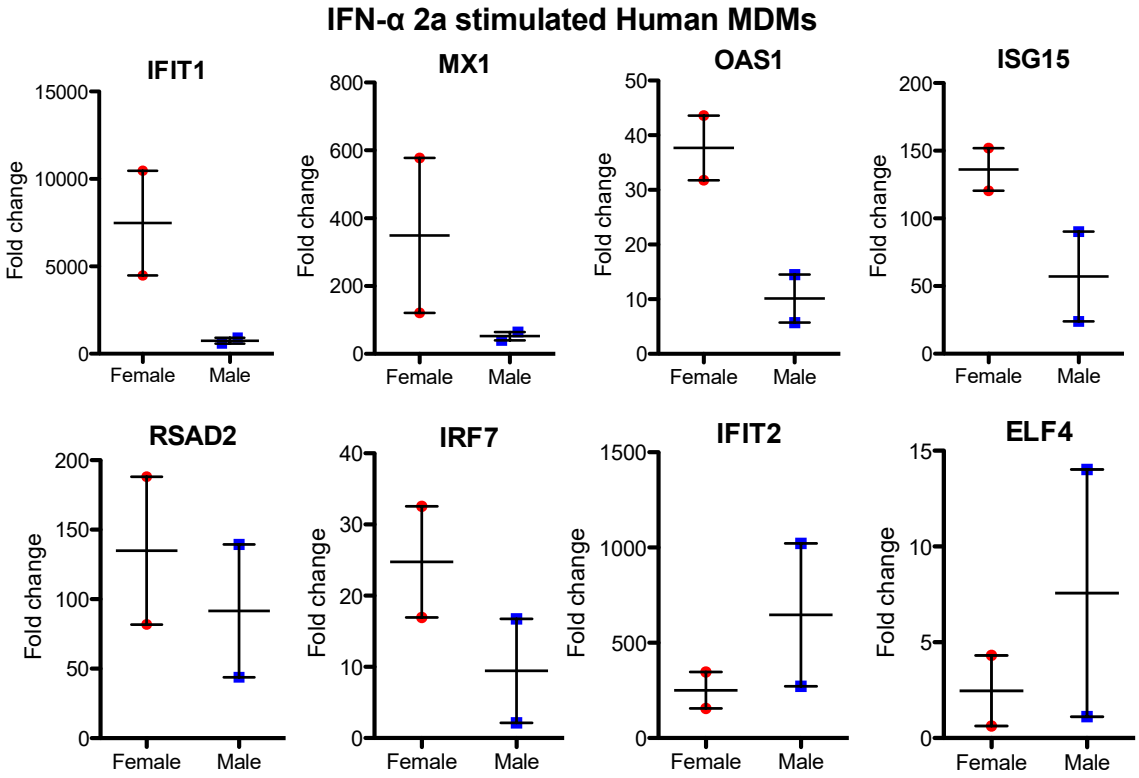

Figure 41: Effect of IFN-α2A stimulation on male and female human MDMs

Higher expression of some ISGs in female macrophages compared to males following IFN-α2A stimulation. IFIT1, IRF7, ISG15, MX1, and OAS1 were more highly upregulated in female macrophages than males. Day 10 macrophages were stimulated by IFN-αA for 6 hours, and gene expression was measured by qPCR. Gene expression changes were normalized to beta-actin. The graphs show data for 2 females and 2 males. The middle bar represents the mean. (Experiment performed by Carol Liu)

Gene symbol	Function	Gene symbol (cont.)	Function (cont.)
Biological processes		*Intracellular processes (cont.)*	
DIAPH2	Development	RLIM	Protein degradation (cont)
ARMCX1		RNF128	
PCSK1N	Endocrine regulation	CSF2RA	Signal Transduction
PGRMC1		EDA	
AGTR2	Homeostasis	EDA2R	
VSIG4	Immune regulation	IL3RA	
CYBB	Microbicidal activity	P2RY10	
Cell cycle		RAB40A	
MAGEH1	Apoptosis	SASH3	
XIAP		BEX4	Transcription
GNL3L	Cell cycle	ELF4	
PIN4		HDAC6	
GPC4		MAMLD1	
HCFC1		SSX2B	
MTM1	Cell differentiation	SSX3	
ENOX2	Cell growth	SSX4B	
FGF16		ZBED1	
Extracellular processes		ALG13	Translation
TRO	Cell Adhesion	FMR1	
SLC6A8	Secretion	RBM3	RNA Binding
TMEM35		RBMX	
CD99	Cell-cell interaction	*RNA gene*	
Intracellular processes		RP11-706O15.7	Long non-coding RNA gene
AP1S2	Intracellular transport	XIST	
SLC25A6		*Structure*	
PRRG3	Ion binding	NAP1L3	Chromatin structure
CLIC2	Ion transport	ARHGAP6	Cytoskeletal structure
GABRE		DMD	
HEPH		FGF13	
MAGT1		SEPT6	
ARSD	Catalytic activity	BGN	Tissue structure
IDS	Lysosomal degradation	*Unknown*	
ACOT9	Metabolism	FAM122C	Unknown
ATP6AP2		HDX	
GK		LONRF3	
GYG2		MID2	
MAOB		MTMR1	
PFKFB1		PLCXD1	
SAT1		RNF113A	
EBP	Protein binding	RP1-142F18.2	
BRCC3	Protein degradation	RP1-232L22_B.1	
CUL4B			

Table 2. ISGs located on the X chromosome.

A database of IFN regulated genes (Inferferome [123]) was cross referenced against a genomics database. Interferon regulated genes that are located on the X chromosome were identified and categorized as above. (Table compiled by Carol Liu)

APPENDIX 4: Sex Differences in HSV infection

Introduction:

There are well established reports of sex differences in the outcome of a variety of viral infections. HIV infection (without antiretroviral therapy) is associated with shorter survival in women than men [124]. There are reported differences in viral encephalomyocarditis [125], vesicular stomatitis [126], and coxsackie virus B3 infection [127]. Females have twice the risk of severe congenital CMV meningitis compared to males, and the memory T helper response to CMV is higher in females than males [128]. There exists a wide body of literature setting precedence for a large and clinically significant difference in outcome between males and females in the setting of a variety of viral infections.

Sex differences in HSV infection in humans

There are two types of herpes simplex virus (HSV) that infect humans. HSV-1 is typically acquired during childhood, usually mild, and produces most cold sores. HSV-2 is primarily acquired as teenagers or adults as a sexually transmitted infection and produces most genital herpes. However, there is overlap, and both types can infect oral and genital areas. There is some sex difference in distribution of HSV-2 with the virus more common in women than men [129, 130], however since it is a sexually transmitted infection, acquisition depends strongly on anatomy, and this may not indicate an intrinsic difference in susceptibility to HSV between the sexes. There are, however, reports of increased incidence of HSV-2 meningitis with females accounting for 75-80%

of cases [131-133], which may suggest a real increased susceptibility to HSV in human females, which proves consistent with our findings in mice.

HSV is a neurotropic and neuroinvasive virus that establishes latency in the cell bodies of neurons in the dorsal root ganglia. HSV infection in humans is characterized by lifelong latency with sporadic reactivation. Immune system control is the major factor affecting reactivation, and both HSV-1 and HSV-2 infection can be severe in infants with limited immune response and individuals with compromised immune systems due to AIDS, cancer, severe burns, or immunosuppressant medication.

Sex differences in HSV infection in mice

Our lab has previously reported a striking difference in mortality between C57BL/6 mice of different sexes following infection with several systemic DNA viruses, including HSV, MCMV, and VV [105]. This difference in mortality was particularly striking with systemic (intraperitoneal) HSV-1 infection, with a 28 fold higher LD50 in males compared to females [105]. Female mice also demonstrated 100 fold higher HSV brainstem titers than males day 6 post infection. However there were no sex differences in serum proinflammatory cytokines (IL-1β, IL-2, IFNγ, and TNFα), suggesting that mortality in females was not due to an overwhelming inflammatory response. These observations suggest that there exist differences in viral defense, viral transit, and/or viral replication in the CNS between males and females that manifests as a very large difference in mortality and brainstem titers.

Properties of Neuroinvasive HSV

HSV-1 is thought to gain access to the CNS through the adrenal glands after peripheral infection [134]. Adrenalectomy prior to infection proved that the virus reached the spinal cord via the adrenals [134]. Virus can be isolated from the adrenal glands as early as 1 hr post infection [135], and by day 3 virus can be isolated from the brainstem of mice. Additionally, there has been reported extensive virus replication in the adrenal cortex with some involvement of the medulla [134, 136]. These reports all implicate the adrenal glands as the major gateway for HSV entry into the CNS.

Neuroinvasive HSV strains were shown to replicate to high titers in adrenal glands and ovaries, migrate to spinal cord, then migrate to the brain. Conversely, nonpathogenic HSV strains were shown not to replicate in adrenal glands [137] or had only transient detection in adrenal glands [138]. However, both neuroinvasive and noninvasive variants are highly neuropathic after direct intracranial injection [139].

We hypothesize that there is a difference in the ability of HSV to replicate in or traverse the adrenal glands in male and female mice. The difference may be due to poor localization or homing of HSV to the adrenals in male mice, poorer replication in the adrenals in males, better peripheral control by the immune system in males, or poor virus crossing from the adrenals to the spinal cord through peripheral nerves in males.

Although our intraperitoneal mouse model does not accurately reflect the route of HSV infection in humans, the information obtained from this study may prove valuable in

understanding sex differences in immune control or neural permissiveness. This has important clinical significance since there is evidence of a sex bias in the rate of HSV meningitis [131-133]. A greater intrinsic ability to enter the female brain or increased permissiveness of neural cells to viral growth in females may be identified in this mouse model. Outside of HSV virology, this work on immune control and CNS entry may be pertinent to the study of multiple sclerosis, which also has a strong female predominance, with CNS access a major limitation.

Experimental Methods:

Mice

Female C57BL/6 mice were ordered from NCI (Frederick, MD) at 6-7 weeks old. They were housed in a specific pathogen free facility (4th Floor CSRB) at Washington University in St. Louis until they reached 8 weeks of age, when they were used for majority of the experiments.

Four Core Genotype Mice breeding stock were originally ordered from Jackson Labs (Bar Harbor, Maine). They were then bred on site in a specific pathogen free facility (SRF) at Washington University in St. Louis. Mice were individually genotyped to determine their sex chromosome complement. Mice were used between 8-12 weeks of age, and transferred to 4th Floor CSRB for infection.

Virus and Intracranial Infection

HSV strain 17 was a kind gift from David Leib (Dartmouth Medical School, Lebanon NH). HSV was propagated in and titered using Vero cells (ATCC) following established protocols [140]. HSV was diluted in sterile DMEM for intraperitoneal infections, or diluted in sterile PBS for intracranial infections.

For intracranial infections, mice were heavily anesthetized with ketamine/xylazine short acting sedative. Diluted HSV was drawn up into a 29.5 gauge insulin syringe. The syringe needle was inserted through a plastic stopper cut at a height to allow adequate penetration of about 4mm into the cortex through the skull, while preventing inserting too deep. Mice were injected with a 10uL volume of diluted HSV into the cortex at the midline. Control mice were injected with an equal volume of sterile PBS.

Antibiotic Treatment

Some cohorts of mice were put on long term trimethoprim-sulfamethoxazole treatment for certain experiments. Sulfamethoxazole and Trimethroprim oral suspension, USP 200mg sulfamethoxazole / 40 mg trimethoprim per 5mL, Grape flavor was purchased from Hi-Tech Pharmacal Co, Inc (Amityville, NY). Approximately ½ tablespoon of well shaken antibiotic suspension was added to the drinking water. New antibiotic was added each time the water was changed, on a schedule of twice per week water changes over a course of 8 week treatment. Antibiotic treatment was continued as described after HSV infection, until mice were sacrificed 28 days p.i.

Radiation mediated Bone Marrow Transplant

Bone marrow transplants were performed with female recipients and male or female bone marrow donors. Recipient 5 week old female Ly5.1 mice were placed on antibiotic water for 1 week prior to gamma irradiation at 6 weeks old. Food was removed the night before irradiation. The recipients were irradiated with 950 rad of gamma radiation over the course of about 20 min. Bone marrow cells were prepared from male or female Ly5.2 donors. Donors were culled with CO_2, femurs and tibias were removed, and bone marrow harvested by centrifugation. Cells were diluted in sterile HBSS, and $2x10^7$ donor bone marrow cells were retroorbitally injected per recipient mouse. Recipients were maintained on Trimethoprim-sulfamethoxazole in the drinking water for 8 weeks. Peripheral blood of each bone marrow chimera and controls were analyzed week 7 post irradiation. Mice were bled via retroorbital bleed with the contralateral eye, and peripheral blood was confirmed as having >97% donor reconstitution in the T cell, B cell, and myeloid cell compartments. At 8 weeks post radiation (recipients are 14 weeks old), mice were infected with $1x10^7$ pfu HSV intraperitoneally. Survival and weight loss was monitored and antibiotic water was maintained out to 28 days post infection.

Busulfan mediated Bone Marrow Transplant

Bone marrow transplants were performed with female recipients and male or female bone marrow donors using the chemotherapy drug Busulfan, to avoid irradiating mice and avoid long term antibiotic treatment. 6 week old Ly5.1 recipient B6 females were toe tagged and individually weighed prior to buslfan administration. Busulfan is made fresh each day and administered based on the individual mouse's weight. To make a 2

mg/mL busulfan suspension, 100 mg of busulfan (Sigma B-2635) is weighed out and added to 1mL of DMSO preincubated in a 55^{o}C water bath. Once dissolved, the busulfan-DMSO mixture is added to 49 mL of sterile PBS preincubated at 55^{o}C. The solution is kept warm in a beaker of 55^{o}C water en route to the mouse facility. 50 mg/kg (or 40 mg/kg) of busulfan is taken up in a 29.5 gauge insulin syringe and allowed to cool before injecting into the mouse intraperitoneally. First dose is given 3 days prior to transplant, followed by a second dose (50 mg/kg or 40 mg/kg) 2 days prior to transplant. Mice are allowed 1 day of rest on the day immediately prior to transplant.

On the day of bone marrow transplant, donor male or female Ly5.2 mice were sacrificed, femurs and tibias removed, and bone marrow harvested by centrifugation. Cells were diluted in sterile HBSS, and 2x10^{7} donor bone marrow cells were retroorbitally injected per recipient mouse. Recipients were allowed to reconstitute their hematopoietic compartment for 8 weeks, without antibiotic treatment. Peripheral blood of each bone marrow chimera and controls were analyzed week 7 post-transplant. Mice were bled via retroorbital bleed with the contralateral eye, and peripheral blood was confirmed as having >97% donor myeloid cells, but only >80% reconstitution in the B cell compartment, and only >75% reconstitution in the T cell compartment. At 8 weeks post-transplant (recipients are 14 weeks old), mice were infected with 1x10^{7} pfu or 3x10^{7} HSV intraperitoneally. Survival and weight loss was monitored out to 28 days post infection. Controls were not busulfan treated, not transplanted, and had no antibiotic exposure.

Results:

HSV entrance into the CNS is the limiting step in systemic HSV model

We sought to answer whether a sex dependent difference in blood brain barrier permeability or entrance to brain exists in this HSV model; and whether the sex difference is due to cells of the hematopoetic compartment. To determine whether entrance into the brain is the limiting step in our model, we infected male and female mice with HSV directly into the cortex via the intracranial route of infection. Interestingly, there is no difference in survival between males and females when infected with 100 pfu HSV intracranially (Fig 42). This suggests that the virus is equally virulent in both sexes when it arrives at its final destination in the brain, and rules out the possibility that virus is cleared faster in the brain or replicates poorer in the brain of males compared to females. This finding implicates a step prior to entry to the brain as being a limiting step in males.

Murine Survival Differences during Systemic HSV infection is not dependent on Sex Chromosome Complement

Female mice are more susceptible than male mice to a variety of DNA viruses, including HSV, CPX, and MCMV [105]. Data in ovarectomized females, castrated males, and castrated males given exogenous estrogen demonstrates that less than half of the survival difference between males and females can be attributed to the presence of estrogens [105]. Androgens have no effect on survival. Therefore the majority of the almost 80 fold difference is susceptibility due to a hormone independent effect. We hypothesized that part of the female susceptibility to viral infection is due to sex

chromosome complement. The X chromosome contains a number of genes important for immune function, including TLR7, TLR8, CD40L, FOXP3, BTK, IL-2 receptor common gamma chain, and many other genes with direct and indirect roles in immune function [141]. Additionally, there is a disproportionately high number of microRNAs located on the X chromosome compared to the autosomes, while there are no miRNAs present on the Y chromosome [142]. Processes such as skewing of X chromosome inactivation and the unequal expression of X chromosome microRNAs may be partially responsible for sex differences in autoimmunity, immunity, and cancer. Female susceptibility to HSV and other viral infections may be due in part to their XX sex chromosome complement.

To test whether sex chromosome complement affects murine survival after HSV infection, we used the Four Core Genotype (FCG) mouse model. The FCG mice have a deletion of the testes determining gene Sry from the Y chromosome, and an insertion of an Sry transgene onto an autosome [143]. This allows production of four genotypes, XX(Sry-) Females, XY-(Sry-) Females, XX (Sry+) Males, and XY-(Sry+) Males. Analysis using this mouse model allows one to draw conclusions based on X gene dosage, Y gene dosage, and X gene imprinting independent of gonadal sex and gonadal hormones. We monitored survival over 28 days with $3x10^7$ pfu HSV/mouse, weight loss, and brainstem HSV titers.

We had expected that mice with the XX chromosome complement (XX F, XX Sry+ M) would have been more susceptible than mice with the XY chromosome complement, if

susceptibility were due to a gene localized on the X chromosome. However, in our experiments with FCG mice infected with $1x10^7$ pfu HSV (Fig 43A) or $3x10^7$ pfu HSV (Fig 43B), we did not see an increased susceptibility in XX bearing mice. In female mice, we paradoxically observed an increased susceptibility in XY- females compared to XX females (Fig 43). We saw no statistical difference in susceptibility between XX (Sry+) males and XY- (Sry+) males (Fig 43). Additionally, the large survival difference we usually see between normal XX Females and XY Males was greatly reduced in these mice. This may indicate a greater underlying difference in response between mice obtained from Jackson Labs (FCG) and mice obtained from NCI (wildtype B6) that will need to be further evaluated.

The unexpected reversal of susceptibility with the XX F and XY-F may suggest that sex chromosome complement is not the main driving factor for the original sex susceptibility difference. Alternatively, the effect of hormones may be masking any effect of sex chromosomes, as the mice used in these experiments had not been gonadectomized prior to puberty.

Determine the sex dependence in the hematopoietic compartment using male-female bone marrow chimeric mice

To confirm a role of the sex chromosome complement in protection against viral challenge, we generated bone marrow chimeric mice from Ly5.1 male or female mice reconstituted into irradiated Ly5.2 recipients, followed by challenge with $3x10^7$ pfu HSV. If the sex difference in survival is due to the sex chromosome complement or differential

responsiveness of male and female hematopoetic cells, we would expect greater mortality in chimeric mice generated with female bone marrow compared to those generated with male bone marrow. We hypothesized that the sex susceptibility phenotype was due to a cell intrinsic difference in the Type I IFN response of the hematopoietic compartment. If so, male resistance and female susceptibility to HSV can be transferred to irradiated recipients by transfer of bone marrow.

To determine whether the sex differences between male and female mice are dependent on the hematopoietic compartment, we studied male/female bone marrow chimeric mice. Bone marrow from wt Ly5.1 female or male mice was used to reconstitute irradiated Ly5.2 male recipients. Chimerism was evaluated by flow cytometry of peripheral mononuclear cells at 6 weeks post reconstitution. Systemic infection with $1x10^7$ pfu HSV was performed at 8 weeks post reconstitution. We expected that reconstitution with male bone marrow would rescue the susceptibility of female mice, and conversely female bone marrow would increase mortality in male mice following HSV infection. Preliminary data from an experiment where male bone marrow was reconstituted into female mice showed promising results with 7/7 mice surviving a $3x10^7$ pfu dose of HSV, a dose at which about 20% of female mice normally survive (data not shown).

In a follow-up experiment, recipient female mice were irradiated with 950 rad, then given a bone marrow transplant from male or female donors. They were then given trimethoprim-sulfamethoxazole antibiotic in the drinking water for 8 weeks prior to

infection with $1x10^7$ pfu HSV. A cohort of control females were age matched, but not irradiated, and not given antibiotic water. Interestingly, both the Male BM → Female recipient and Female BM→ Female recipient groups were highly resistant to HSV infection (Fig 44). However, the age matched female controls had about 80% lethality, consistent with previous survival data for female mice. The fact that the Female BM → Female recipient group did not phenocopy Female controls, but rather the Male BM → Female recipient group, suggests that there is something in bone marrow chimera procedure itself that is making these mice unexpectedly resistant to HSV. The two main differences between the experimental groups and the control group are exposure to radiation and long term antibiotic use.

Determine the effect of long term antibiotic use on HSV susceptibility

To test whether exposure to antibiotics affects HSV susceptibility, we treated B6 females with trimethoprim-sulfamethoxazole in the drinking water for 8 weeks, or age matched controls with no antibiotic exposure, then infected mice with $1x10^7$ pfu HSV. The antibiotic treated mice appeared to be protected from HSV with higher survival and lost less weight than controls (Fig 45). However the survival in the control group was also higher than expected in this experiment, so definitive conclusions unfortunately cannot be drawn, and this experiment needs to be repeated.

The bone marrow chimera experiment was repeated a second time, with female B6 mice irradiated with 950 rad, then given a bone marrow transplant from male or female donors. This time, both the bone marrow female recipients and the age matched control female mice were given antibiotics in the drinking water for 8 weeks before HSV

infection. The results from this experiment showed that all three groups were protected from HSV (Fig 46), and notably there was no statistical difference between mice given male bone marrow or female bone marrow. This may suggest that exposure to long term antibiotics alone may improve survival from HSV viral infection.

One hypothesis is that the existing female gut flora makes mice more susceptible to certain infections including HSV, compared to males. Antibiotic treatment may be altering commensal gut flora composition by converting the female microbiome to a more “male” or more protective microbiome. This remains to be tested. An alternative explanation is that older mice are more resistant against acute HSV infection. We have previously infected female or male B6 mice at 8 weeks old in our initial characterization of the sex difference during acute infection. However, mice used in the radiation experiments were irradiated at 6 weeks old and infected at 14 weeks old. Mice in the antibiotic experiments were treated starting at 6 weeks old and infected at 14 weeks old. However, we routinely have controls that are aged along with the radiated mice that show the expected high mortality, so we consider resistance secondary to aging to be less likely.

Determine the effect of radiation using non irradiative busulfan BMT

Additionally, we wanted to test whether radiation accounted for the initial result seen in Fig 44. To test whether radiation alone was responsible for the unexpected protection in both the Male BM→ Female recipient and Female BM → Female recipient cohorts, we decided to perform bone marrow chimeras using a non-irradiative method. Busulfan is a chemotherapy drug used to treat leukemias, lymphomas, and other myeloproliferative

disorders, and also routinely as a conditioning agent prior to bone marrow transplantation in humans and mice [144]. Female recipients were given a split dose of Busulfan (100 mg/kg) to ablate the stem cell niche in bone marrow. On day 4, the mice were given a bone marrow transplant from female donors. They were then allowed to reconstitute for 8-10 weeks with no antibiotic treatment prior to infection with $1x10^7$ pfu HSV. The female mice given female bone marrow appears to be similarly susceptible to female controls (Fig 47A). Unfortunately the controls showed much higher survival than expected so the dynamic range of this experiment is limited. Since these age-matched controls did not receive busulfan, radiation, or antibiotics, we would have expected them to match the 80% lethality rate of previous experiments in B6 females, instead we observed only 20% lethality. In this experiment, however, we observed a high level of toxicity at the 100 mg/kg split dose of busulfan, with several mice dying following the second dose of busulfan. The surviving mice were well reconstituted with donor marrow, with 85% T cells, 92% B cells, and >97% myeloid cells donor derived.

This busulfan bone marrow chimera experiment was repeated with a lower dose of busulfan (80 mg/kg split dose) and a higher innoculum of HSV ($3x10^7$ pfu) to obtain more reliable and reproducible survival data with fewer deaths due to busulfan. We saw minimal protective effect with male BM that was not significant with the number of mice used (Fig 47B). However, there was a trend of increased survival in the male BM recipients compared to female controls. At the lower dose of busulfan, we did not observe any deaths due to busulfan toxicity. However, there is some mixed chimerism 8

weeks post bone marrow transplant, with 75% T cells, 80% B cells, and >97% myeloid cells donor derived.

Discussion:

This recent work has opened up several new avenues of investigation. The finding that HSV is equally virulent in males and females when given intracranially strongly suggests that the block is downstream of entering the CNS, possibly at the level of the adrenal glands. The experiments with the Four Core Genotype mice imply that sex chromosome complement is probably not the driving factor for female susceptibility, but this must be investigated in a cleaner gonadectomized model. Other additional experiments have introduced the gut microbiome and antibiotic treatment as possible factors involved in resistance and susceptibility to acute HSV. Finally, busulfan treated bone marrow chimeras evaluated the hypothesis that protection is at least partially due to components of the hematopoietic system.

HSV enters CNS through adrenal glands

Our results with intracranial infections of male and female mice clearly demonstrate that HSV is equally lethal when CNS entry is bypassed (Fig 42), whereas a very significant sex difference exists when virus is given intraperitoneally [145]. Via intraperitoneal infection the sex difference in CNS entry is demonstrated by the greatly increased brainstem titers in females compared to males [105]. According to extensive literature research, HSV-1 is thought to gain access to the CNS through the adrenal glands after peripheral infection. Via all peripheral routes of infection (footpad, intranasal, intraperitoneal, intravenous), virus appears to spread preferentially to adrenals and

ovaries [146]. Adrenalectomy prior to infection proved that virus reaches the spinal cord through the adrenals [134]. Virus can be isolated from the adrenal glands as early as 1 hour post infection [135], and there is extensive virus replication in the adrenal cortex with some involvement of the medulla after around 1 day post infection [134]. By day 2, virus can be detected in the lower thoracic spinal cord, and virus can be isolated from the brainstem by day 3, indicating a quick progression to the CNS though an adrenal gland entry.

There are neuroinvasive strains of HSV and noninvasive strains of HSV. We expected that by identifying their differences, we would be able to identify what regulates HSV entry into the CNS. Neuroinvasive HSV strains were shown to replicate to high titers in adrenal glands and ovaries (testes are not colonized), migrate to spinal cord, then migrate to the brain [146]. Conversely, nonpathogenic HSV strains were shown not to replicate in adrenal glands [137] or had only transient detection in adrenal glands [138]. However, both neuroinvasive and noninvasive variants are highly neuropathic after direct intracranial injection [139], paralleling our intracranial infection results between males and females. We hypothesize that there is a difference in the ability of HSV to replicate in or traverse the adrenal glands in male and female mice.

The Adrenal Medulla

The adrenal medulla is of ectodermal origin, and derives from neural crest cells that migrated during embryonic development. The medulla is highly innervated with a very rich nerve supply. A large proportion of fibers projecting to adrenal gland are destined to

innervate chromaffin cells, which are considered modified post-ganglionic neuroendocrine cells. Importantly, chromaffin cells are innervated by preganglionic neurons (not postganglionic neurons) that synapse in the medulla to directly innervate the chromaffin cells. There are no intermediate cells between the adrenal glands and CNS, indicating that this is a very direct pathway into the CNS.

The adrenal cortex mainly produces cortisol, aldosterone, and androgens, while the medulla chiefly produces epinephrine and norepinephrine. In contrast to the direct innervation of the medulla, the cortex is regulated by neuroendocrine hormones secreted from the pituitary gland which are under the control of the hypothalamus, as well as by the renin-angiotensin system.

Necropsy reports after acute HSV infection implicates adrenal glands

The hypothesis that HSV enters through the adrenals is consistent with our previous necropsy reports on mice at 6 days pi with $3x10^7$ pfu HSV (Dr Suellen Greco). Three independent reports indicated that there was extensive adrenal necrosis involving both the cortex and medulla, with moderate to severe lesions in the medulla and mild to moderate lesions in the cortex. There was also necrosis of peripheral nerves noted in the vicinity of the adrenal and kidney. Other notable features included presence of intranuclear inclusion bodies, centrilobar hepatocellular degeneration, lymphoid necrosis in the white pulp of spleen and lymph nodes, leucopenia, and lymphopenia. There was little inflammatory infiltrate noted in the organs of these mice; such changes in inflammatory cell populations were noted primarily in the spleen and lymph nodes.

Females showed elevations in transaminases and there were particularly notable differences in the medullary necrosis, with often severe lesions in the females and none in the males. Illness in these mice is thought to be certainly related to sequelae of adrenal necrosis, and may have been further complicated by hepatocellular degeneration. These necropsy reports strongly implicate the adrenal medulla in the sex differences in viral susceptibility, given the extensive necrosis seen in females compared to males.

Sex differences in adrenal gland morphology

Given that this information suggested a block at the level of the adrenal glands, we investigated the obvious differences between male and female adrenal glands. There are some dramatic anatomic differences. Notably, female adrenal glands are much larger (size and weight) than age matched males. There is an increased volume of both the adrenal cortex and medulla. At 9 weeks old, female adrenal glands are about two fold heavier than males [147]. Females also have a unique X zone in the adrenal cortex that is not present in males at the age ranges used in our experiments. The X zone is thought to be a remnant of the fetal adrenal zone, and degenerates after puberty in male mice, whereas the X zone persists until first pregnancy in female mice.

This literature review and preliminary work suggests a block in HSV access to the CNS in males at the level of the adrenal glands. This may be due to poor localization of HSV to the adrenals in male mice, poorer replication in adrenals in male mice, better peripheral control by the immune system in male mice, or poorer virus crossing from the

adrenals to the spinal cord through peripheral nerves in males. This model will need further study to fully evaluate these hypotheses.

Effect of antibiotic treatment on HSV mortality

Although we have only very preliminary evidence, our experiments involving antibiotic treatment suggest that there may be some protective effect of antibiotics against HSV mortality. The parallel observation that C57BL/6 mice purchased from NCI have a very large sex phenotype between males and females, while Four Core Genotype mice obtained through Jackson Labs does not replicate this sex difference phenotype between XX Females and XY Males, also supports the idea that some gut microbiome differences may be playing a role. Although clearly there are genetic differences between C57BL/6 mice and Four Core Genotype mice that have yet to be ruled out, these two lines of evidence may suggest that male and female murine gut flora would also be of interest for future study as mice bred in different facilities would theoretically have distinct microbiome compartments. If this holds true under further testing, then we might hypothesize that female gut flora is distinct from male gut flora, and female gut flora somehow allows susceptibility to HSV, while male gut flora is protective. It is possible that antibiotic treatment in previous experiments converts the female microbiome to a more “male” microbiome, although these suppositions have yet to be substantiated and require extensive further investigation.

Future Experiments:

A substantial amount of preliminary work has been completed in the investigation of the sex difference phenotype following systemic HSV infection, but it has raised more questions than it has solved. This work has led us to several important avenues, including the possibility of a barrier to CNS entry at the level of the adrenal glands, a possible dependence on antibiotic treatment or normal flora variation in mice housed in different facilities, as well as the possible contribution of sex chromosomes. Additional experiments to address these questions should be completed in the future. Here we have outlined a series of experiments designed to follow up on our preliminary findings.

Adrenal gland titers in males and females

Adrenal glands, spleen, liver, ovaries/testes, spinal cord, brainstem, and cortex have already been harvested from male and female mice infected with $1x10^7$ pfu HSV ip. We have frozen organs from 5 males and 5 females each on day 1, day 3, and day 6 post infection. We would expect to see higher adrenal titers in females than in males. We also expect virus to enter the CNS earlier in females and reach a higher titer in spinal cord, brainstem, and cortex in females. The frozen organs are ready to be tittered.

Adrenal gland histology in males and females

Adrenal glands from males and females infected with $3x10^7$ pfu HSV should be obtained for H&E sections at day 1 and/or day 3 pi. Adrenal gland sections would be assessed for presence of lesions or intranuclear inclusion bodies, necrosis of cortex and medulla, necrosis of peripheral nerves, and presence of inflammatory infiltrate. We

expect more medullary destruction in females, with possible necrosis of peripheral nerves. We expect very mild lesions if any in males.

Adrenalectomy prior to acute HSV infection

Plans should be made to adrenalectomize male and female mice 4 weeks prior to infection with $3x10^7$ pfu HSV. Mice will be anesthetized with a ketamine/xylazene short acting sedative and surgically prepared. Adrenal glands will be bilaterally removed using a 1.5 cm dorsal midline incision over the 13^{th} rib. Adrenal glands located in the fat pad that covers the cranial portion of the kidney will be removed. Incisions will be closed with absorbable suture, and skin incisions closed with stainless steel wound clips. Staples will be removed 7-10 days post-operatively. Adrenalectomized animals will be maintained with 0.9% sodium chloride drinking water, and may require a corticosteroid added to drinking supplement to increase survivability. Mice will be allowed 4-6 weeks to recover from surgery prior to infection with HSV. Adrenalectomized mice will be infected and monitored for survival and weight loss. Other cohorts will be sacrificed at specific times post infection to assess organ titers. We expect adrenalectomy to be protective in both sexes. Adrenalectomy may prevent HSV entry into the CNS as assessed by viral plaque assay of spinal cord, brainstem, and cortex.

Repeat 8 week antibiotic experiment

Plans should be made to repeat the previous antibiotic experiment, using a cohort of 10 mice placed on trimethoprim-sulfamethoxazole in drinking water for 8 weeks prior to infection with $3x10^7$ pfu HSV (higher dose). Control cohort of 10 mice will be on normal

water, housed in same facility, and age matched for 8 weeks prior to infection. This experiment will confirm whether antibiotics alone are protective.

Compare Jackson mice vs NCI mice (males and females)

To compare mice housed in different facilities, we will obtain 10 female/5 male C57Bl/6 mice from NCI (normal vendor for wildtype B6 mice) and 10 female/5 male C57Bl/6 mice from Jackson Labs (original vendor for Four Core Genotype mice). We will infect these mice at 8 weeks old with $3x10^7$ pfu HSV. We have consistently seen a very dramatic difference in survival between males and females from NCI. This experiment will confirm whether the survival difference between XX F and XY M are minimized in Jackson mice, as suggested by the preliminary Four Core Genotype mice survival data. If so, this may point to the gut microbiome as a possible contributor to the observed sex difference in male and female B6 mice from NCI.

Ovariectomize and castrate Four Core Genotype mice prior to HSV infection

To further evaluate the effect of sex chromosomes in the absence of hormonal influences, we will castrate males and ovariectomize females prior to HSV infection. Male mice (XX M, XY M) will be castrated at 3 weeks old, prior to onset of puberty. Mice will be anesthetized with a ketamine/xylazene short acting sedative and surgically prepared. A midline incision will be made in the scrotum, then an incision in the tunica albuginea of the first testicle. The testes, vas deferens, and attached testicular fat will be pulled out of the incision. The blood vessels supplying the testes will be cauterized, and

testes and vas deferens severed. The procedure will be repeated on the contralateral testicle. The scrotum incision will be closed using sterile tissue glue.

Female mice (XX F, XY F) will be ovariectomized at 3 weeks old, prior to onset of puberty. Females will also be anesthetized with ketamine/xylazene and prepared under sterile operating conditions. A dorsal midline skin incision will be made caudal to the posterior border of the ribs. The peritoneum will be cut to enter the abdominal cavity. The ovary and periovarian fat will be lifted out, and the fallopian tube will be clamped. The ovary is removed by cutting above the clamped area, and the blood vessels will be cauterized. The uterine horn is returned into the abdomen, and the peritoneum closed with absorbable suture. The skin incision is closed using wound clips. The procedure is repeated on the contralateral side.

Mice will be followed for post-operative care and watched for signs of dehydration, weight loss, and proper wound healing. Analgesics will be used post operatively as needed. Wound clips will be removed 1 week after surgery. At 8 weeks old, male and female mice will be infected with $3x10^7$ pfu HSV and monitored for survival and weight loss. This experiment will determine if there is any sex chromosome effect in absence of any masking effect due to hormones.

Figures:

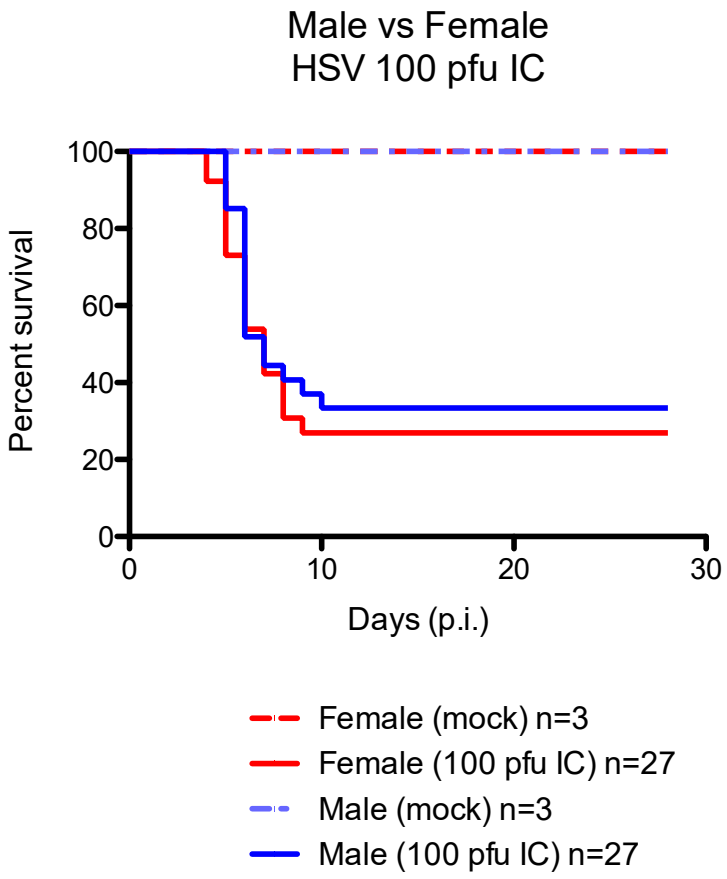

Figure 42: Male and Female B6 mice are equally susceptible to HSV via direct intracranial infection

B6 males (blue line) and B6 females (red line) were infected with 100 pfu HSV intracranially. Mice were followed for survival out to 28 days post infection. There is no statistical difference between survival after intracranial infection in male and female mice.

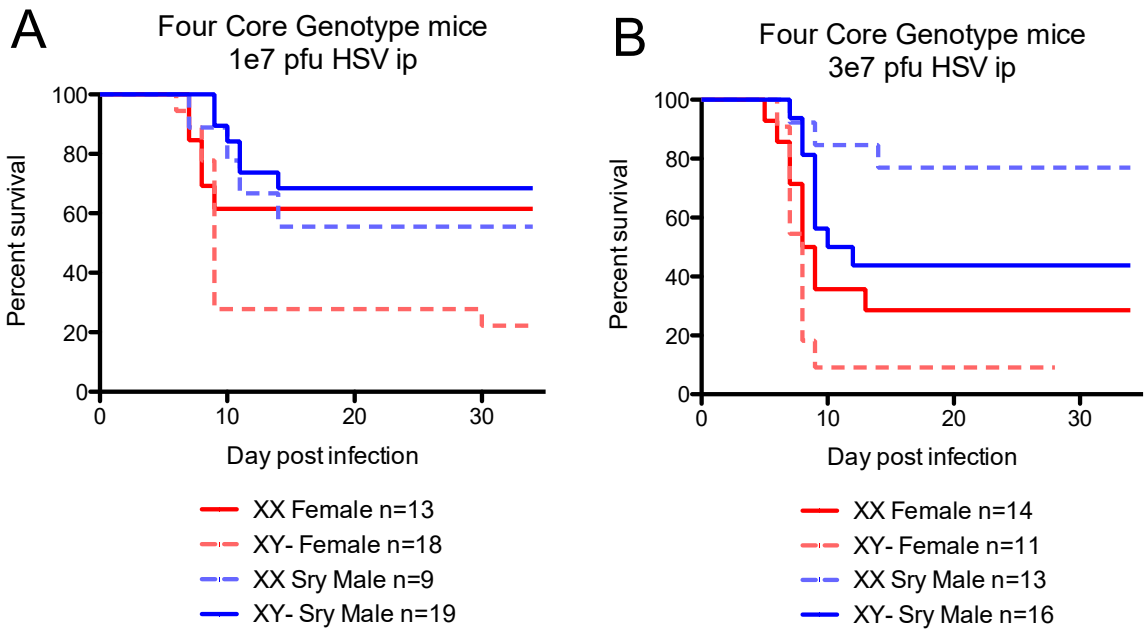

Figure 43: XX sex chromosome complement does not increase HSV susceptibility

Four Core Genotype mice were infected with (A) 1e7 pfu HSV or (B) 3e7 pfu HSV intraperitoneally. XX Female (red solid), XY Female (red dashed), XX male (blue dashed), XY Male (blue solid). Note that there is no statistical difference between Four Core Genotype XX Females (red solid) and XY Males (blue solid) at either dose, contrary to the large sex difference seen in C57BL/6 mice obtained from NCI. There also is no increased susceptibility in XX bearing mice, contrary to expectations.

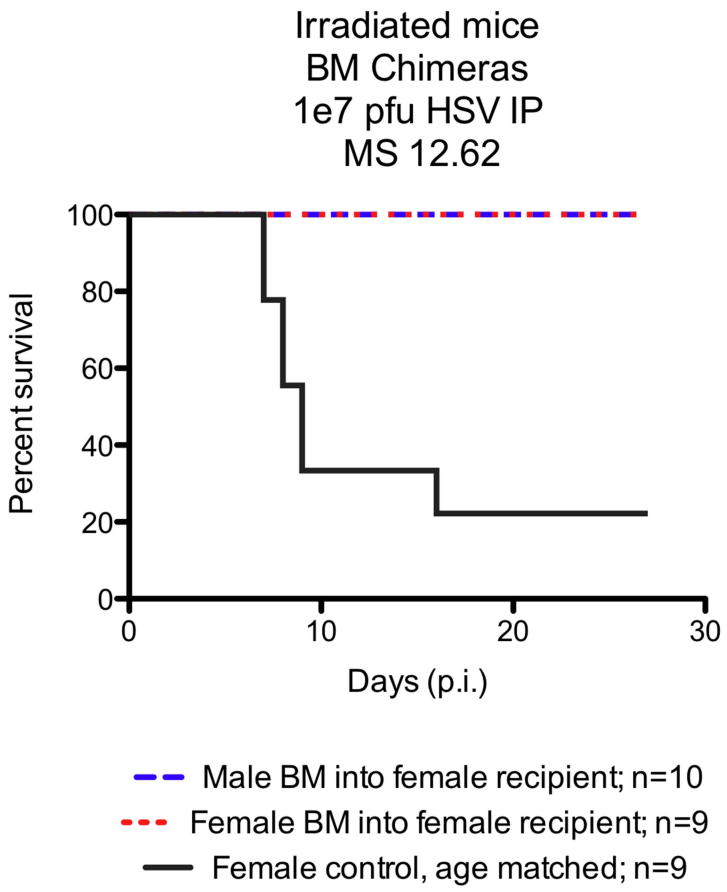

Figure 44: Irradiated mice on antibiotic treatment are resistant to systemic HSV infection

Recipient female Ly5.1 mice were irradiated with 950 rad, then given bone marrow from male (blue dashed) or female (red dashed) Ly5.2 donors. Recipients were given Trimethoprim-sulfamethoxazole in the drinking water for 8 weeks prior to infection with 1e7 pfu HSV intraperitoneally. Control females were age matched, but not irradiated, and not given antibiotic water (black solid). Note that Female BM into Female recipient mice unexpectedly does not phenocopy nonirradiated, non antibiotic treated Female controls.

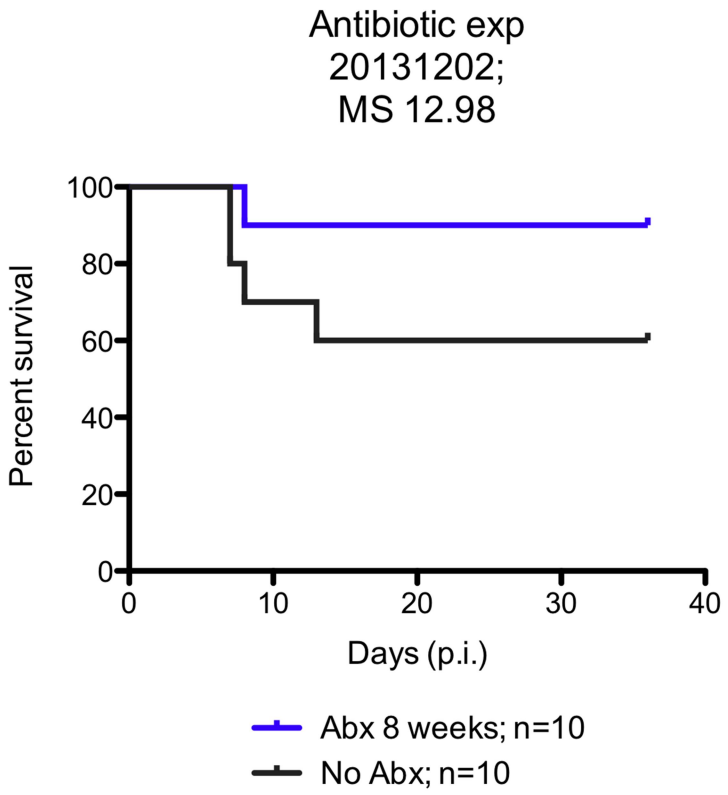

Figure 45: Long term Antibiotic treatment maybe protective against systemic HSV infection

B6 females were treated with trimethoprim-sulfamethoxazole in the drinking water for 8 weeks (blue) or left untreated (black), then infected with 1e7 pfu HSV intraperitoneally. This may suggest some protective effect due to long term antibiotic treatment. This should be repeated.

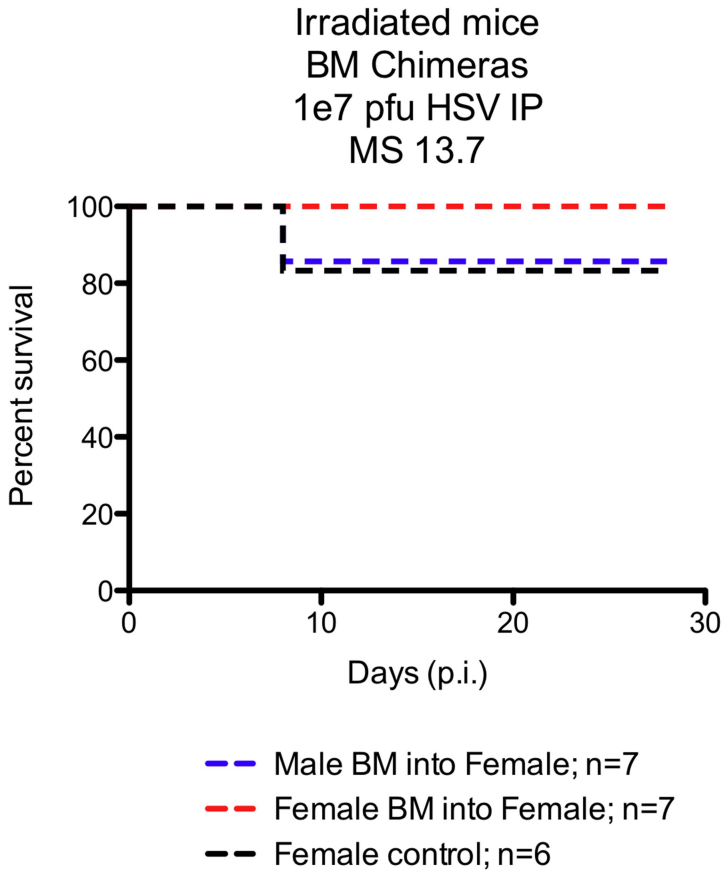

Figure 46: Irradiated mice on antibiotic treatment are resistant to HSV; non-irradiated controls on antibiotic treatment are also resistant to HSV

Recipient female Ly5.1 mice were irradiated with 950 rad, then given bone marrow from male (blue dashed) or female (red dashed) Ly5.2 donors. Recipients were given Trimethoprim-sulfamethoxazole in the drinking water for 8 weeks prior to infection with 1e7 pfu HSV intraperitoneally. Control females were age matched and also given antibiotic water, but not irradiated (black dashed). Compare to Figure 44, where non-irradiated controls were not given antibiotic water. All groups exposed to long term antibiotic treatment are highly resistant to systemic HSV in this model.

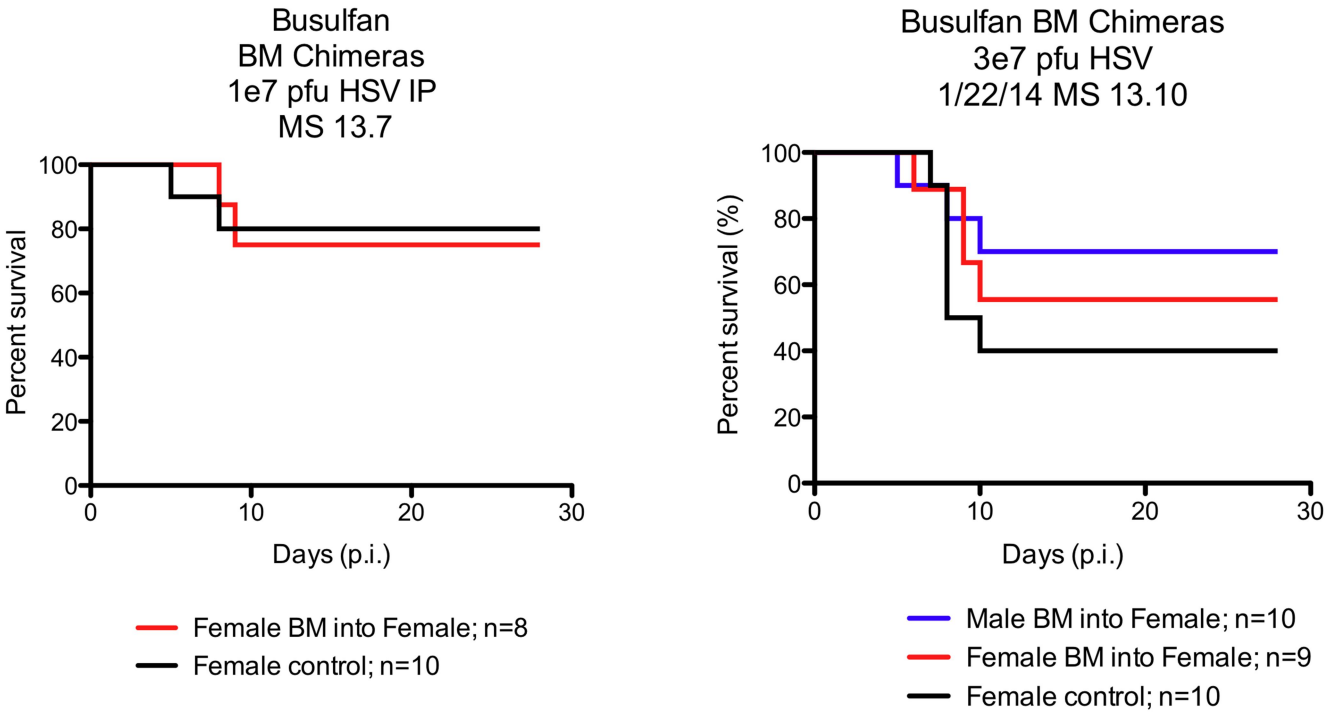

Figure 47: Effect of Busulfan mediated bone marrow transplant on HSV susceptibility

(A) Recipient female Ly5.1 mice were given 100 mg/kg busulfan split dose (50 mg/kg day 1, 50 mg/kg day 2), rested on day 3, and transplanted with bone marrow from female Ly5.2 donors on day 4. Mice were allowed to reconstitute for 8 weeks with no antibiotic treatment, then infected with 1e7 pfu HSV intraperitoneally. (B) Same protocol was followed, except recipient female mice were given 80 mg/kg busulfan split dose (40 mg/kg day 1, 40 mg/kg day 2), and following 8 weeks of reconstitution, mice were infected with 3e7 pfu HSV intraperitoneally. In both experiments, controls were not busulfan treated and not transplanted, and had no antibiotic exposure.

REFERENCES

1. Parker, S., et al., *Human monkeypox: an emerging zoonotic disease.* Future microbiology, 2007. **2**: p. 17-34.
2. Reynolds, M.G. and I.K. Damon, *Outbreaks of human monkeypox after cessation of smallpox vaccination.* Trends Microbiol, 2012.
3. Van Vliet, K., et al., *Poxvirus Proteomics and Virus-Host Protein Interactions.* Microbiology and Molecular Biology Reviews, 2009. **73**(4): p. 730-749.
4. Campbell, J.A., et al., *Zoonotic orthopoxviruses encode a high-affinity antagonist of NKG2D.* J Exp Med, 2007. **204**(6): p. 1311-7.
5. Cosman, D., et al., *ULBPs, novel MHC class I-related molecules, bind to CMV glycoprotein UL16 and stimulate NK cytotoxicity through the NKG2D receptor.* Immunity, 2001. **14**(2): p. 123-33.
6. Lenac, T., et al., *Murine cytomegalovirus regulation of NKG2D ligands.* Med Microbiol Immunol, 2008. **197**(2): p. 159-66.
7. Campbell, J.A., *Immune Receptor Targeting by Orthopoxvirus MHC Class I-like protein*, in *Department of Immunology*. 2009, Washington University in Saint Louis: Saint Louis, Missouri. p. 166.
8. Campbell, J.A., et al., *Cutting Edge: FcR-Like 5 on Innate B Cells Is Targeted by a Poxvirus MHC Class I-Like Immunoevasin.* The Journal of Immunology, 2010. **185**(1): p. 28-32.
9. Haga, C.L., et al., *Fc receptor-like 5 inhibits B cell activation via SHP-1 tyrosine phosphatase recruitment.* Proc Natl Acad Sci USA, 2007. **104**(23): p. 9770-5.
10. Lazear, E., et al., *Crystal structure of the cowpox virus-encoded NKG2D ligand OMCP.* J Virol, 2013. **87**(2): p. 840-50.
11. Jonjić, S., B. Polić, and A. Krmpotić, *Viral inhibitors of NKG2D ligands: Friends or foes of immune surveillance?* Eur. J. Immunol., 2008. **38**(11): p. 2952-2956.
12. Obeidy, P. and A.F. Sharland, *NKG2D and its ligands.* Int J Biochem Cell Biol, 2009. **41**(12): p. 2364-7.
13. Davis, R.S., *Fc receptor-like molecules.* Annu Rev Immunol, 2007. **25**: p. 525-60.
14. Wilson, T.J., A. Fuchs, and M. Colonna, *Cutting Edge: Human FcRL4 and FcRL5 Are Receptors for IgA and IgG.* The Journal of Immunology, 2012.
15. Schreeder, D.M., et al., *Cutting Edge: FcR-Like 6 Is an MHC Class II Receptor.* The Journal of Immunology, 2010. **185**(1): p. 23-27.
16. Zafirova, B., et al., *Altered NK cell development and enhanced NK cell-mediated resistance to mouse cytomegalovirus in NKG2D-deficient mice.* Immunity, 2009. **31**(2): p. 270-82.
17. Earl, P.L., et al., *Preparation of cell cultures and vaccinia virus stocks.* Current protocols in protein science / editorial board, John E Coligan [et al], 2001. **Chapter 5**: p. Unit5.12.
18. Earl, P.L., et al., *Preparation of cell cultures and vaccinia virus stocks.* Curr Protoc Protein Sci, 2001. **Chapter 5**: p. Unit5 12.

19. Falkner, F.G. and B. Moss, *Transient dominant selection of recombinant vaccinia viruses.* J Virol, 1990. **64**(6): p. 3108-11.
20. Kato, S.E., et al., *An alternative genetic method to test essential vaccinia virus early genes.* J Virol Methods, 2004. **115**(1): p. 31-40.
21. Nybakken, G.E., et al., *Structural basis of West Nile virus neutralization by a therapeutic antibody.* Nature, 2005. **437**(7059): p. 764-9.
22. Dokun, A.O., et al., *Specific and nonspecific NK cell activation during virus infection.* Nat Immunol, 2001. **2**(10): p. 951-6.
23. Zhang, X., R. Goncalves, and D.M. Mosser, *The isolation and characterization of murine macrophages.* Curr Protoc Immunol, 2008. **Chapter 14**: p. Unit 14.1.
24. Aricescu, A.R., W. Lu, and E.Y. Jones, *A time- and cost-efficient system for high-level protein production in mammalian cells.* Acta Crystallogr D Biol Crystallogr, 2006. **62**(Pt 10): p. 1243-50.
25. Won, W.J., et al., *Fc receptor homolog 3 is a novel immunoregulatory marker of marginal zone and B1 B cells.* J Immunol, 2006. **177**(10): p. 6815-23.
26. Carayannopoulos, L.N., et al., *Ligands for murine NKG2D display heterogeneous binding behavior*, in *Eur. J. Immunol.* 2002. p. 597-605.
27. Chapman, J.L., et al., *Animal models of orthopoxvirus infection.* Veterinary pathology, 2010. **47**(5): p. 852-870.
28. Lodoen, M., et al., *NKG2D-mediated natural killer cell protection against cytomegalovirus is impaired by viral gp40 modulation of retinoic acid early inducible 1 gene molecules.* J Exp Med, 2003. **197**(10): p. 1245-53.
29. Lodoen, M.B., et al., *The cytomegalovirus m155 gene product subverts natural killer cell antiviral protection by disruption of H60-NKG2D interactions.* J Exp Med, 2004. **200**(8): p. 1075-81.
30. Krmpotic, A., et al., *NK cell activation through the NKG2D ligand MULT-1 is selectively prevented by the glycoprotein encoded by mouse cytomegalovirus gene m145.* J Exp Med, 2005. **201**(2): p. 211-20.
31. Lenac, T., et al., *The herpesviral Fc receptor fcr-1 down-regulates the NKG2D ligands MULT-1 and H60.* J Exp Med, 2006. **203**(8): p. 1843-50.
32. Fang, M., L.L. Lanier, and L.J. Sigal, *A role for NKG2D in NK cell-mediated resistance to poxvirus disease.* PLoS Pathog, 2008. **4**(2): p. e30.
33. Ehrlich, L.I.R., et al., *Engagement of NKG2D by cognate ligand or antibody alone is insufficient to mediate costimulation of human and mouse CD8+ T cells.* Journal of immunology (Baltimore, Md : 1950), 2005. **174**(4): p. 1922-1931.
34. Jamieson, A.M., et al., *The role of the NKG2D immunoreceptor in immune cell activation and natural killing.* Immunity, 2002. **17**(1): p. 19-29.
35. Gainey, M.D., et al., *Viral MHC class I inhibition evades CD8+ T-cell effector responses in vivo but not CD8+ T-cell priming.*, in *Proc Natl Acad Sci USA*. 2012.
36. Dement-Brown, J., et al., *Fc receptor-like 5 promotes B cell proliferation and drives the development of cells displaying switched isotypes.* Journal of Leukocyte Biology, 2012. **91**(1): p. 59-67.
37. Zhu, Z., et al., *FCRL5 exerts binary and compartment-specific influence on innate-like B-cell receptor signaling.* Proceedings of the National Academy of Sciences of the United States of America, 2013.

38. Stall, A.M., S.M. Wells, and K.P. Lam, *B-1 cells: unique origins and functions.* Semin Immunol, 1996. **8**(1): p. 45-59.
39. LeBien, T.W. and T.F. Tedder, *B lymphocytes: how they develop and function.* Blood, 2008. **112**(5): p. 1570-80.
40. Hardy, R.R., *B-1 B cell development.* J Immunol, 2006. **177**(5): p. 2749-54.
41. Choi, Y.S. and N. Baumgarth, *Dual role for B-1a cells in immunity to influenza virus infection.* J Exp Med, 2008. **205**(13): p. 3053-64.
42. Gray, D., M. Gray, and T. Barr, *Innate responses of B cells.* Eur. J. Immunol., 2007. **37**(12): p. 3304-10.
43. Duan, B. and L. Morel, *Role of B-1a cells in autoimmunity.* Autoimmun Rev, 2006. **5**(6): p. 403-8.
44. Alugupalli, K.R. and R.M. Gerstein, *Divide and conquer: division of labor by B-1 B cells.* Immunity, 2005. **23**(1): p. 1-2.
45. Bahram, S., et al., *MIC and other NKG2D ligands: from none to too many.* Curr Opin Immunol, 2005. **17**(5): p. 505-9.
46. Serbina, N.V., et al., *Monocyte-mediated defense against microbial pathogens.* Annu Rev Immunol, 2008. **26**: p. 421-52.
47. Mosser, D.M. and J.P. Edwards, *Exploring the full spectrum of macrophage activation.* Nat Rev Immunol, 2008. **8**(12): p. 958-69.
48. Rees, A.J., *Monocyte and macrophage biology: an overview.* Semin Nephrol, 2010. **30**(3): p. 216-33.
49. Auffray, C., M.H. Sieweke, and F. Geissmann, *Blood monocytes: development, heterogeneity, and relationship with dendritic cells.* Annu Rev Immunol, 2009. **27**: p. 669-92.
50. Hubert, P., et al., *Antibody-dependent cell cytotoxicity synapses form in mice during tumor-specific antibody immunotherapy.* Cancer Res, 2011. **71**(15): p. 5134-43.
51. Lefebvre, M.-L., et al., *Ex vivo-activated human macrophages kill chronic lymphocytic leukemia cells in the presence of rituximab: mechanism of antibody-dependent cellular cytotoxicity and impact of human serum.* J Immunother, 2006. **29**(4): p. 388-97.
52. Helguera, G., et al., *Visualization and quantification of cytotoxicity mediated by antibodies using imaging flow cytometry.* J Immunol Methods, 2011. **368**(1-2): p. 54-63.
53. Renaudineau, Y., et al., *Monoclonal anti-CD20 antibodies: mechanisms of action and monitoring of biological effects.* Joint Bone Spine, 2009. **76**(5): p. 458-63.
54. Goh, Y.S., et al., *Human IgG isotypes and activating Fcγ receptors in the interaction of Salmonella enterica serovar Typhimurium with phagocytic cells.* Immunology, 2011. **133**(1): p. 74-83.
55. Nuutila, J. and E.-M. Lilius, *Flow cytometric quantitative determination of ingestion by phagocytes needs the distinguishing of overlapping populations of binding and ingesting cells.* Cytometry A, 2005. **65**(2): p. 93-102.
56. Beliard, R., et al., *A human anti-D monoclonal antibody selected for enhanced FcgammaRIII engagement clears RhD+ autologous red cells in human volunteers as efficiently as polyclonal anti-D antibodies.* British Journal of Haematology, 2008. **141**(1): p. 109-19.

57. Kumpel, B.M., *Efficacy of RhD monoclonal antibodies in clinical trials as replacement therapy for prophylactic anti-D immunoglobulin: more questions than answers.* Vox Sang, 2007. **93**(2): p. 99-111.
58. Béliard, R., *Monoclonal anti-D antibodies to prevent alloimmunization: lessons from clinical trials.* Transfus Clin Biol, 2006. **13**(1-2): p. 58-64.
59. Getahun, A. and B. Heyman, *Studies on the mechanism by which antigen-specific IgG suppresses primary antibody responses: evidence for epitope masking and decreased localization of antigen in the spleen.* Scand J Immunol, 2009. **70**(3): p. 277-87.
60. Diefenbach, A., et al., *Ligands for the murine NKG2D receptor: expression by tumor cells and activation of NK cells and macrophages.* Nat Immunol, 2000. **1**(2): p. 119-26.
61. van der Poel, C.E., et al., *Functional characteristics of the high affinity IgG receptor, FcγRI.* J Immunol, 2011. **186**(5): p. 2699-704.
62. Edberg, J.C., et al., *The CY domain of the Fcgamma RIa alpha-chain (CD64) alters gamma-chain tyrosine-based signaling and phagocytosis.* J Biol Chem, 2002. **277**(43): p. 41287-93.
63. Ravetch, J.V. and J.P. Kinet, *Fc receptors.* Annu Rev Immunol, 1991. **9**: p. 457-92.
64. Bruhns, P., et al., *Specificity and affinity of human Fcgamma receptors and their polymorphic variants for human IgG subclasses.* Blood, 2009. **113**(16): p. 3716-25.
65. Harrison, P.T. and J.M. Allen, *High affinity IgG binding by FcgammaRI (CD64) is modulated by two distinct IgSF domains and the transmembrane domain of the receptor.* Protein Eng, 1998. **11**(3): p. 225-32.
66. Lu, J., et al., *Crystal structure of Fcgamma receptor I and its implication in high affinity gamma-immunoglobulin binding.* J Biol Chem, 2011. **286**(47): p. 40608-13.
67. Karupiah, G., et al., *Different roles for CD4+ and CD8+ T lymphocytes and macrophage subsets in the control of a generalized virus infection.* J Virol, 1996. **70**(12): p. 8301-9.
68. Rivera, R., et al., *Murine alveolar macrophages limit replication of vaccinia virus.* Virology, 2007. **363**(1): p. 48-58.
69. Pullyblank, A.M., P.J. Guillou, and J.R. Monson, *Interleukin 1 and tumour necrosis factor alpha may be responsible for the lytic mechanism during anti-tumour antibody-dependent cell-mediated cytotoxicity.* Br J Cancer, 1995. **72**(3): p. 601-6.
70. Klimp, A.H., et al., *A potential role of macrophage activation in the treatment of cancer.* Crit Rev Oncol Hematol, 2002. **44**(2): p. 143-61.
71. Barnes, N., et al., *FcgammaRI-deficient mice show multiple alterations to inflammatory and immune responses.* Immunity, 2002. **16**(3): p. 379-89.
72. Ioan-Facsinay, A., et al., *FcgammaRI (CD64) contributes substantially to severity of arthritis, hypersensitivity responses, and protection from bacterial infection.* Immunity, 2002. **16**(3): p. 391-402.
73. Ceuppens, J.L., et al., *Defect in the membrane expression of high affinity 72-kD Fc gamma receptors on phagocytic cells in four healthy subjects.* J Clin Invest, 1988. **82**(2): p. 571-8.
74. van de Winkel, J.G., et al., *Molecular basis for a familial defect in phagocyte expression of IgG receptor I (CD64).* J Immunol, 1995. **154**(6): p. 2896-903.
75. Nimmerjahn, F., et al., *FcγRIV deletion reveals its central role for IgG2a and IgG2b activity in vivo.* Proceedings of the National Academy of Sciences of the United States of America, 2010. **107**(45): p. 19396-19401.

76. Langlet, C., et al., *CD64 Expression Distinguishes Monocyte-Derived and Conventional Dendritic Cells and Reveals Their Distinct Role during Intramuscular Immunization.* Journal of immunology (Baltimore, Md : 1950), 2012. **188**(4): p. 1751-1760.
77. Nimmerjahn, F., et al., *FcgammaRIV: a novel FcR with distinct IgG subclass specificity.* Immunity, 2005. **23**(1): p. 41-51.
78. Lanier, L.L., *DAP10- and DAP12-associated receptors in innate immunity.* Immunol Rev, 2009. **227**(1): p. 150-60.
79. Chahroudi, A., et al., *Vaccinia virus tropism for primary hematolymphoid cells is determined by restricted expression of a unique virus receptor.* J Virol, 2005. **79**(16): p. 10397-407.
80. Davis, R.S., et al., *Identification of a family of Fc receptor homologs with preferential B cell expression.* Proc Natl Acad Sci USA, 2001. **98**(17): p. 9772-7.
81. Radaev, S. and P. Sun, *Recognition of immunoglobulins by Fcgamma receptors.* Mol Immunol, 2002. **38**(14): p. 1073-83.
82. Davis, R.S., et al., *Differential B cell expression of mouse Fc receptor homologs.* Int Immunol, 2004. **16**(9): p. 1343-53.
83. Zhou, Q. and G.S. Salvesen, *Viral caspase inhibitors CrmA and p35.* Methods Enzymol, 2000. **322**: p. 143-54.
84. Xue, X., et al., *Structural basis of chemokine sequestration by CrmD, a poxvirus-encoded tumor necrosis factor receptor.*, in *PLoS Pathog*. 2011. p. e1002162.
85. Cunnion, K.M., *Tumor necrosis factor receptors encoded by poxviruses.*, in *Mol. Genet. Metab.* 1999. p. 278-282.
86. Lleo, A., et al., *Is autoimmunity a matter of sex?* Autoimmun Rev, 2008. **7**(8): p. 626-30.
87. Davidson, A. and B. Diamond, *Autoimmune diseases.* N Engl J Med, 2001. **345**(5): p. 340-50.
88. Beagley, K.W. and C.M. Gockel, *Regulation of innate and adaptive immunity by the female sex hormones oestradiol and progesterone.* FEMS immunology and medical microbiology, 2003. **38**(1): p. 13-22.
89. Marriott, I. and Y.M. Huet-Hudson, *Sexual dimorphism in innate immune responses to infectious organisms.* Immunologic research, 2006. **34**(3): p. 177-192.
90. McClelland, E.E. and J.M. Smith, *Gender specific differences in the immune response to infection.* Archivum immunologiae et therapiae experimentalis, 2011. **59**(3): p. 203-213.
91. Klein, S.L., A. Jedlicka, and A. Pekosz, *The Xs and Y of immune responses to viral vaccines.* The Lancet infectious diseases, 2010. **10**(5): p. 338-349.
92. Klein, S.L., *Sex differences in prophylaxis and therapeutic treatments for viral diseases.* Handbook of experimental pharmacology, 2012(214): p. 499-522.
93. Klein, S.L., *Sex influences immune responses to viruses, and efficacy of prophylaxis and treatments for viral diseases.* BioEssays : news and reviews in molecular, cellular and developmental biology, 2012. **34**(12): p. 1050-1059.
94. Marriott, I. and Y.M. Huet-Hudson, *Sexual dimorphism in innate immune responses to infectious organisms.* Immunol Res, 2006. **34**(3): p. 177-92.
95. Bouman, A., M.J. Heineman, and M.M. Faas, *Sex hormones and the immune response in humans.* Hum Reprod Update, 2005. **11**(4): p. 411-23.

96. Garcia-Gomez, E., B. Gonzalez-Pedrajo, and I. Camacho-Arroyo, *Role of sex steroid hormones in bacterial-host interactions.* Biomed Res Int, 2013. **2013**: p. 928290.
97. Schroder, J., et al., *Gender differences in human sepsis.* Arch Surg, 1998. **133**(11): p. 1200-5.
98. McClelland, E.E. and J.M. Smith, *Gender specific differences in the immune response to infection.* Arch Immunol Ther Exp (Warsz), 2011. **59**(3): p. 203-13.
99. Robinson, D.P., et al., *Elevated 17beta-estradiol protects females from influenza A virus pathogenesis by suppressing inflammatory responses.* PLoS Pathog, 2011. **7**(7): p. e1002149.
100. Pinheiro, I., L. Dejager, and C. Libert, *X-chromosome-located microRNAs in immunity: might they explain male/female differences? The X chromosome-genomic context may affect X-located miRNAs and downstream signaling, thereby contributing to the enhanced immune response of females.* Bioessays, 2011. **33**(11): p. 791-802.
101. Arnold, A.P. and X. Chen, *What does the "four core genotypes" mouse model tell us about sex differences in the brain and other tissues?* Front Neuroendocrinol, 2009. **30**(1): p. 1-9.
102. Gleicher, N. and D.H. Barad, *Gender as risk factor for autoimmune diseases.* J Autoimmun, 2007. **28**(1): p. 1-6.
103. Robinson, D.P., et al., *Sex chromosome complement contributes to sex differences in coxsackievirus B3 but not influenza A virus pathogenesis.* Biol Sex Differ, 2011. **2**: p. 8.
104. Scofield, R.H., et al., *Klinefelter's syndrome (47,XXY) in male systemic lupus erythematosus patients: support for the notion of a gene-dose effect from the X chromosome.* Arthritis Rheum, 2008. **58**(8): p. 2511-7.
105. Geurs, T.L., et al., *Sex differences in murine susceptibility to systemic viral infections.* Journal of autoimmunity, 2012. **38**(2-3): p. J245-53.
106. Meier, A., et al., *Sex differences in the Toll-like receptor-mediated response of plasmacytoid dendritic cells to HIV-1.* Nat Med, 2009. **15**(8): p. 955-9.
107. Chang, J.J., et al., *Higher expression of several interferon-stimulated genes in HIV-1-infected females after adjusting for the level of viral replication.* J Infect Dis, 2013. **208**(5): p. 830-8.
108. van Pesch, V., et al., *Characterization of the murine alpha interferon gene family.* Journal of virology, 2004. **78**(15): p. 8219-8228.
109. Theofilopoulos, A.N., et al., *Type I interferons (alpha/beta) in immunity and autoimmunity*, in *Annu Rev Immunol*. 2005. p. 307-336.
110. Lavoie, T.B., et al., *Binding and activity of all human alpha interferon subtypes.* Cytokine, 2011. **56**(2): p. 282-9.
111. Tassiulas, I., et al., *Amplification of IFN-alpha-induced STAT1 activation and inflammatory function by Syk and ITAM-containing adaptors.* Nat Immunol, 2004. **5**(11): p. 1181-9.
112. Pasieka, T.J., et al., *Functional genomics reveals an essential and specific role for Stat1 in protection of the central nervous system following herpes simplex virus corneal infection.* Journal of virology, 2011. **85**(24): p. 12972-12981.
113. Pasieka, T.J., et al., *Host responses to wild-type and attenuated herpes simplex virus infection in the absence of Stat1.* Journal of virology, 2009. **83**(5): p. 2075-2087.

114. Pasieka, T.J., et al., *Bioluminescent imaging reveals divergent viral pathogenesis in two strains of Stat1-deficient mice, and in αßγ interferon receptor-deficient mice.* PloS one, 2011. **6**(9): p. e24018.
115. Ambarus, C.A., et al., *Systematic validation of specific phenotypic markers for in vitro polarized human macrophages.* Journal of immunological methods, 2012. **375**(1-2): p. 196-206.
116. Melchjorsen, J., et al., *Early innate recognition of herpes simplex virus in human primary macrophages is mediated via the MDA5/MAVS-dependent and MDA5/MAVS/RNA polymerase III-independent pathways.* Journal of virology, 2010. **84**(21): p. 11350-11358.
117. Génin, P., A. Vaccaro, and A. Civas, *The role of differential expression of human interferon-A genes in antiviral immunity.* Cytokine & growth factor reviews, 2009. **20**(4): p. 283-295.
118. Yamaoka, T., et al., *Biologic and binding activities of IFN-alpha subtypes in ACHN human renal cell carcinoma cells and Daudi Burkitt's lymphoma cells.* Journal of interferon & cytokine research : the official journal of the International Society for Interferon and Cytokine Research, 1999. **19**(12): p. 1343-1349.
119. Vogel, S.N., R.M. Friedman, and M.M. Hogan, *Measurement of antiviral activity induced by interferons alpha, beta, and gamma.* Current protocols in immunology / edited by John E Coligan [et al], 2001. **Chapter 6**: p. Unit 6.9.
120. Moran, D.M., E.R. Kern, and J.C. Overall, *Synergism between recombinant human interferon and nucleoside antiviral agents against herpes simplex virus: examination with an automated microtiter plate assay.* The Journal of infectious diseases, 1985. **151**(6): p. 1116-1122.
121. Menachery, V.D., T.J. Pasieka, and D.A. Leib, *Interferon regulatory factor 3-dependent pathways are critical for control of herpes simplex virus type 1 central nervous system infection.* Journal of virology, 2010. **84**(19): p. 9685-9694.
122. Menachery, V.D. and D.A. Leib, *Control of herpes simplex virus replication is mediated through an interferon regulatory factor 3-dependent pathway.* Journal of virology, 2009. **83**(23): p. 12399-12406.
123. Samarajiwa, S.A., et al., *INTERFEROME: the database of interferon regulated genes*, in *Nucleic Acids Research*. 2009. p. D852-D857.
124. Santoro-Lopes, G., et al., *Gender and survival after AIDS in Rio de Janeiro, Brazil.* J Acquir Immune Defic Syndr Hum Retrovirol, 1998. **19**(4): p. 403-7.
125. Curiel, R.E., et al., *Does the gender difference in interferon production seen in picornavirus-infected spleen cell cultures from ICR Swiss mice have any in vivo significance?* J Interferon Res, 1993. **13**(6): p. 387-95.
126. Barna, M., et al., *Sex differences in susceptibility to viral infection of the central nervous system.* J Neuroimmunol, 1996. **67**(1): p. 31-9.
127. Huber, S.A. and B. Pfaeffle, *Differential Th1 and Th2 cell responses in male and female BALB/c mice infected with coxsackievirus group B type 3.* J Virol, 1994. **68**(8): p. 5126-32.
128. Villacres, M.C., et al., *Predominant type 1 CMV-specific memory T-helper response in humans: evidence for gender differences in cytokine secretion.* Hum Immunol, 2004. **65**(5): p. 476-85.

129. Brazzale, A.G., et al., *Seroprevalence of herpes simplex virus type 1 and type 2 among the Indigenous population of Cape York, Far North Queensland, Australia.* Sex Health, 2010. **7**(4): p. 453-9.
130. Smith, J.S. and N.J. Robinson, *Age-specific prevalence of infection with herpes simplex virus types 2 and 1: a global review.* J Infect Dis, 2002. **186 Suppl 1**: p. S3-28.
131. Landry, M.L., J. Greenwold, and H.R. Vikram, *Herpes simplex type-2 meningitis: presentation and lack of standardized therapy.* Am J Med, 2009. **122**(7): p. 688-91.
132. Omland, L.H., B.F. Vestergaard, and J.H. Wandall, *Herpes simplex virus type 2 infections of the central nervous system: A retrospective study of 49 patients.* Scand J Infect Dis, 2008. **40**(1): p. 59-62.
133. Glynn, J.R., et al., *Herpes simplex virus type 2 trends in relation to the HIV epidemic in northern Malawi.* Sex Transm Infect, 2008. **84**(5): p. 356-60.
134. Hill, T.J., D.L. Yirrell, and W.A. Blyth, *Infection of the adrenal gland as a route to the central nervous system after viraemia with herpes simplex virus in the mouse.* J Gen Virol, 1986. **67 (Pt 2)**: p. 309-20.
135. Potratz, D., et al., *Herpes simplex virus type 1 and 2 in the adrenal glands: replication and histopathology.* Arch Virol, 1986. **90**(3-4): p. 207-22.
136. Burgos, J.S., et al., *Herpes simplex virus type 1 infection via the bloodstream with apolipoprotein E dependence in the gonads is influenced by gender.* J Virol, 2005. **79**(3): p. 1605-12.
137. Peles, E., et al., *Importance of the HpaI-P sequence for herpes simplex virus-1 replication in the adrenal glands.* Arch Virol, 1990. **113**(3-4): p. 151-63.
138. Berkowitz, C., et al., *Herpes simplex virus type 1 (HSV-1) UL56 gene is involved in viral intraperitoneal pathogenicity to immunocompetent mice.* Arch Virol, 1994. **134**(1-2): p. 73-83.
139. Podlech, J., K. Weise, and D. Falke, *Colonization of adrenal glands and ovaries of mice by HSV-2 variants. I. Virological studies.* Arch Virol, 1990. **110**(3-4): p. 165-77.
140. Rader, K.A., et al., *In-Vivo Characterization of Site-Directed Mutations in the Promoter of the Herpes-Simplex Virus Type-1 Latency-Associated Transcripts.* Journal of General Virology, 1993. **74**: p. 1859-1869.
141. Libert, C., L. Dejager, and I. Pinheiro, *The X chromosome in immune functions: when a chromosome makes the difference.* Nature reviews Immunology, 2010. **10**(8): p. 594-604.
142. Pinheiro, I., L. Dejager, and C. Libert, *X-chromosome-located microRNAs in immunity: might they explain male/female differences? The X chromosome-genomic context may affect X-located miRNAs and downstream signaling, thereby contributing to the enhanced immune response of females.* BioEssays : news and reviews in molecular, cellular and developmental biology, 2011. **33**(11): p. 791-802.
143. Arnold, A.P. and X. Chen, *What does the "four core genotypes" mouse model tell us about sex differences in the brain and other tissues?* Frontiers in neuroendocrinology, 2009. **30**(1): p. 1-9.
144. Ashizuka, S., et al., *Busulfan-conditioned bone marrow transplantation results in high-level allogeneic chimerism in mice made tolerant by in utero hematopoietic cell transplantation.* Exp Hematol, 2006. **34**(3): p. 359-68.
145. Geurs, T.L., et al., *Sex differences in murine susceptibility to systemic viral infections.*, in *J. Autoimmun.* 2012. p. J245-53.

146. Burgos, J.S., et al., *Non-invasive bioluminescence imaging for monitoring herpes simplex virus type 1 hematogenous infection*, in *Microbes and Infection*. 2006. p. 1330-1338.
147. Bielohuby, M., *The mouse adrenal gland: age- and gender- dependent alterations of growth and function*. 2007. p. 1-84.

CURRICULUM VITAE

Michel M. Sun
226 N. Boyle Ave, Apt 2N
St Louis, MO 63108
(973) 960-6745
sunmi@wusm.wustl.edu

EDUCATION

08/2008-present Washington University in St Louis — St. Louis, MO
M.D/Ph.D in Immunology
Ph.D expected May 2016
M.D. expected May 2016

08/2004-05/2008 Rutgers University — New Brunswick, NJ
B.A. Chemistry
B.A. Cell Biology & Neuroscience
GPA 3.986

LABORATORY EXPERIENCE

07/2010-present Department of Immunology, Washington University in St Louis
PhD Student
Advisor: Anthony French, M.D., Ph.D.

OMCP Mediated Cowpox Virulence and its Dependence on the Immune Receptors NKG2D and FCRL5.
This project involves the investigation and characterization of a secreted cowpox immunoevasion protein (OMCP) and evaluation of its role in modulating host defense *in vivo*. We have previously described OMCP binding to the activating receptor NKG2D in NK cells as well as the orphan receptor FCRL5 on innate B cells. We investigated the impact of OMCP targeting of these receptors on cowpox virus virulence *in vivo* using both intraperitoneal and intranasal routes of infection. By using NKG2D-deficient, FCRL5-deficient, and wild type mice, as well as recombinant cowpox viruses lacking OMCP or expressing a mutated form of OMCP that does not bind NKG2D, we were able to delineate the impact of OMCP targeting of each receptor. We found that OMCP's virulence *in vivo* could largely be attributed to blocking NKG2D-mediated NK cell responses with no apparent effect due to binding to FCRL5 bearing innate B cells.

08/2006-05/2008 Department of Chemistry and Chemical Biology, Rutgers University
Undergraduate Student
Advisor: John W Taylor, Ph.D.

Synthesis and Study of a Broadly Neutralizing HIV-1 Epitope Designed for Helix Stabilization.

I completed a Henry Rutgers Scholars Thesis project involving the design, synthesis, and evaluation of a series of conformationally constrained analogs of the alpha helical 4E10 epitope of the HIV viral envelope protein gp41. A library of peptides with cyclic side chain bridges (i, i+4 lactam bridged; i, i+7 para-(aminomethyl)phenylacetic acid bridged), as well as their isosteric acyclic analogs were synthesized by solid phase peptide synthesis, secondary structure content assessed by circular dichroism spectropolarimetry, and 4E10 antibody binding affinity evaluated by ELISA.

08/2007-05/2008 Center for Advanced Biotechnology and Medicine, Robert Wood Johnson Medical School

Research Assistant

Advisor: Gail Ferstandig Arnold, Ph.D.

Application of Synthetic HIV-1 Epitope Helices for Vaccine Design.

The most promising peptides in my library were identified and evaluated for usefulness as boosting immunogens in a vaccination protocol. Synthesis of 4E10 peptide epitope analogs was performed to focus the immune response on the native alpha helical structure of gp41 with the hypothesis that helically constrained epitope analogs may act as more potent immunogenic vaccine components than unconstrained peptide.

TEACHING EXPERIENCE

08/2010-05/2011 Washington University in St Louis Medical School

Physiology Teaching Assistant

Responsible for leading small group conferences for the first year medical school Physiology class, and running review sessions after each block throughout the year. Also assisted in writing, editing, and grading exams and homework assignments.

2007-2008 Douglass College Weekend Academy

Laboratory Teaching Assistant

Instruction of a chemistry lab for a community outreach program aimed at high school girls with a strong prior interest in a career in science, engineering, and/or math. Lectured on topics in inorganic chemistry (color experiments involving metal-ion complexes), physical chemistry (Tindall effect), organic chemistry (polymer synthesis), and biological/theoretical chemistry (protein data bank exploration), etc.

AWARDS AND HONORS

2012-2014 Infectious Disease Training Grant T32-AI007172
2007-2008 Henry Rutgers Scholar
2007-2008 Aresty Scholars Research Award
2008 Enzon Award for Excellence in Chemistry
2007 American Chemical Society (ACS) Analytical Chemistry Award

2007 Departmental Organic Chemistry Lab Award
2007 Bruce Garth Award (for outstanding service to the community in chemistry)
2007 Phi Lambda Upsilon, Chemistry Honor Society (chapter secretary)
2006 Alpha Epsilon Delta, Premed Honor Society
2004-2008 Peter F.E. Marapodi Scholarship
2004-2008 Edward J. Bloustein Distinguished Scholars Program Scholarship
2004-2008 Rutgers Presidential Academic Scholarship

PUBLICATIONS

1. Sun, M., T.L. Geurs, J.A. Campbell, D.M. Lippold, R.S. Davis, L.N. Carayannopoulos, and A.R. French. OMCP mediated cowpox virulence and its dependence on the immune receptors NKG2D and FCRL5 in vivo. Submitted **2014**.
2. Lazear, E., M. Sun, C.A. Nelson, L.N. Carayannopoulos, A.R. French, and D.H. Fremont. Cowpox virus OMCP antazonizes NKG2D via an unexpected binding orientation. Submitted **2014**.
3. Fogel, L.A., M.M. Sun, T.L. Geurs, L.N. Carayannopoulos, and A.R. French. Markers of Nonselective and Specific NK Cell Activation. *J. Immunol.* 190 (12), **2013**.

Conference Abstracts

4. Sun M, Taylor JW. Synthesis and Study of a Broadly Neutralizing HIV-1 Epitope Designed for Helix Stabilization. Columbia University Undergraduate Research Symposium; *Columbia Undergrad Sci J*, Volume 3, Issue 1, April **2008**.